

STELLAR EVOLUTION ON THE BORDERLINE OF  
WHITE DWARF AND NEUTRON STAR FORMATION

*Cover:* Image of the Bug Nebula, one of the brightest and most extreme planetary nebulae known. Planetary nebulae are thought to be the remnant of the envelope of an AGB star, ejected in about 1,000 to 10,000 years. In the center of this nebula lies a white dwarf with an estimated temperature of about 250,000 degrees Celsius. The white dwarf itself is surrounded by a dark torus, seen at the upper right, which withdraws the star from being visible. The plumes and bubbles surrounding the central star reveal a violent past of this system.

Image credits: ESA/NASA & Albert Zijlstra

©2007 Arend Jan Poelarends  
Alle rechten voorbehouden.

This thesis was typeset by the author in L<sup>A</sup>T<sub>E</sub>X using the CLASSICTHESIS package and printed by Uitgeverij BOXPRESS in Oisterwijk.

ISBN-10: 90-393-4442-6  
ISBN-13: 978-90-393-4442-2

STELLAR EVOLUTION  
ON THE BORDERLINE  
OF WHITE DWARF AND  
NEUTRON STAR  
FORMATION

STEREVOLUTIE OP DE GRENS VAN DE  
VORMING VAN WITTE DWERGEN EN  
NEUTRONENSTERREN

(met een samenvatting in het Nederlands)

PROEFSCHRIFT

ter verkrijging van de graad van doctor aan  
de Universiteit Utrecht op gezag van de  
rector magnificus, prof. dr. W.H. Gispen,  
ingevolge het besluit van het college voor  
promoties in het openbaar te verdedigen op  
woensdag 24 januari 2007 des middags te 12.45 uur

door

AREND JAN THEODOOR POELARENDS

geboren op 31 augustus 1979 te Zwolle

PROMOTOR: PROF. DR. N. LANGER

This research has been supported by the  
Netherlands Organization for Scientific Research (NWO).

# CONTENTS

---

|     |   |     |
|-----|---|-----|
| 1   | INTRODUCTION  | 1   |
| 1.1 | The history of stellar evolution  | 1   |
| 1.2 | Single star evolution   | 3   |
| 1.3 | Chemical evolution of the universe  | 5   |
| 1.4 | Super AGB stars   | 7   |
| 1.5 | This thesis   | 7   |
| 2   | THE SUPERNOVA CHANNEL OF SUPER AGB STARS  | 11  |
| 2.1 | Introduction  | 12  |
| 2.2 | Numerical methods   | 14  |
| 2.3 | Pre-AGB evolution and the initial mass range for SAGB stars                             | 15  |
| 2.4 | The TP-SAGB stellar evolution models  | 20  |
| 2.5 | The SAGB population synthesis model   | 23  |
| 2.6 | Results   | 30  |
| 2.7 | Concluding remarks  | 38  |
| 3   | SUPERNOVAE FROM MASSIVE METAL-POOR AGB STARS  | 43  |
| 3.1 | Introduction  | 44  |
| 3.2 | Models, detailed and synthetic  | 45  |
| 3.3 | Evolution to the AGB  | 48  |
| 3.4 | Evolution on the TPAGB  | 54  |
| 3.5 | Results   | 59  |
| 3.6 | Observational implications  | 67  |
| 3.7 | Discussion and conclusions  | 71  |
| 4   | NUCLEOSYNTHESIS IN SUPER AGB STARS  | 73  |
| 4.1 | Introduction  | 74  |
| 4.2 | Models, full and synthetic  | 75  |
| 4.3 | Results   | 83  |
| 4.4 | Discussion  | 95  |
| 4.5 | Conclusions   | 96  |
| 4.6 | Appendix: Fitting details   | 97  |
| 5   | THE EFFECTS OF BINARY EVOLUTION ON THE DYNAMICS OF CORE COLLAPSE AND NEUTRON-STAR KICKS | 99  |
| 5.1 | Introduction  | 100 |
| 5.2 | Binary evolution and the pre-core-collapse core structure of massive stars              | 101 |
| 5.3 | A dichotomous kick scheme   | 109 |
| 5.4 | Discussion and future work  | 113 |

|     |                            |     |
|-----|----------------------------|-----|
| 6   | NEDERLANDSE SAMENVATTING   | 117 |
| 6.1 | De evolutie van sterren    | 117 |
| 6.2 | De evolutie van het heelal | 122 |
| 6.3 | Dit proefschrift           | 123 |
|     | BIBLIOGRAPHY               | 127 |
|     | ACKNOWLEDGMENTS            | 137 |
|     | CURRICULUM VITAE           | 141 |

## INTRODUCTION

---

On the evening of November 11th, 1572 Tycho Brahe discovered the first supernova in modern times, shaking his worldview that the cosmos, e.g., the sphere of the stars, everything beyond the orbit of Saturn, was unchanging and eternal as Aristotle, the great Greek philosopher, had claimed. Numerous questions arose about the nature of this so called *Nova Stella*? Was it something close to the earth, was it a peculiar comet, condensed from fiery gasses? As the star faded in the months after its discovery and became invisible in 1574, leaving the world in awe and shocked, Brahe proved that the new star was something in the supra-lunar world, in the realm of the aether which was apparently not as unchangeable and eternal as Aristotle had proposed (Pannekoek 1951, pp. 166-168). A new era had begun, in which the state of the universe became more and more a scientific question rather than one of philosophy or religion.

### 1.1 THE HISTORY OF STELLAR EVOLUTION

It still took more than 300 years before man's wondering about the stars had crystallized into a physical theory; before a picture emerged about what a star really is, how it evolves, and what happens at the end of the evolution, in the most violent phase, the actual supernova explosion.

At the beginning of the 20th century, pioneering work was done by Emden and Eddington (who formulated the equations of the stellar structure) and Schwarzschild (theory of radiation). Although it was already known that nuclear reactions played an important role in stellar evolution, George Gamow was the first in 1929 to propose the idea that the main source of energy of stars has to be hydrogen fusion. After this breakthrough, it still took about ten years before Hans Bethe and Carl von Weizsacker in 1938 worked out the theory of thermonuclear fusion, including the so important proton-proton chain and CNO cycle. A whole new field opened, where stellar evolution and nuclear physics were coming together, and which is still very active.

Don Clayton, one of the pioneering founders of the theory of the origin of the chemical elements in stars, writes in his book (Clayton 1983, pp. 1-2):

The key to the history of the stellar interior was found in the nuclear laboratory. The conceptual framework there revolves around the sequence of nuclear reactions that occur

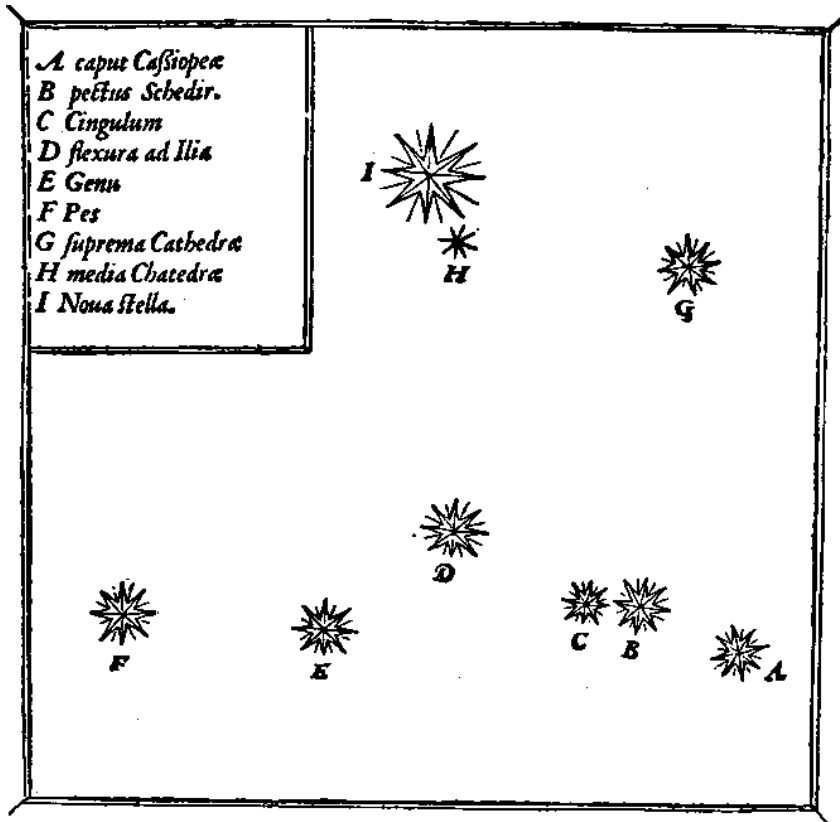


Figure 1. The *Nova Stella* (new star) in Cassiopeia (marked with I) as observed by Tycho Brahe in 1572. Figure obtained from [Pannekoek \(1951\)](#).

in the interiors of stars and the three major functions of those reactions: (1) they provide, like a giant nuclear reaction, the internal power that allows the stars to shine for long periods of time without cooling off; (2) they synthesize heavy elements from lighter ones; and (3) they determine the evolution of the star. The proper sequence of reactions was and is being found by careful laboratory study of nuclear reactions, the early demonstrations of which prompted Eddington to exclaim in 1920, "And what is possible in the Cavendish Laboratory may not be too difficult in the sun."



## 1.2 SINGLE STAR EVOLUTION

In the following decades a new picture of stellar evolution emerged. Many fundamental processes however, are still poorly understood, for example the theory of convection and mixing or the effects of rotation and magnetic fields, but the basic evolution is well established, i.e., the evolutionary path from main sequence through the red giant branch to (1) the asymptotic giant branch and the white dwarf stage or (2) towards a supernova explosion. Also, the main nuclear fusion stages from hydrogen, via helium, carbon, neon, oxygen, and silicon, to iron and nickel are well established (Weaver et al. 1978).

All stars begin their life from a gas cloud that starts contracting under its own gravity. Due to this contraction, the temperature and the density at the center rise. This process can continue until the conditions are suitable for the ignition of hydrogen in the center. A new star is born! The fusion of hydrogen into helium produces a lot of energy, maintaining a pressure gradient that makes the star stable against gravity. The temperature and density inside the star remain almost constant until this energy source is exhausted. This phase is called the main sequence and takes about 80% of the lifetime of the star. When hydrogen as energy source is exhausted, the star starts contracting again. If the conditions become favorable to ignite helium, the whole cycle starts again. After helium core burning, the evolution of low and intermediate mass stars and massive stars becomes significantly different, and below we will discuss them in two different paragraphs.

**MASSIVE STARS AND SUPERNOVAE** Massive stars are defined as stars that experience a collapse of the iron core. The minimum mass for massive stars lies around  $10 M_{\odot}$ . The evolution of massive stars proceeds through all major and advanced burning stages, e.g., hydrogen, helium, carbon, neon, oxygen, and silicon, which progressively takes shorter amounts of time. Once silicon burning is completed and an iron core is formed, instabilities develop, resulting eventually in a collapse of the core and an explosion of the star. At the time of explosion the star possesses a complex shell structure, and shock a wave from the explosion, travels through these shells and heats the material, resulting in various nucleosynthesis processes, producing  $\sim 1/2$  of the heavy elements up to uranium (see for a review Woosley et al. 2002).

**LOW MASS STARS AND WHITE DWARF** Low mass stars develop, after hydrogen and helium core burning, an electron-degenerate carbon oxygen core which is too cool to ignite carbon burning. After core helium burning, the convective envelope moves down and penetrates in the helium layer until it reaches the boundary of the core. At this

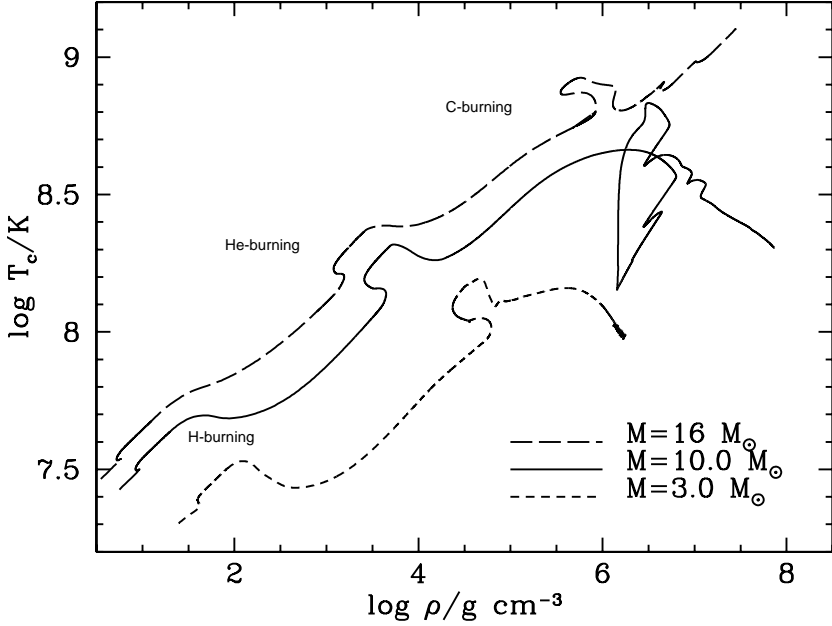


Figure 2. Evolution of the core as a function of central density,  $\rho_c$ , and the central temperature,  $T_c$ , for three different masses. The long-dashed line shows the evolution for a  $16 M_\odot$  star, the solid line for a  $9 M_\odot$  star, and the short-dashed line for a  $3 M_\odot$  stars. The major burning stages are indicated. The  $3 M_\odot$  star undergoes hydrogen and helium burning, while the  $10 M_\odot$  and the  $16 M_\odot$  star undergo also carbon burning. Not shown are the subsequent burning stages for the  $16 M_\odot$  star, i.e., neon, oxygen, and silicon burning. In general the core properties follows a line of  $\rho \propto T^3$ , but the  $3 M_\odot$  and  $10 M_\odot$  stars deviate from this because of the cooling of the core by neutrinos.

point in time, a double shell structure develops: the center of the star is formed by a contracting degenerate carbon oxygen core, which is surrounded by both a helium and a hydrogen burning shell. This structure is unstable and helium shell flashes develop, resulting in thermal pulses that are characteristic for asymptotic giant branch (AGB) stars (see [Iben & Renzini 1983](#); [Herwig 2005](#) for a review). During this thermally pulsing AGB (TPAGB) phase, the star has a high mass loss rate, which removes the entire envelope in a short time, leaving a naked carbon oxygen core which evolves into a white dwarf.

This thesis studies stars at the transition between AGB stars and supernovae. Specifically Super-AGB stars are studied that ignite carbon

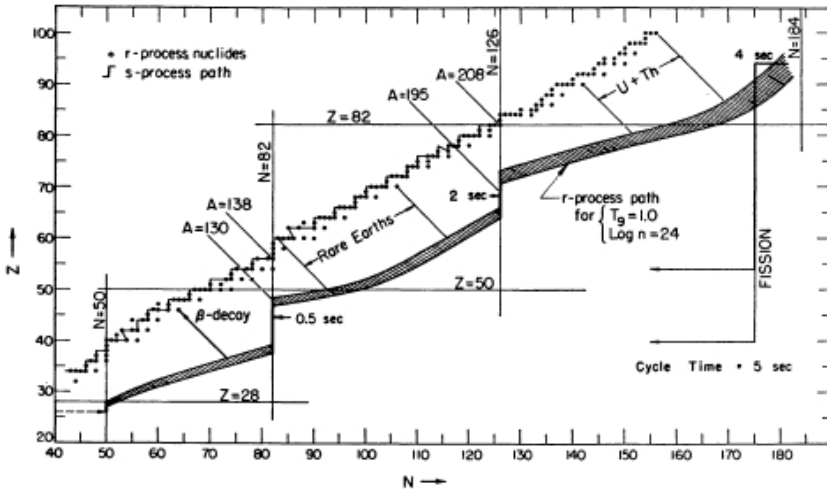


Figure 3. Diagram that shows the paths that the *r*- and *s*-process follow through the nuclear chart. The *s*-process path, with its main site in the helium intershell of AGB stars, goes right through the valley of stability, and is characterized by a low neutron flux. The *r*-process path goes far from the valley of stability, through unstable isotopes with high neutron numbers, and is characterized by a high neutron flux in explosive environments. Both processes are able to synthesize elements beyond iron up to high atomic numbers. Figure obtained from Seeger et al. (1965)

in their cores but retain on the TPAGB a similar configuration as AGB stars, and have cores that are so massive, that at least some of them are able to reach a critical mass – the Chandrasekhar mass – and explode as a supernova.

1.3 CHEMICAL EVOLUTION OF THE UNIVERSE

Both types of stars (low mass and high mass stars) contribute to the chemical evolution of the universe. The abundance pattern we observe today in the solar system is completely different from the chemical pattern produced by the Big Bang and is the result of enrichment in chemical elements from supernovae and AGB stars.

Almost all isotopes with mass numbers lower than  $\sim 90$  are synthesized in advanced burning phases of stars. Half of all trans-iron isotopes are made in the *r*-process, the other half is made in the *s*-process. The *r*-process stand for rapid neutron capture process and is characterized by high neutrons densities, which are likely available in explosive en-

vironments and lead to a nucleosynthesis path far from stability in which the time to capture a neutron is shorter than the time to decay (see Figure 3). The *s*-process stands for slow, since the time to capture a neutron is longer than the time to decay, and is characterized by low neutron densities, mainly in the helium intershells of AGB stars, and follows the valley of stability.

### 1.3.1 Carbon enhanced metal poor stars as tracers

Central in the quest for understanding of the origin of the *r*- and *s*-process in the universe, are the so-called (very) metal poor stars (see for a review [Beers & Christlieb 2005](#)), who reflect the nucleosynthesis at earlier epochs in the evolution of the universe.

Many of those (V)MP stars actually are enriched in carbon, the so-called carbon enhanced metal poor stars (CEMP). The discovery of CEMP stars that show enhancements in both *r*-process elements and *s*-process elements ([Hill et al. 2000](#)) have stirred up the debate about possible formations scenarios of these CEMP *r+s* stars ([Jonsell et al. 2006](#); [Wanajo et al. 2006](#)). The double enhancement requires both pollution from an AGB star and a supernova, which is a puzzle for both stellar evolution and nucleosynthesis.

A wide range of scenarios have been suggested, including the possibility of a binary star system with one of the components being a star between 8 and 10  $M_{\odot}$  that first undergoes a AGB evolution in which the pollution of the companion with *s*-process occurred, followed by an explosion caused by electron captures on  $^{20}\text{Ne}$ , in which the companion gets polluted by *r*-process elements ([Barbuy et al. 2005](#); [Wanajo et al. 2006](#)).

Another possible *r+s* scenario requires a binary system with an AGB star of low metallicity. During its evolution, the AGB star transfers *s*-processed matter to the observed star and the carbon oxygen core of the AGB is able to grow to the Chandrasekhar mass due to a low mass loss rate. Once the carbon oxygen core reaches the Chandrasekhar mass, a thermonuclear runaway starts and the degenerate core explodes, leading to a so-called Type 1.5 supernova ([Iben & Renzini 1983](#); [Zijlstra 2004](#)), polluting the observed star with *r*-process elements.

Both scenarios can possibly explain the enhancement of *r*- and *s*-elements in CEMP and require stars in the mass range of 4  $M_{\odot}$  to 7.5  $M_{\odot}$  (SN1.5) or 8  $M_{\odot}$  up to 10  $M_{\odot}$ .

## 1.4 SUPER AGB STARS

Super-AGB (SAGB) stars are formed in a small mass range between AGB stars and massive stars.

Characteristic for SAGB stars is the second dredge-up, which they experience after the end of core He-burning, in the same way as the less massive, intermediate mass AGB stars do. In this process, the convective envelope extends inward and reduces the mass of the helium core until only a very thin shell remains. This inward movement is caused by the ignition of carbon inside the semi-degenerate core, which generates enough energy to let the star expand, which in turn reduces the opacity and drives the convection down. The configuration the star resembles after this second dredge-up is very similar to AGB stars that are lower in mass (Frost et al. 1998). The degenerate core is surrounded by the He- and H-shell, and as in the AGB stars this double-shell burning on a degenerate core is unstable and leads eventually to thermal pulses, i.e., the periodic extinction and ignition of the hydrogen and helium shell sources (Nomoto 1987a; Ritossa et al. 1996; Iben et al. 1997; Garcia-Berro et al. 1997; Ritossa et al. 1999).

Since the temperature is not high enough to start neon burning, the electron degeneracy in the core increases, but the H-free core may still continue to grow. If the core mass reaches the Chandrasekhar mass of  $1.375 M_{\odot}$ , these SAGB stars explode, due to electron captures on  $^{24}\text{Mg}$  and  $^{20}\text{Ne}$  (Miyaji et al. 1980a; Miyaji & Nomoto 1987; Hashimoto et al. 1993), as a electron capture supernova (ECSN).

## 1.5 THIS THESIS

In this thesis we study the evolution and final fates of these SAGB stars. We determine the transition masses between AGB and SAGB stars, and between SAGB and massive stars and how sensitive these transition masses are on the choice of different input physics, e.g., convection criterion and convective overshooting. The evolution on the TPSAGB is by the mass loss rate, and the efficiency of hot bottom burning and dredge-up, but all are quite uncertain. We study these uncertainties in detail and give conclusions for the final fate, pre-supernova luminosity, remnant masses and chemical yields.

**CHAPTER 2: SUPERNOVAE FROM MASSIVE AGB STARS** In this chapter we study the evolution of SAGB stars at solar metallicity. We find, from stellar evolution models, that the initial mass range for SAGB evolution is  $7.5 < M/M_{\odot} < 9.25$ . This mass range significantly depends on the choice of input parameters, such as the treatment of convection and the use of overshooting. For stellar models which are computed with the Ledoux criterion and without the use of overshoot-

ing or rotation, we find a shift in initial mass of about  $2.5 M_{\odot}$  to larger masses.

The final evolution is determined by the competition between the two major players at the TPSAGB, mass loss and core growth. Both are, however, very uncertain. We used a synthetic model to parametrize different scenarios. Our standard scenario is based on the empirical mass loss rate by [van Loon et al. \(2005\)](#) and a dredge-up parametrization according to [Karakas et al. \(2002\)](#). We find a very narrow mass range between  $9.0 < M / M_{\odot} < 9.25$  for which SAGB stars are able to explode as an electron capture supernova. A lower, but still reasonable, mass loss rate would make the ECSN range wider by  $\sim 0.35 M_{\odot}$ . If SAGB stars, however, do not experience any third dredge-up, the initial mass range would widen with  $\sim 0.25 M_{\odot}$ . For the different scenario's we find supernova rates between 3% and 20%.

### CHAPTER 3: SUPERNOVAE FROM MASSIVE METAL-POOR AGB STARS

In this chapter we study the evolution of SAGB stars and the dependence on the initial metallicity. We investigate how the mass range for ECSN widens for lower metallicities where stellar winds may be weaker, and under which conditions carbon deflagration supernovae from AGB stars (SN 1.5) occur. Using six different combinations of model parameters, we study the effects of dredge-up and mass loss on the TPSAGB evolution. We find that for our preferred parameter set the initial mass range for ECSN stars is widening from  $0.25 M_{\odot}$  at solar metallicity to almost  $2 M_{\odot}$  at  $\log Z / Z_{\odot} = -3$ , and that the minimum initial mass for ECSN shifts from  $9 M_{\odot}$  at solar metallicity to  $6.3 M_{\odot}$  at  $\log Z / Z_{\odot} = -3$ . Our model predicts Type 1.5 SNe, but only for metallicities lower than about  $\log Z / Z_{\odot} = -3$ . We investigate the dependence of these results on our assumptions on mass loss and dredge-up during the TP-SAGB and find larger initial mass ranges and hence higher supernova rates when we decrease the efficiency of the dredge-up or the mass loss rate. We discuss observational consequences of metal-poor SNe from SAGB stars, in particular their relevance to understand observed *s*- and *r*-enhancements in extremely metal-poor stars in our Galaxy, and the large number of neutron stars found in Galactic globular clusters.

### CHAPTER 4: NUCLEOSYNTHESIS IN SUPER AGB STARS

Using a synthetic model based on [Izzard et al. \(2006b\)](#), we follow the TPSAGB evolution at solar metallicity, to calculate chemical yields. We study the effects of model uncertainties, particularly mass loss, convective overshooting and the efficiency of hot bottom burning and third dredge-up, and their respective effects on the yields. We find, that in the context of galactic chemical evolution, the chemical yields from SAGB stars are not important. We did not include in these calculations the possible

yields from the  $s$ - and/or  $r$ -process.

CHAPTER 5: THE EFFECTS OF BINARY EVOLUTION ON THE DYNAMICS OF CORE COLLAPSE AND NEUTRON STAR KICKS This chapter investigates and discusses the possibility of ECSN progenitors in a binary. We find that the initially more massive stars in binary systems with masses in the range  $8 - 11 M_{\odot}$  are likely to undergo an electron-capture supernova, while single stars in the same mass range would end as ONeMg white dwarfs. We suggest that the core collapse in an electron-capture supernova (and possibly in the case of relatively small iron cores) leads to a prompt or fast explosion rather than a very slow, delayed neutrino-driven explosion and that this naturally produces neutron stars with low-velocity kicks. This leads to a dichotomous distribution of neutron star kicks, as inferred previously, where neutron stars in relatively close binaries attain low kick velocities.





A. J. T. Poelarends, F. Herwig, N. Langer, A. Heger

*submitted to Astrophysical Journal*

**ABSTRACT** We study the late evolution of solar metallicity stars in the transition region between white dwarf formation and core collapse. This includes the super-asymptotic giant branch (super-AGB, SAGB) stars, which have massive enough cores to ignite carbon burning and form an oxygen-neon (ONe) core. The most massive SAGB stars have cores that may grow to the Chandrasekhar mass because of continued shell-burning. Then they encounter instability and collapse, triggering a so called electron capture supernovae (ECSN).

From stellar evolution models we find that the initial mass range for SAGB evolution is  $7.5\text{--}9.25 M_{\odot}$ . We perform calculations with three different stellar evolution codes to investigate the sensitivity of this mass range to some of the uncertainties in current stellar models. The mass range significantly depends on the treatment of semiconvective mixing and convective overshooting. To consider the effect of a large number of thermal pulses, as expected in SAGB stars, we construct synthetic SAGB models that include a semi-analytical treatment of dredge-up, hot-bottom burning, and thermal pulse properties. This enables us to compute the evolution of the main properties of SAGB stars from the onset of thermal pulses until the core reaches the Chandrasekhar mass or is uncovered by the stellar wind. Thereby, we determine the stellar initial mass ranges that produces ONe-white dwarfs and electron-capture supernovae. The latter is found to be  $9.0\text{--}9.25 M_{\odot}$  for our fiducial model, implying that electron-capture supernovae would constitute about 4% of all supernovae in the local universe. Our synthetic approach allows us to explore the uncertainty of this number imposed by by uncertainties in the third dredge-up efficiency and ABG mass loss rate. We find that for both processes, the most optimistic approach leads to about a doubling of the number of electron-capture supernovae, which provides a firm upper limit to their contribution to all supernovae of  $\sim 20\%$ .

## 2.1 INTRODUCTION

It is well known that, for a given initial chemical composition, it is the initial stellar mass which essentially determines the final fate of a star: lower masses produce white dwarfs, higher masses neutron stars and supernovae. The transition region between white dwarf and neutron star formation, however, is notoriously difficult and avoided in most comprehensive stellar evolution calculations. This is unsatisfactory, since the region of uncertainty is rather large, i.e.  $7\text{--}12 M_{\odot}$  and might thus encompass as much as about half of all supernovae.

Of particular interest in this context is the evolution of so called super-asymptotic giant branch (SAGB) stars, with which here we mean stars that ignite carbon non-explosively, but also undergo thermal pulses (Siess 2006). These stars may end their lives either as massive ONe-white dwarfs (Nomoto 1984a), or as electron capture supernovae (ECSNe), where the core collapse is triggered by electron captures before neon ignition (Wheeler et al. 1998; Wanajo et al. 2003). Stars of larger initial mass ignite hydrostatic neon burning, form an iron core, and lead to classical core collapse supernovae (CCSNe).

The upper mass limit of SAGB stars is affected by the second dredge-up, which may occur after core He-exhaustion, and which drastically reduces the mass of the helium core. At this point and throughout the following early SAGB phase carbon burning transforms the CO core into an ONe core (Nomoto 1987a; Ritossa et al. 1996; Iben et al. 1997; Garcia-Berro et al. 1997; Ritossa et al. 1999). Since the temperature is not high enough to ignite neon, the core cools, electron degeneracy in the core increases, and the structure of the SAGB star outside of the ONe-core resembles the situation in the most massive CO-core AGB stars (Frost et al. 1998, for a general review of AGB evolution see Iben & Renzini 1983; Habing 1996 and Herwig 2005). The degenerate core is surrounded by the He- and H-shell sources, which eventually produce thermal pulse due to the instability of the helium shell source (Yoon et al. 2004).

In this situation, the mass of the H-free core continues to grow. If the core mass can grow to the Chandrasekhar mass of  $1.375 M_{\odot}$ , the core will collapse triggered by electron captures on  $^{24}\text{Mg}$  and  $^{20}\text{Ne}$ , and the star will perform an ECSN (Miyaji et al. 1980a; Miyaji & Nomoto 1987; Hashimoto et al. 1993). Recent studies by Ritossa et al. (1996); Garcia-Berro et al. (1997); Iben et al. (1997); Ritossa et al. (1999) and Siess (2006) have shown that the mass fraction of  $^{24}\text{Mg}$  in the ONe-core is smaller than previously thought, which diminishes the role of electron captures on  $^{24}\text{Mg}$ . While Gutiérrez et al. (2005) found that unburnt carbon in the degenerate ONe core could trigger an explosion at densities of  $\sim 10^9 \text{gcm}^{-3}$ , we disregard this possibility furtheron as it seems speculative at present and has little direct observational support.

However, the initial mass range for this to occur is certainly constrained by our considerations below.

For which initial mass range the SAGB evolution can lead to core collapse depends on core growth and mass loss of SAGB stars. Larger mass loss rates lead to a shorter duration of the SAGB phase: For very high SAGB mass loss, there is no time for any significant core growth, and the initial mass range for ECSNe will be very small. On the other hand, the core growth rate in SAGB stars depends on the the hydrogen shell burning and thus on two crucial factors, hot-bottom burning (Ventura et al. 2005), and the efficiency of the third dredge-up.

Previous studies of SAGB stars have concentrated on the evolution of the stellar cores (Nomoto 1984a, 1987a). According to these models, stars with helium cores between  $2.0$  and  $2.5 M_{\odot}$  form ONe cores and explode as ECSN, leaving a neutron star less massive than  $1.3 M_{\odot}$ . Ritossa et al. (1996, 1999), Iben et al. (1997) and Garcia-Berro et al. (1997) studied the evolution of complete SAGB stellar models in detail. They describe SAGB thermal pulses, and an outward mixing event which they called dredge-out, in which the convective envelope connects to a convection zone on top of the helium burning layer. Siess (2006), who studied the effects of the carbon flame and of thermonuclear reactions on the structure of the ONe core, finds similar results.

Thermal pulses in AGB evolutionary models require high numerical resolution, both in time and space. The interpulse period decreases with increasing core mass to eventually only a few years for the most massive AGB star. In order to follow the evolution of SAGB stars with very high core masses, orders of magnitude more thermal pulses have to be computed compared to low-mass AGB stars, which experience only tens of thermal pulses. For this reason, no detailed stellar evolution calculations through the entire super-TP-AGB phase exist. Ritossa et al. (1999) attempted to characterize stars that would end as ECSN. Based on the assumption of a constant SAGB mass loss rate of  $10^{-4} M_{\odot} / \text{yr}$ , they speculated that out of their set of four calculated models (9, 10, 10.5 and  $11 M_{\odot}$ ) only the  $11 M_{\odot}$  model would explode as an ECSN. The other models would lose all their envelope before the core has grown enough, and their final fate would be an ONe white dwarf. Eldridge & Tout (2004c) determine a minimum mass for supernova explosion around  $7 M_{\odot}$  (with overshooting), or around  $9 M_{\odot}$  (without overshooting), again without being able to calculate the stellar evolution models through the final phases.

The SAGB evolution is characterized by a considerable uncertainty in the SAGB mass loss rate, and in the 3rd dredge-up efficiency. To explore this uncertainty would require to compute several model grids. We therefore take a different approach and use the fact that TP-AGB stars, after a brief transition phase, reach a quasi-steady state in which the important structural quantities evolve in a simple and predictable

way as function of time. This approach of synthetic AGB modeling has already been successfully used for low and intermediate-mass AGB stars (Marigo et al. 1996).

In the following, we first describe the detailed stellar evolution models (Sect. 2.2) and identify the initial mass range for SAGB stars by calculating the pre-AGB evolution phase up to the end of the second dredge-up and possibly C-ignition, using three different stellar evolution codes (Sect. 2.3). Next, we describe our SAGB stellar evolution models (Sect. 2.4), and our synthetic SAGB evolution model (Sect. 2.5). We present our results in Sect. 2.6 and concluding remarks in Sect. 2.7.

## 2.2 NUMERICAL METHODS

We use three different stellar evolution codes to calculate the evolution of solar metallicity stars up to the end of the second dredge-up, or to Ne-ignition. We used the codes STERN (Langer 1998; Heger et al. 2000), EVOL (Blöcker 1995; Herwig 2000) and KEPLER (Weaver et al. 1978; Heger et al. 2000). All three codes use the OPAL opacities (Iglesias & Rogers 1996), and are equipped with up-to-date input physics, including a nuclear network with all relevant thermonuclear reactions.

For our investigation, the most relevant difference between the codes concerns the treatment of convective and semiconvective mixing. As we will see, these affect the He-core mass after central He-burning, and thereby the final fate of the stellar model. STERN and KEPLER use the Ledoux-criterion to determine convective instability, and take semiconvection into account. In KEPLER, fast semiconvection mixing is assumed. This leads to more efficient mixing in semiconvective zones than adopting the semiconvective diffusion coefficient of Langer et al. (1983) as it is used in the STERN code. Additionally, in KEPLER convection zones are widened by one extra grid point where fast mixing is assumed, to allow for convective overshooting. In the EVOL code, convective boundaries are determined by the Schwarzschild criterion, and semiconvection is not treated as a separate mixing process. Mixing beyond convective boundaries is treated by adopting an exponentially decaying diffusion coefficient (Herwig et al. 1997; Herwig 2000). Such mixing may be induced by convective overshooting (Freytag et al. 1996), or internal gravity waves (Denissenkov & Tout 2003), or a combination of both (Young et al. 2005). For the pre-AGB evolution, the overshoot parameter in EVOL has been set to  $f = 0.016$ , which was shown by Herwig (2000) to reproduce the observed main sequence width in the HR diagram of young open clusters. Effectively, the strength of mixing in KEPLER lies between that of STERN (slow semiconvective mixing) and that of EVOL (Schwarzschild criterion for convection = very fast mixing in semiconvective regions).

The EVOL code has previously been used to study low-mass (e.g.

Herwig & Austin 2004) and massive AGB stars (Herwig 2004a,b). KEPLER has in the past been applied to study massive stars (Woosley et al. 2002), but has not previously been used for AGB simulations. STERN has been used for low mass AGB stars (Langer et al. 1999; Herwig et al. 2003; Siess et al. 2004) as well as for massive stars (Heger et al. 2000; Heger & Langer 2000).

### 2.3 PRE-AGB EVOLUTION AND THE INITIAL MASS RANGE FOR SAGB STARS

In order to identify the processes that lead to SAGB star formation we calculate stellar evolution sequences with initial masses between  $6.5 M_{\odot}$  and  $13 M_{\odot}$ , starting from the zero age main sequence until the completion of the second dredge-up or neon ignition (Table 1). Up to the end of the second DUP, no mass loss is taken into account. The initial metallicity of our models is  $Z = 0.02$ . The effects of rotation or magnetic fields are not taken into account.

#### 2.3.1 *H- and He-core burning*

The evolution of stars toward the SAGB has been studied previously by Ritossa et al. (1996); Iben et al. (1997); Garcia-Berro et al. (1997); Ritossa et al. (1999); Siess (2006), and our simulations qualitatively confirm these results, although quantitative differences occur. In our STERN models, a consequence of including semiconvection is that during core helium burning, a semiconvective layer limits the mixing between the inner helium burning core and the outer convective core, which still grows in mass (see also Fig. 4 below). This decreases the lifetime of the core helium burning phase, because the available amount of helium is reduced, and leads to smaller helium and CO-core masses compared to models which use the Schwarzschild criterion for convection.

Girardi et al. (2000) studied the effect of convective overshooting on the maximum initial mass for which stars do not ignite carbon,  $M_{\text{up}}$ , and which defines the lower limit of SAGB stars. They find for models without overshooting a value of  $M_{\text{up}}$  of  $6 M_{\odot} \dots 7 M_{\odot}$ , while a moderate amount of overshooting reduces this by  $1 M_{\odot}$ . In our models we find  $M_{\text{up}} = 7.5 M_{\odot}$  (EVOL/KEPLER), while our STERN models – without any overshooting – give  $M_{\text{up}} = 9.0 M_{\odot}$ .

#### 2.3.2 *The second dredge-up*

The occurring of the second dredge-up is a key differences between SAGB stars and massive stars that encounter Fe-core collapse. After core-He exhaustion, the core resumes contraction while the envelope

Table 1. Summary of our detailed stellar evolution sequences. The columns give the model identifier, the initial mass ( $M_{\odot}$ ), the helium core mass prior to the second dredge-up ( $M_{\odot}$ ), the helium core mass after the second dredge-up ( $M_{\odot}$ ), information the end of the simulation, and the final fate of the sequence according to our fiducial SAGB evolution properties (mass loss, dredge-up, as described in Sect. 2.6.4)

| Model | $M_i$ | pre-2DU | post-2DU | comments                  | fate   |
|-------|-------|---------|----------|---------------------------|--------|
| S5.0  | 5.0   | 0.91    | 0.84     | 14 TP                     | CO WD  |
| S8.5  | 8.5   | 1.73    | 1.02     | 10 TP                     | CO WD  |
| S9    | 9     | 1.90    | 1.07     | 30 TP                     | ONe WD |
| S9.5  | 9.5   | 2.00    | 1.11     |                           | ONe WD |
| S10   | 10    | 2.14    | 1.16     | 55 TP                     | ONe WD |
| S10.5 | 10.5  | 2.30    | 1.20     |                           | ONe WD |
| S11   | 11    | 2.45    | 1.23     |                           | ONe WD |
| S11.5 | 11.5  | 2.61    | 1.27     | 15 TP                     | ONe WD |
| S12   | 12    | 2.79    | 1.32     | dredge-out                | ECSN   |
| S12.5 | 12.5  | 2.95    | 2.95     | dredge-out                | CCSN   |
| S13.0 | 13    | 3.13    | 3.13     | Neon ignition             | CCSN   |
| S16.0 | 16    | 4.33    | 4.33     | Neon ignition             | CCSN   |
| E6.5  | 6.5   | 1.59    | 0.99     |                           | CO WD  |
| E7.5  | 7.5   | 1.90    | 1.07     |                           | ONe WD |
| E8.5  | 8.5   | 2.27    | 1.24     |                           | ONe WD |
| E9.5  | 9.5   | 2.65    | 1.43     |                           | CCSN   |
| E10.0 | 10.0  | 2.82    | 2.82     | dredge-out                | CCSN   |
| E10.5 | 10.5  | 3.00    | 3.00     | Neon ignition             | CCSN   |
| K8    | 8.0   | 1.808   | 1.168    |                           | ONe WD |
| K8.5  | 8.5   | 1.955   | 1.247    |                           | ONe WD |
| K9    | 9.0   | 2.130   | 1.338    |                           | ONe WD |
| K9.1  | 9.1   | 2.161   | 1.357    |                           | ECSN   |
| K9.2  | 9.2   | 2.190   | 1.548    | Neon ignition             | CCSN   |
| K9.3  | 9.3   | 2.221   | 1.603    | Neon ignition             | CCSN   |
| K9.4  | 9.4   | 2.253   | 1.690    | Neon ignition             | CCSN   |
| K9.5  | 9.5   | 2.283   | 1.799    | Neon ignition             | CCSN   |
| K10   | 10.0  | 2.439   | 2.315    | Neon ignition             | CCSN   |
| K10.5 | 10.5  | 2.598   | 2.596    | Neon ignition             | CCSN   |
| K11   | 11.0  | 2.759   | 2.759    | Neon ignition             | CCSN   |
| E0099 | 9.0   | 2.15    | 1.17     | $f_{\text{over}} = 0.004$ |        |

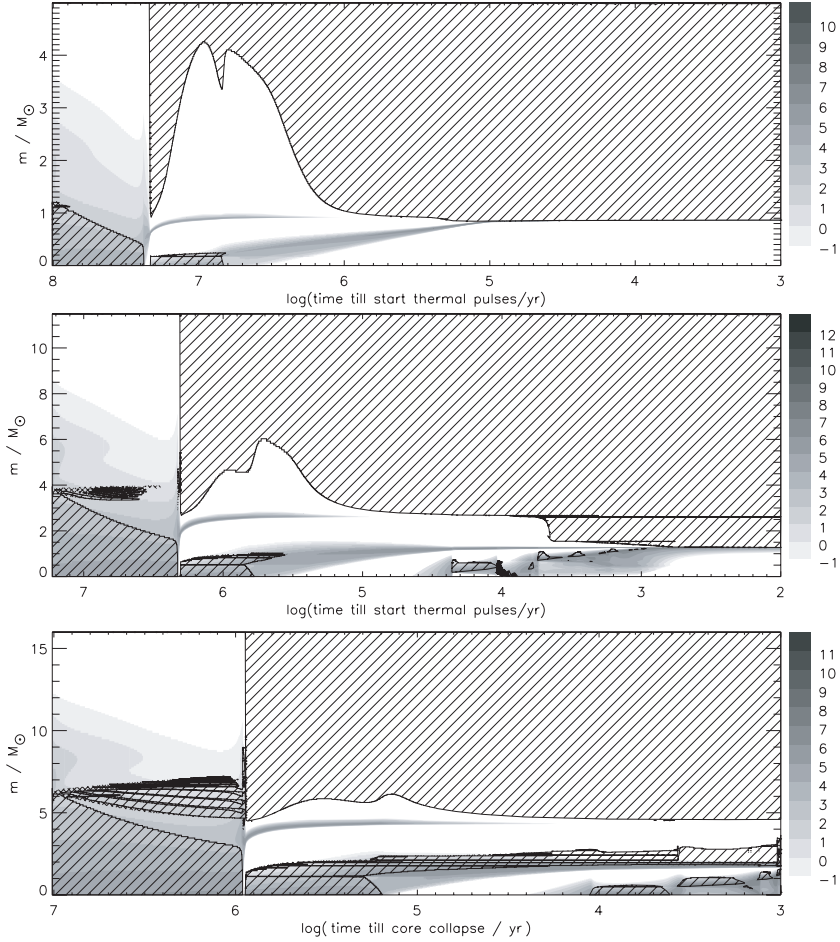


Figure 4. Time evolution of convection zones and energy generation for three evolution sequences with different mass, computed with STERN. The initial masses and evolution scenarios are: top panel:  $5 M_{\odot}$ , massive AGB, middle panel:  $11.5 M_{\odot}$ , SAGB, lower panel:  $16.0 M_{\odot}$  star, Fe-core, CCSN. The energy generation from nuclear burning is shown in greyscale with a legend to the side in units of  $\log \text{ erg/g/s}$ .

expands. As the star evolves up the asymptotic giant branch the envelope convection deepens, and eventually penetrates into the H-free core. Only due to this mixing event is the H-free core mass sufficiently reduced so that an electron-degenerate core can form which then cools before neon burning can ignite. If the core mass after the 2nd dredge-up is smaller than the Chandrasekhar mass, an electron-degenerate core will form and the He- and H-shells will eventually start the thermal pulse cycle.

The dependence of the late evolutionary phases, including the second dredge-up, on the initial mass is illustrated in the Kippenhahn-diagrams of three sequences computed with the STERN code shown in Figure 4. All models evolved through core-H and core-He burning. In the  $5.0 M_{\odot}$  models, the hydrogen burning shell extinguishes, and the second dredge-up reduces the helium core mass by about  $0.2 M_{\odot}$ . When the helium shell source gets close to the bottom of the convective envelope, hydrogen reignites, and the thermal pulse cycle starts. For the  $11.5 M_{\odot}$  model, central hydrogen and helium burning is followed by off-center carbon ignition. During the carbon burning phase the size of the helium core is reduced by a deep second dredge-up, after which the core becomes degenerate and thermal pulses develop. In the  $16.0 M_{\odot}$  case, convective core H- and He-burning is followed by core C-burning, and no 2nd dredge-up occurs. Neon ignites hydrostatically, and subsequent burning will lead to the formation of an iron core.

In accord with previous work (Ritossa et al. 1996; Iben et al. 1997; Garcia-Berro et al. 1997; Ritossa et al. 1999; Siess 2006), the second dredge-up reduces the helium core mass to values below the Chandrasekhar mass in our EVOL and STERN models. This leads to a clear definition of the upper mass limit of SAGB stars, as the critical mass between the occurrence and non-occurrence of the second dredge-up. In the first case, neon ignition is always avoided, in the second case the helium core mass is so large ( $\sim 2.8 M_{\odot}$ ) that neon always ignites. Our KEPLER models show a more complicated behavior: some show a second dredge-up depth which leaves helium cores with masses in between  $1.4 M_{\odot}$  and  $2.8 M_{\odot}$ . However, those with post-dredge-up helium cores above the Chandrasekhar limit all ignite core neon burning. We conclude that a second dredge-up down to the Chandrasekhar mass is required for an ECSN to occur, which thus defines our upper SAGB mass limit. This is also in line with the recent results of Eldridge & Tout (2004b), who do indeed find neon shell flashes in some of their most massive models undergoing the second dredge-up; however the dredge-up does proceed to the Chandrasekhar mass, and the suggested fate of these models is that of an ECSN.

Figure 5 shows the helium core masses obtained in our detailed stellar evolution models. While the core mass after the 2nd dredge-up increases with initial mass for models computed with all three codes,



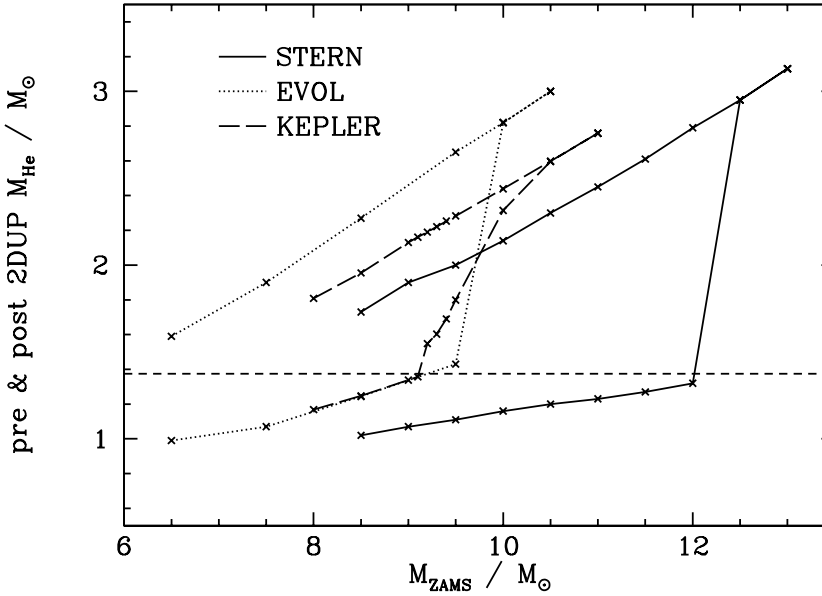


Figure 5. Helium core masses for stars of various initial masses, as obtained using different stellar evolution codes (solid line: STERN, dashed line: KEPLER, dotted line: EVOL). The upper part of the line shows the maximum size of the helium core, prior to the second dredge-up. The lower part shows the size of the helium core just after the completion of the second dredge-up and prior to the onset of the TP-AGB. The light dashed horizontal line gives the lower limit for the final helium core mass for which the star may experience an electron-capture supernova.

differences arise with respect to the critical mass for second dredge-up. KEPLER and EVOL have similar final core masses, however they differ with respect to the maximum core masses. These differences are related to the treatment of convection and overshooting. STERN uses the Ledoux-criterion for determining the convective boundaries, which naturally gives rise to smaller cores than the Schwarzschild-criterion. In these models no rotation was included, which – if included – would give significantly larger cores, due to rotationally induced mixing during the hydrogen and helium burning phases (Heger et al. 2000).

Using EVOL and KEPLER we find the transition between stars with and without a deep second dredge up at  $\sim 9.25 M_{\odot}$ . On the other hand, using STERN we find that stars more massive than  $12 M_{\odot}$  do not experience a deep second dredge-up. The models in the mass range between  $12 M_{\odot}$  and  $12.5 M_{\odot}$  show a convective shell that develops on

top of the helium burning layer (the so called dredge-out, c.f. [Ritossa et al. 1999](#)) which connects through a semiconvective layer with the bottom of the hydrogen-rich convective envelope. We find that protons are mixed into this hot layer and burn quickly. For a proper treatment of this interaction a coupled scheme of burning and mixing is needed to follow the subsequent evolution of these stars. Therefore, it remains unclear whether this semiconvective layer dissolves and on what time scale. If it would, the helium core masses would be reduced to just below the Chandrasekhar mass. If the semiconvective layer remains for the rest of the evolution of the star, it would allow neon to ignite in the core and eventually lead to Fe-core collapse supernova. This renders the upper mass limit for SAGB stars according to the STERN models somewhat ambiguous in the range  $12...12.5 M_{\odot}$ .

In the EVOL models, the convective core overshooting was calibrated as to reproduce the observed width of the main sequence. However, stars rotate, and the STERN code usually takes this into account. The effect of rotation also widens the main-sequence and in this way STERN models with rotation can reproduce the observed main-sequence width as well ([Heger & Langer 2000](#)). In this study we compute non-rotating models with STERN, in order to avoid the complex question of how rotational mixing affects SAGB properties. As a drawback, the initial mass range for SAGB stars found with STERN is offset compared to the EVOL/KEPLER models by  $\approx 2.75 M_{\odot}$ . Since the non-rotating STERN models do not reproduce the well-established main-sequence width, we prefer here the results of the EVOL/KEPLER models to derive the initial mass range for SAGB stars. Based on those, the upper mass limit for SAGB stars – and thus electron capture supernovae – is about  $9.25 M_{\odot}$  (Figure 5). Without knowledge about the subsequent phase – the thermally pulsing SAGB phase – we can only say that the lower limit for electron capture supernovae will not be lower than  $7.5 M_{\odot}$ , since stars with a lower mass form highly degenerate CO cores.

## 2.4 THE TP-SAGB STELLAR EVOLUTION MODELS

### 2.4.1 *Thermal pulses and hot bottom burning*

Double shell burning of H and He on degenerate cores leads to periodic thermonuclear instabilities. These He-shell flashes or thermal pulses are an important site for nucleosynthesis in AGB stars, and cause mixing of the intershell region and — by way of the third dredge-up — mixing of processed material to the surface [Iben & Renzini \(1983\)](#); [Busso et al. \(1999\)](#); [Herwig \(2005\)](#). Thermal pulses of SAGB stars are similar to thermal pulses of CO-core AGB stars ([Ritossa et al. 1996](#)). In order to obtain quantitative information on these SAGB thermal pulse cycles, we calculate such model sequences for several initial masses (Table 1).

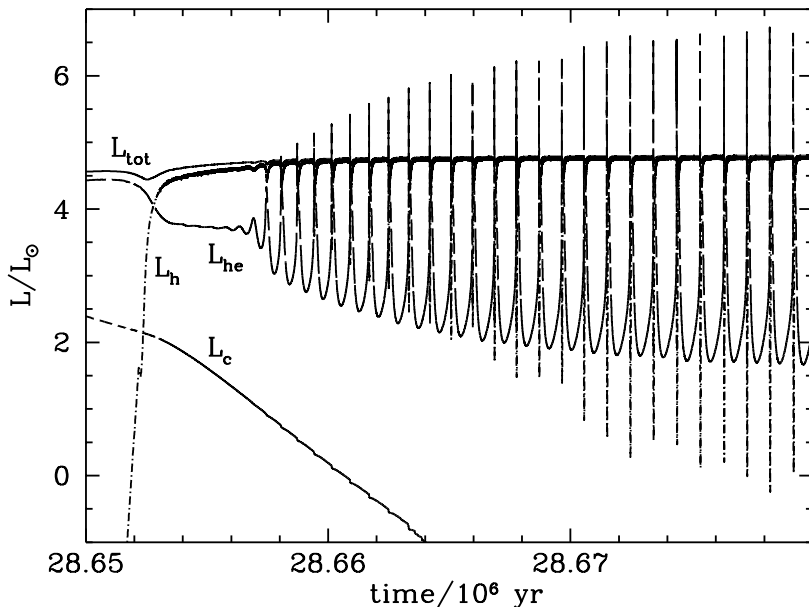


Figure 6. Nuclear burning luminosity contributions and total luminosity as a function of time at the onset of the thermal pulse phase for a  $9 M_{\odot}$  star calculated with STERN. At the time of second dredge-up hot-bottom burning starts, shown in the figure as a steep rise of the hydrogen luminosity.

As in massive AGB stars, most of the luminosity is produced by hot-bottom burning. During hot-bottom burning, fresh nuclear material is transported convectively into the H-shell, burning ashes in the form of He are also transported out of the shell, upward into the envelope. In the more massive SAGB stars this hot-bottom burning starts immediately after the completion of the second dredge-up, and can proceed at very high temperatures. In our STERN models we obtain values of  $1.0 \times 10^8 \text{K}$  ( $10 M_{\odot}$  with  $M_c = 1.16 M_{\odot}$  after 30 thermal pulses) and  $1.1 \times 10^8 \text{K}$  ( $11.5 M_{\odot}$  with  $M_c = 1.27 M_{\odot}$  already at the first thermal pulse). The EVOL models show a similar trend with the  $9.0 M_{\odot}$  model (Eo09) reaching temperatures at the bottom of the convective envelope of  $1.13 \times 10^8 \text{K}$  after the 12th pulse.

Hot-bottom burning could be stronger than in our calculations, e.g. due to convective overshooting at the bottom of the convective envelope, or due to a larger convective efficiency than assumed in most MLT based stellar evolution calculations. In that case, the accretion of He on the core may be so much reduced that the core does not or only very

slowly grow. We have performed some test calculations with enhanced convective extra mixing during the hot-bottom phase. These tests show a stationary H-shell with no core growth. Whether this theoretical possibility is occurring in real stars is not clear because the physics of a convective boundary inside the H-shell is poorly known.

SAGB stars show a He-peak luminosity during thermal pulses of around  $\log L/L_{\odot} \sim 6$ , which is significantly lower than obtained in low mass AGB stars which reach luminosities up to  $\log L/L_{\odot} \sim 8$ . This may explain why the third dredge-up is less efficient in terms of the dredge-up parameter  $\lambda$  (see Sect. 2.4.2).

Extending the trend seen from low-mass to massive AGB stars, SAGB stars have smaller intershell masses (in the STERN  $9M_{\odot}$  model of  $7 \times 10^{-4}M_{\odot}$  at a core mass of  $1.06M_{\odot}$ ), and the interpulse time is also lower, ranging from 50 yr for the  $11.5M_{\odot}$  SAGB star with core mass of  $1.27M_{\odot}$  to 1000 yr for a SAGB star with a mass of  $9.0M_{\odot}$ .

#### 2.4.2 Efficiency of the 3rd dredge-up

The growth of the core during the TP-SAGB may be decreased by the dredge-up of material after a thermal pulse. The efficiency of the dredge-up is expressed through the dredge-up parameter  $\lambda = \Delta M_{\text{H}}/\Delta M_{\text{DUP}}$ , where  $\Delta M_{\text{H}}$  is the core mass increase due to H-burning during the interpulse phase, and  $\Delta M_{\text{DUP}}$  is the mass that is dredged up by the convective envelope.

In the models calculated with STERN we did not observe any dredge-up. This result is consistent with results for non-rotating low mass AGB-stars (Siess et al. 2004) from the same code which are also calculated using the Ledoux-criterion for convection. Ritossa et al. (1996) and Siess & Pumo (2006) find a similar result. The recent models of Doherty & Lattanzio (2006) find very efficient dredge-up, e.g.  $\lambda \approx 0.7$  for a  $9.5M_{\odot}$  model. Observations clearly require a 3rd dredge-up in low and intermediate mass AGB stars, since we see its result in terms of carbon and s-process enrichment in real AGB stars. However, the efficiency of the 3rd dredge-up in massive and SAGB stars is not constrained observationally.

In order to get an idea about the efficiency of the 3rd dredge-up in super AGB stars and the robustness of our and previous results, we studied the behavior of the thermal pulses also with the EVOL code. We calculated a  $9M_{\odot}$  model (E0099) until the 12th pulse. This model was computed with a four times smaller factor for the overshooting than the other EVOL models ( $f_{\text{over}} = 0.004$ ) until the TP-AGB. This gives the star a smaller core than the regular models. On the TP-AGB a value of  $f_{\text{over}} = 0.008$  was used. The first thermal pulse starts after the completion of the second dredge-up, when the bottom of the convective envelope is at  $m_{\text{r}} = 1.17M_{\odot}$ . The surface luminosity after 12 pulses

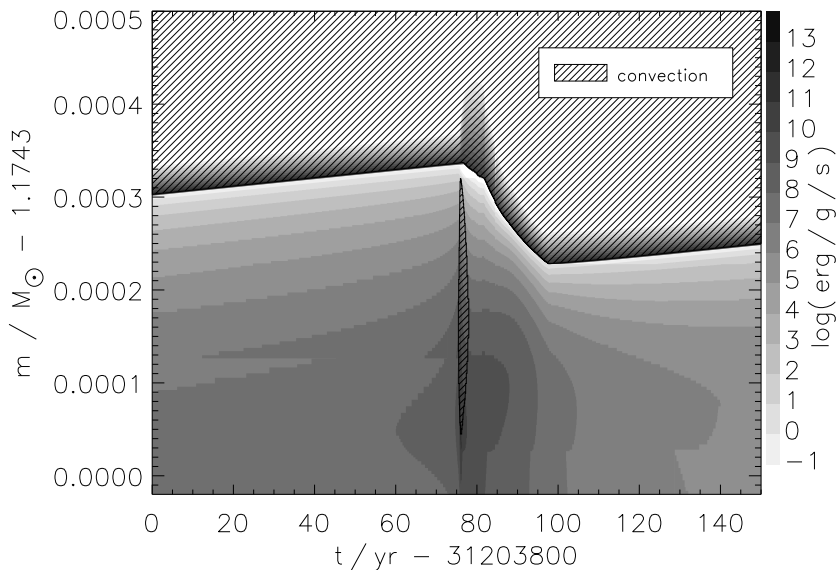


Figure 7. Evolution of the SAGB He-shell flash during the 12th pulse computed with the EVOL code(Eo09). The dredge-up efficiency equals  $\lambda = 0.5$ .

is  $\log L / L_{\odot} = 5.07$ , the maximum helium luminosity during the 12th pulse  $\log L_{\text{He}} / L_{\odot} = 6.17$ , and the duration of the interpulse period is  $\sim 500\text{yr}$ .

After the eighth pulse, the ensuing mixing has the characteristics of a ‘hot’ dredge-up, first described for massive low-metallicity AGB stars by Herwig (2004a) and then found by Chieffi et al. (2001) for  $Z = 0$  models. Any small amount of mixing of protons into the hot  $^{12}\text{C}$ -rich layers — performed here by diffusive exponential overshooting — leads to violent H-burning which increases the convective instability. Like a flame, this corrosive hydrogen burning enforces the penetration of the convective envelope into the intershell (see Fig. 7). For this situation, we find efficient dredge-up ( $\lambda \sim 0.5$ ), i.e. half of the interpulse core growth is dredged up, reducing the average pulse cycle core growth rate.

## 2.5 THE SAGB POPULATION SYNTHESIS MODEL

Mass loss and the dredge-up are the two most important but also most uncertain processes that determine the final evolution of SAGB stars. Here we employ a simplified synthetic model that allows us to estimate the effect of different assumptions concerning these two processes on

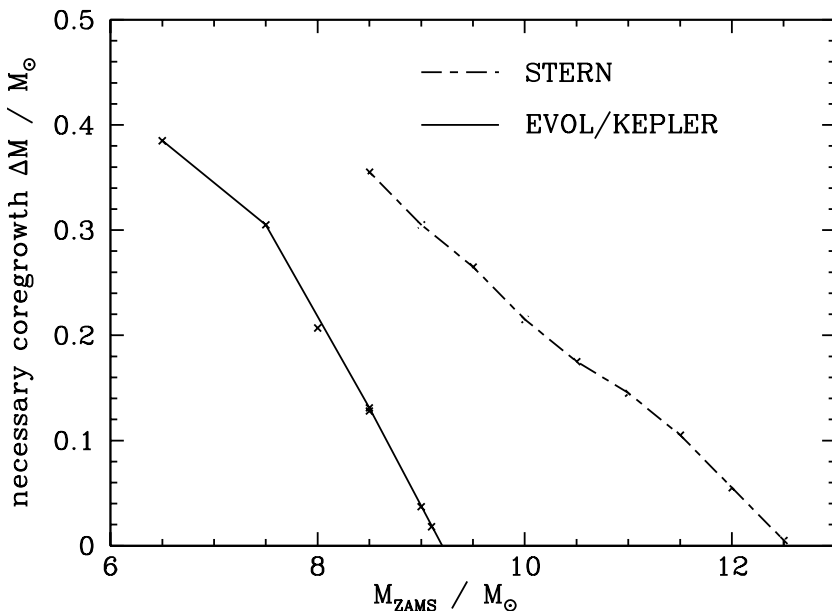


Figure 8. Mass  $\Delta M_{\text{H}}$  by which the core needs to grow during the TP-AGB in order to reach the Chandrasekhar mass, as function of the initial mass. The upper boundary is given by stars that do not have a second dredge-up, so their cores are larger than the Chandrasekhar mass.

the initial mass range for ECSNe.

### 2.5.1 A simple estimate

We start with a simple back-of-the-envelope estimate: Stars that have, after carbon burning, a helium core mass larger than the Chandrasekhar mass ( $M_{\text{Ch}}$ ) explode as CCSN. The Chandrasekhar mass of a cold iron core is  $M_{\text{Ch-eff}} = 1.375 M_{\odot}$  (Sugimoto & Nomoto 1980; Nomoto 1981). In order to form an ECSN, the core mass has to grow from the beginning of the TP-AGB  $M_{\text{c}}(2\text{DUP})$  to the Chandrasekhar mass by

$$\Delta M_{\text{H}} = M_{\text{Ch}} - M_{\text{c}}(2\text{DUP}). \quad (2.1)$$

This value depends strongly on the initial mass as Figure 8 shows.

Whether the core is able to grow by this amount depends only on the mass of the envelope, the core growth rate and the mass loss rate. Given these quantities,  $\Delta M_{\text{H,max}}$  is the maximum mass that the core

can grow. The timescale on which the envelope of the star will be lost is

$$\tau_{\text{env}} = \frac{M_{\text{env}}}{dM/dt_{\text{env}}}, \quad (2.2)$$

and multiplied by the core growth rate this gives the maximum value that the core can grow.

The core growth rate due to nuclear burning is  $dM_c/dt$ . Due to the 3rd dredge-up, the value for the core growth rate can decrease. We correct for this by introducing a factor  $1 - \lambda$ . This gives an approximate relation for the growth of the core during the TP-SAGB phase

$$\Delta M_{\text{H,max}} = \frac{M_{\text{env}}}{dM/dt_{\text{env}}} \times (1 - \lambda) dM_c/dt. \quad (2.3)$$

For a typical, but constant, core growth rate of  $\dot{M}_c = 5 \cdot 10^{-7} M_{\odot} \text{yr}^{-1}$ , and an envelope mass of  $M_{\text{env}} = 10 M_{\odot}$ , Fig. 9 shows  $\Delta M_{\text{H,max}}$  as a function of the mass loss rate, for two different values of  $\lambda$  (no dredge-up and  $\lambda = 0.9$ ).

Figure 8 shows that in order to have an initial mass range for ECSN of, for example,  $1 M_{\odot}$ , the core growth during the SAGB phase must be of the order  $0.1 - 0.2 M_{\odot}$ . Figure 9 shows that if SAGB mass loss is larger than  $\approx 10^{-4} M_{\odot}/\text{yr}$  such a core growth can not be achieved, even for inefficient 3rd dredge-up. For mass loss rates below  $\approx 10^{-6} M_{\odot}/\text{yr}$ , however, a core growth of a few  $0.1 M_{\odot}$  is predicted even if  $\lambda = 0.9$ . Compared with the empirical mass loss rates derived by Lo5 (Table 2) it is clear that the initial mass range for ECSN is sensitive to the third dredge-up.

### 2.5.2 Synthetic SAGB evolution

A quantitative estimate of the initial mass range for ECSN can be obtained through a synthetic model for the TP-AGB phase, similar to that of Izzard et al. (2004, hereafter Io4) for AGB stars, which is based on detailed AGB models from Karakas (Karakas et al. 2002). The extension to SAGB stars is made by fitting the TP-AGB evolution of detailed stellar evolution models (STERN) presented above, specifically over the mass range between  $7$  and  $11.5 M_{\odot}$  in initial mass.

Based on the SAGB STERN evolution sequences with up to 30 thermal pulses, we derive fits for luminosity, radius, and Q-factor (see Sect. 2.5.2), as function of the core mass ( $M_c$ ), the envelope mass ( $M_{\text{env}}$ ) and as secondary parameters the metallicity ( $Z$ ) and the envelope hydrogen abundance ( $X_{\text{H}}$ ). Since the SAGB evolution models have entered into a quasi-steady state regime, these fits are good approximations for the subsequent evolution of SAGB stars during the TP-AGB in mass (total, core and envelope), luminosity and radius.

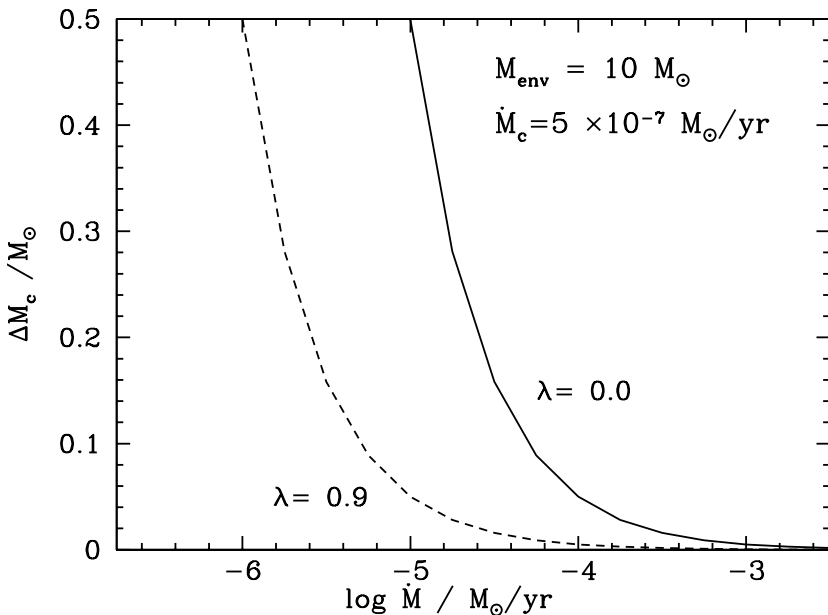


Figure 9. Expected core growth during the TP-SAGB (Eq. 2.3) as function of the mass loss rate, for two different dredge-up efficiencies  $\lambda$  as labeled. A constant mass loss rate, an envelope mass of  $10 M_{\odot}$ , and a constant core growth rate of  $5 \times 10^{-7} M_{\odot}/\text{yr}^{-1}$  are assumed.

We then use these analytic expression as basis for our synthetic TP-SAGB model. As starting values for our synthetic SAGB calculation we use total mass, core mass, and envelope hydrogen abundance after the second dredge-up. First the luminosity is calculated from the initial core and envelope mass, then the radius is calculated, which is a function of the previously calculated luminosity and the envelope mass, and finally the core growth is calculated and integrated over a timestep  $dt$ . From these quantities, the effective temperature, mass loss rate, the resulting new mass of the envelope, and the new mass of the core are calculated. The newly begotten core mass and envelope mass are used as input for the next timestep.

In following subsections we describe the basic outline of our synthetic model (for details we refer to [Izzard et al. 2004](#)).

#### *Luminosity and Radius*

We follow [Io4](#) in their attempt to model the luminosity with two terms, one which contains a core-mass-luminosity relation (CMLR) and one term due to hot-bottom burning. The total luminosity of the star can



now be written as (cf. their Eq. 29)

$$L = f_d(f_t L_{\text{CMLR}} + L_{\text{env}}) L_{\odot}, \quad (2.4)$$

where  $L_{\text{CMLR}}$  is the core mass-luminosity relation given by

$$L_{\text{CMLR}} = 3.7311 \cdot 10^4 \times \max[(M_c / M_{\odot} - 0.52629)(2.7812 - M_c / M_{\odot}), 1.2(M_c / M_{\odot} - 0.48)] \quad (2.5)$$

if the core mass at the first thermal pulse,  $M_{c,1\text{TP}}$  is  $\leq 0.58 M_{\odot}$  and

$$L_{\text{CMLR}} = \max[4(18160 + 3980Z) \times (M_c / M_{\odot} - 0.4468) - 4000, 10], \quad (2.6)$$

if  $M_{c,1\text{TP}} < 0.58 M_{\odot}$ , which is not used in this work, but will be used in a later paper.

$L_{\text{env}}$  is the contribution due to hot-bottom burning (e.g., I04:32),

$$L_{\text{env}} = 1.50 \cdot 10^4 \left( \frac{M_{\text{env}}}{M_{\odot}} \right)^{1.3} \left[ 1 + 0.75 \left( 1 - \frac{Z}{0.02} \right) \right] \times \max \left[ \left( \frac{M_c}{M_{\odot}} + \frac{1}{2} \frac{\Delta M_{c,\text{nodup}}}{M_{\odot}} - 0.75 \right)^2, 0 \right]. \quad (2.7)$$

$M_c$  is the core mass,  $M_{\text{env}}$  is the envelope mass.  $\Delta M_{c,\text{nodup}}$  is the change in core mass without third dredge-up and is defined by  $\Delta M_{c,\text{nodup}} = M_{c,\text{nodup}} - M_{c,1\text{TP}}$  with  $M_{c,\text{nodup}}$  the core mass as if there was no third dredge-up and  $M_{c,1\text{TP}}$  the core mass at the first thermal pulse.  $Z$  is the metallicity. Note that we use a lower exponent than I04 in the contribution of the envelope mass, i.e. 1.3 instead of 2, which resulted in good fits for models between 7 and  $11.5 M_{\odot}$ .

The function

$$f_t = \min \left[ \left( \frac{\Delta M_{c,\text{nodup}} / M_{\odot}}{0.04} \right)^{0.2}, 1.0 \right] \quad (2.8)$$

accounts for the steep rise in luminosity at the beginning of the TP-AGB. The function

$$f_d = 1 - 0.2180 \exp[-11.613(M_c / M_{\odot} - 0.56189)] \quad (2.9)$$

corrects for the short timescale dips in the luminosity during the thermal pulse cycle.

For the fit to the radius we use an expression of the same form as given by I04, but with coefficients adjusted to the STERN models:

$$\log(f_{\text{rR}}) = -0.26 + 0.75 \log(L / L_{\odot}) - 0.41 \log M_{\text{env}} / M_{\odot} \quad (2.10)$$

with

$$f_r = 0.09 \log (M_{\text{env}} / M_{\text{env,1TP}}) \quad (2.11)$$

a factor that accounts for the removal of the envelope, where  $M_{\text{env,1TP}}$  is the mass of the envelope at the first thermal pulse. This correction factor is determined by a fit to a  $9 M_{\odot}$  model to which an extreme mass loss rate of  $10^{-3} M_{\odot} / \text{yr}$  was applied. For envelope masses below  $M_{\text{env}} = 2 M_{\odot}$  the fit predicts too large radii and it is not valid for temperatures below 2500 K as calculated from  $R$  and  $L$ .

### *Third Dredge-up*

For the dependence of the third dredge-up on the initial mass we use the data from [Karakas et al. \(2002\)](#). Our own EVOL SAGB models, however, show smaller dredge-up ( $\lambda = 0.5$  for  $M_{\text{ini}} = 9 M_{\odot}$ ) than the extrapolation of the [Karakas et al. \(2002\)](#) data (Figure 10). We therefore extend the fit to higher masses with a relation that reflects our own data at  $M_{\text{ini}} = 9 M_{\odot}$ . To simulate a situation with no dredge-up, we also include in our synthetic code an option to set  $\lambda = 0$ . As discussed in § 2.4.2 the dredge-up efficiency does not depend on the particular assumption on the overshooting.

### *Core growth and hot-bottom burning*

The growth rate of the He core in the inter-pulse phase is given by

$$\frac{dM_c}{dt} = Q \times L \quad (2.12)$$

where  $L$  is the total luminosity of the star, and  $Q$  is the efficiency of the H-shell to produce core material. Helium burning is mostly inactive in these phases.  $Q$  gives the mass of nuclear ashes accreted onto the core per energy released by the star.  $Q$  depends on several model properties, especially on the hot-bottom burning efficiency, and less on the chemical composition of the envelope. For massive AGB and SAGB stars its strength depends on the envelope mass. If the hot-bottom burning is efficient,  $Q$  can be small (see discussion in § 2.4.1), and the core may not significantly grow at all. Fig. 11 shows the decrease of  $Q$  with increasing envelope mass. We parameterize  $Q$  as

$$Q = \min[1.43 \times 10^{-11}, 1.40 \times 10^{-11} + \frac{4.166 \times 10^{-12}}{X_{\text{H}}} - 1.5 \times 10^{-12} \frac{M_{\text{env}}}{M_{\odot}}]. \quad (2.13)$$

This parameterization is in reasonable agreement with [Io4](#) who set  $Q$  to  $1.585 \times 10^{-11} M_{\odot} L_{\odot}^{-1} \text{yr}^{-1}$ , [Hurley et al. \(2000\)](#) who found  $1.27 \times 10^{-11} M_{\odot} L_{\odot}^{-1} \text{yr}^{-1}$ , and  $1.02 \times 10^{-11} M_{\odot} L_{\odot}^{-1} \text{yr}^{-1}$  in [Wagenhuber & Groenewegen \(1998\)](#).

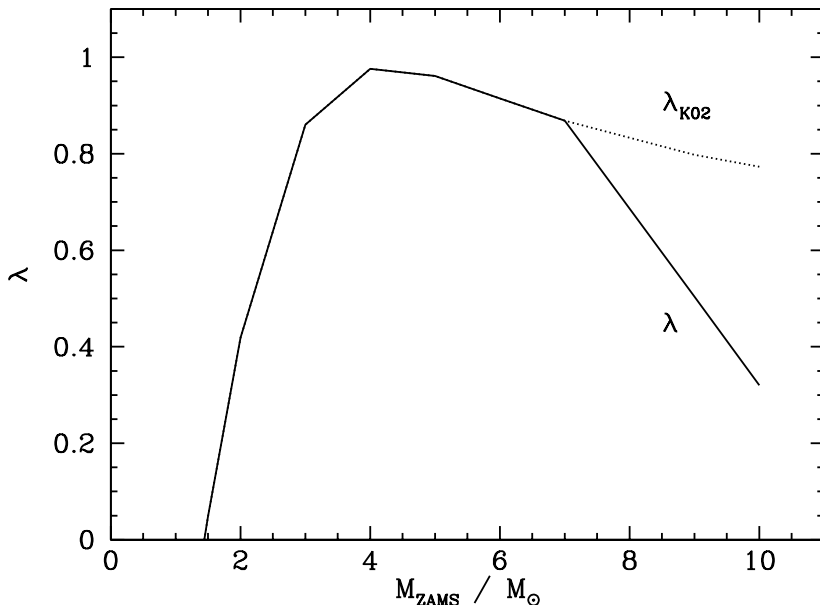


Figure 10. Dredge-up efficiency as a function of initial mass. The dotted line extrapolates the data by [Karakas et al. \(2002\)](#), while the solid line gives the modification based on our SAGB dredge-up stellar evolution sequence.

### Mass loss

As discussed in § 2.5.1 the mass loss of SAGB stars may be the most important ingredient to determine the initial mass range of ECSN. SAGB stars are O-rich (because of hot-bottom burning), and have stellar parameters around  $\log T_{\text{eff}} = 3.5$  and  $\log L/L_{\odot} = 5$  at solar metallicity. It is not clear what the dominant mass loss mechanism for these stars is. Are they cool enough to develop dust-driven winds or is mass loss simply driven by radiation pressure?

Table 2 shows a compilation of observational and theoretical mass loss rates. We preferentially use the observed mass loss rates for massive AGB stars and red supergiants by [van Loon et al. \(2005\)](#) (hereafter L05). If dust-formation does not play an important role, then the Reimers mass loss rate ([Reimers 1975](#)), may be applicable. It is derived from observations of RGB stars with a small range in temperatures and radii, however, [Schröder & Cuntz \(2005\)](#) have revised the Reimers rate. For the more massive RSG stars their new approach, which also includes surface gravity, gives about three times larger mass loss than the Reimers formula. This places it within a factor of 2 of the obser-

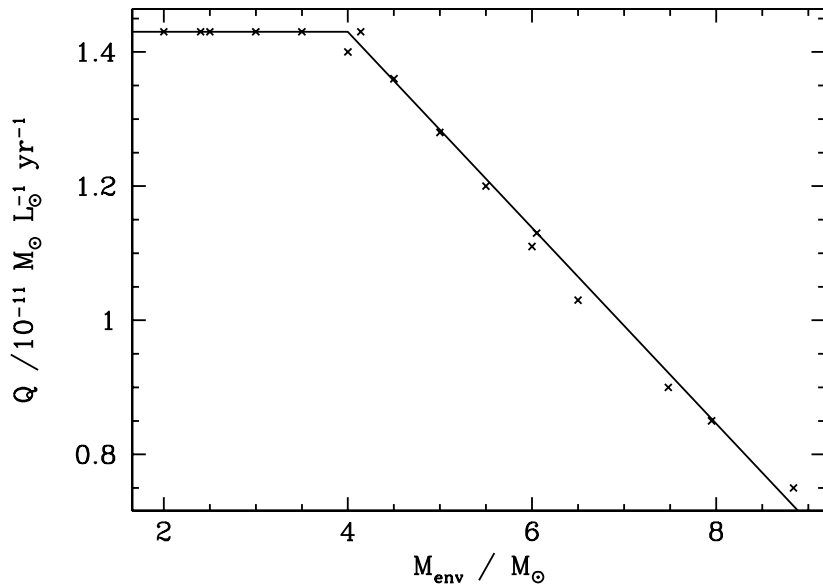


Figure 11. Ashes accreted on core per unit stellar energy release ( $Q$ ) as a function of the mass of the envelope. For envelopes less massive than of  $4 M_{\odot}$  there is no hot-bottom burning.

vational mass loss determination by L05. The mass loss formula by Vassiliadis & Wood (1993) (hereafter VW93), which is often used for AGB star evolution calculations, is also close to the observational value. The AGB mass loss formulated by Bloeker (1995), and based on the hydrodynamic wind models by (Bowen 1988) has a higher luminosity exponent, and gives very high mass loss rates for SAGB stars. From our first estimate in Sect. 2.5.1 it is clear that with the Bloeker mass loss SAGB stars would never explode as ECSN.

## 2.6 RESULTS

We perform a series of synthetic calculations, with two assumptions on third dredge-up and three assumptions on mass loss. For dredge-up we assume either the parameterization of § 2.5.2 or  $\lambda = 0$ . For mass loss, we consider the cases Reimers, L05, and VW93 (§ 2.5.2).

Table 2. Mass loss rates for SAGB stars with a typical value for the luminosity of  $\log L/L_{\odot} = 5$  and an effective temperature of  $T_{\text{eff}} = 3000\text{K}$ .

|                        | Type         | Rate                                       |
|------------------------|--------------|--|
| Reimers ( $\eta = 1$ ) | Red Giants   | $\sim 5 \cdot 10^{-6} M_{\odot}/\text{yr}$ |
| Reimers ( $\eta = 4$ ) | Red Giants   | $\sim 2 \cdot 10^{-5} M_{\odot}/\text{yr}$ |
| Schröder & Cuntz       | Super Giants | $\sim 1 \cdot 10^{-5} M_{\odot}/\text{yr}$ |
| van Loon               | AGB/RSG      | $\sim 3 \cdot 10^{-5} M_{\odot}/\text{yr}$ |
| Blöcker                | AGB          | $\sim 6 \cdot 10^{-3} M_{\odot}/\text{yr}$ |
| Vassiliadis & Wood     | AGB          | $\sim 4 \cdot 10^{-5} M_{\odot}/\text{yr}$ |

Table 3. Mass limits and supernova number fractions as a function of the dredge-up efficiency and mass loss prescription. The lower limit  $M_{\text{low}}$  and the upper limit  $M_{\text{high}}$  are both given in  $M_{\odot}$ .

|                        | $\lambda = \text{parameterized}$ |                   |      | $\lambda = 0$    |                   |      |
|------------------------|----------------------------------|-------------------|------|------------------|-------------------|------|
|                        | $M_{\text{low}}$                 | $M_{\text{high}}$ | % EC | $M_{\text{low}}$ | $M_{\text{high}}$ | % EC |
| Reimers ( $\eta = 4$ ) | 8.67                             | 9.25              | 8.4  | 7.86             | 9.25              | 19.7 |
| VW93                   | 9.03                             | 9.25              | 3.2  | 8.82             | 9.25              | 6.2  |
| Lo5                    | 9.00                             | 9.25              | 3.6  | 8.76             | 9.25              | 7.1  |

### 2.6.1 Initial mass range for ECSN

The resulting initial mass ranges for ECSN are illustrated in Figure 12 for the case with parameterized  $\lambda$ , and in Figure 13 for  $\lambda = 0$ . Stars that end their evolution as white dwarf, i.e. below the Chandrasekhar mass, do not explode as ECSNe. With the parameterized prescription for the third dredge-up, the width of the initial mass window for which ECSN occurs is between  $0.25 M_{\odot}$  and  $0.65 M_{\odot}$ , depending on the assumed mass loss rate. The mass loss prescriptions of Lo5 and of VW93 give an initial mass window of  $0.20 - 0.25 M_{\odot}$ . With zero dredge-up, the core grows at the maximum possible rate. The width of the initial mass window for ECSN is between  $1.4 M_{\odot}$  for the Reimers mass loss rate and  $0.45 - 0.5 M_{\odot}$  for the VW93 and Lo5 mass loss rates.

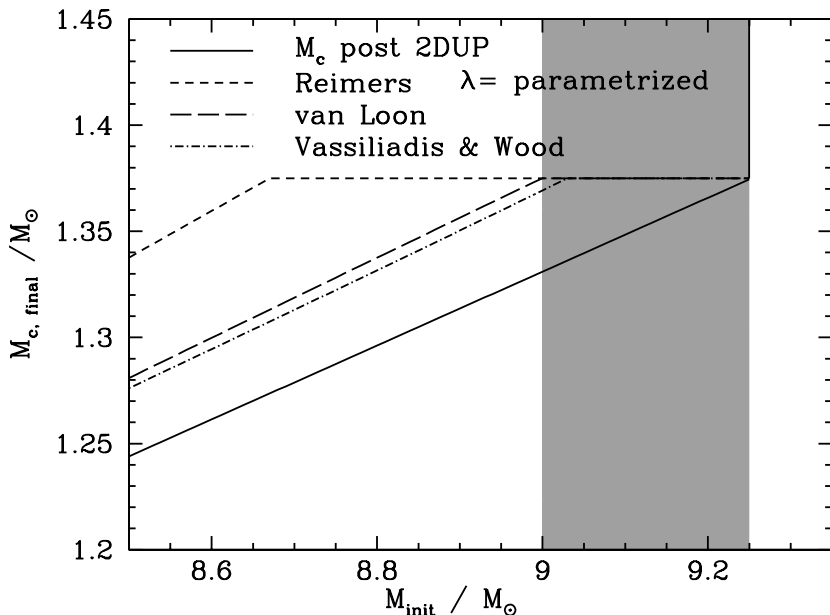


Figure 12. Final core mass as a function of initial mass based on synthetic SAGB calculations. The solid line indicates the the post second dredge-up core mass, the short dashed line indicates the final core mass using the Reimers mass loss rate ( $\eta = 4$ ), the dashed line using the L05 mass loss rate, and the dash-dotted line using the VW93 mass loss rate. The shaded region indicates the initial mass range for ECSNe for the L05 mass loss rate.

### 2.6.2 ECSN fraction

Based on the inferred mass ranges from the synthetic model, we determine the ratio of the number of ECSNe to the total number of SNe. Table 3 gives an overview of the results for the cases of parameterized dredge-up and without dredge-up ( $\lambda = 0$ ), assuming the Salpeter IMF. The value of  $\lambda$  has a strong influence on the predicted fractions. With the parameterized dredge-up and the VW93 or L05 mass loss rates the ECSN fraction of all supernovae is about 3.5%. With the Reimers mass loss rate 8% of all supernovae are ECSN. The largest ECSN fraction of 20% is obtained without dredge-up and using the Reimers mass loss rate.

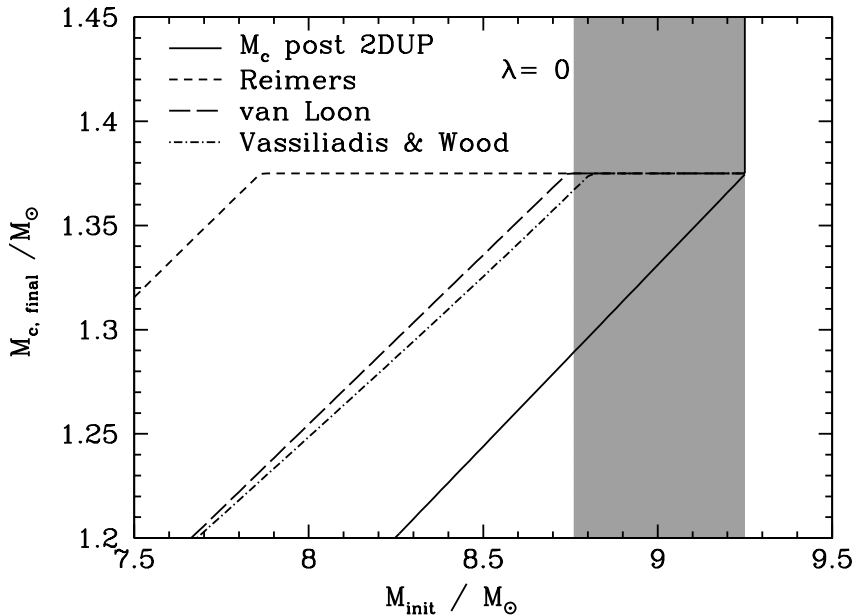


Figure 13. Same as Figure 12 but for calculations assuming no dredge-up.

### 2.6.3 Final masss and SN properties

Figure 14 shows the initial-final mass relation for the mass range from  $1.0 M_{\odot}$  to  $14 M_{\odot}$  using the parameterized dredge-up prescription and the Lo5 mass loss rate. For ECSNe, we find a large spread in progenitor and envelope masses. The least massive SAGB SN progenitors lose almost their entire envelope, growing the core just barely enough to still make an electron capture supernovae before the envelope is lost. The most massive SAGB SN progenitors, on the other hand, undergo very little TP-AGB mass loss before they explode, and contain a massive hydrogen-rich envelope at that time.

This diversity is a natural consequence of the competition between core growth and mass loss during the SAGB stage, and thus independent of the choice of mass loss rate and dredge-up parametrisation. The expected envelope mass range, from almost zero to about  $8 M_{\odot}$  (Fig. 15), implies a diversity of supernova light curves of ECSNe, which may range from light curves of so called Type IIb and Type IIL supernovae to those of typical Type IIP supernovae (Falk & Arnett 1977; Young 2004).

However, ECSNe may show three properties which might allow to distinguish them from ordinary Type II supernovae. First, they

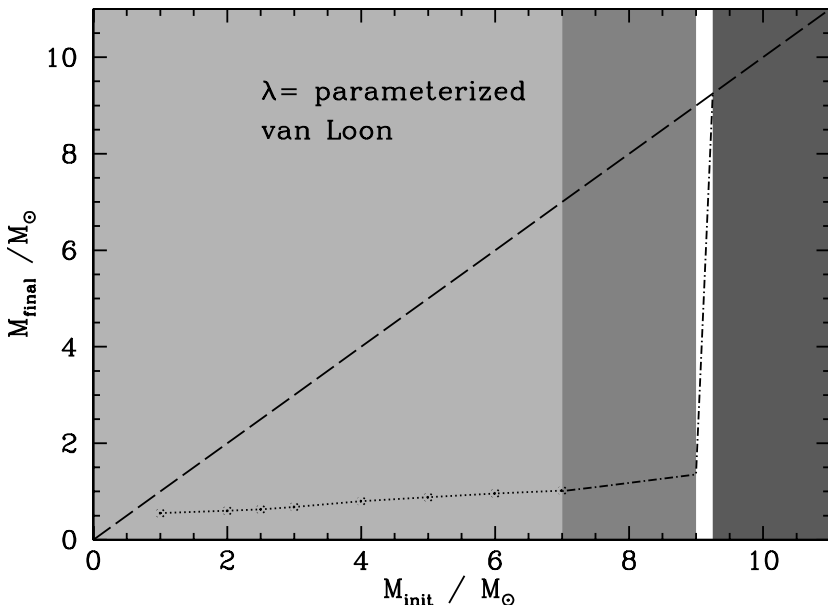


Figure 14. Final mass of the remnant as a function of the initial mass. Remnant regimes are shaded as *light grey*: CO-white dwarf; *grey*: ONE white dwarf; *white*: ECSN; *dark grey*: CCSN. The final mass is either the WD mass or the stellar mass at the time of SN explosion. The dashed line indicates the line of initial mass equal final mass.

might produce low-energy explosions (Kitaura et al. 2006) and possibly low neutron star kicks (Podsiadlowski et al. 2004). A consequence of the low explosion energy may be a small nickel mass produced by the explosion, and thus a low luminosity of the tail of the light curve which is produced by the decay of  $^{56}\text{Ni}$  and  $^{56}\text{Co}$  (Kitaura et al. 2006). The Type IIP SN 1997D may provide an example (Chugai & Utrobin 2000). Second, however, the enormous mass loss rate of the supernova progenitor (Fig. 17) star may produce clear signatures of a supernova-circumstellar medium interaction in the supernova light. Such signatures are in particular exceptionally a bright and long-lasting light curve (Sollerman et al. 2001), and narrow hydrogen emission lines superimposed to a typical SN II spectrum (Pastorello et al. 2002). Third, ECSN progenitors are extremely bright, with luminosities of the order of  $10^5 L_{\odot}$  (Fig. 16). Thus, progenitor identifications on pre-explosion images (Maund & Smartt 2005; Hendry et al. 2006) might be able to identify ECSNe. They may be distinguished from very massive ( $> 20 M_{\odot}$ ) progenitors of similar luminosity by their much cooler



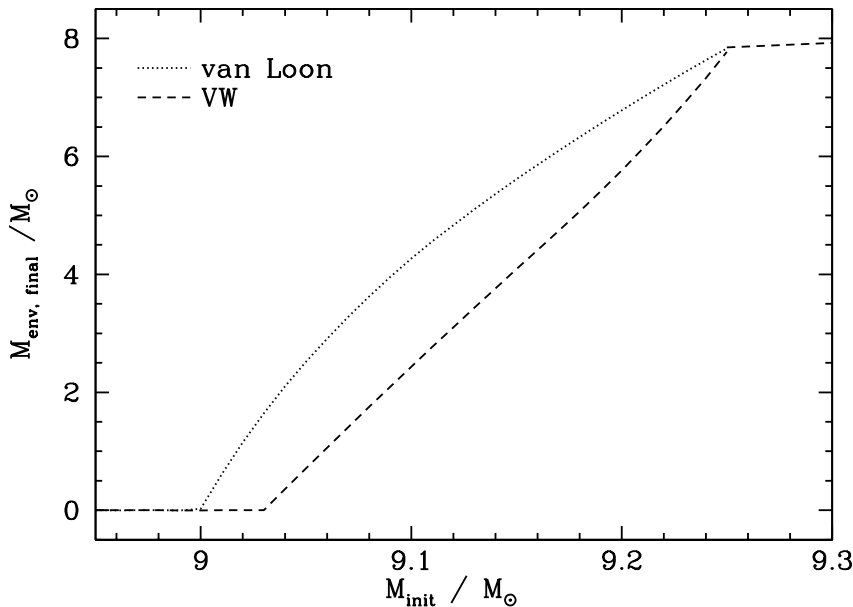


Figure 15. Mass of the envelope just prior to the explosion as function of the initial mass for two mass loss rates.

effective temperatures ( $< 3000\text{K}$  for ECSN progenitors versus  $\sim 3400\text{K}$  for CCSN progenitors).

#### 2.6.4 The reference model, examples

As shown above, the results of our synthetic SAGB calculations employing the VW93 and the Lo5 mass loss prescriptions are rather similar. Since it is unclear whether the Reimers mass loss rate is really applicable, and as the Lo5 mass loss rate relies on very recent observations, we adopt the latter as the fiducial mass loss prescription for our synthetic SAGB modeling. Concerning the third dredge-up efficiency, we adopt the mass dependant formulation shown in Fig. 10 as our reference efficiency. These assumptions define our reference model for the synthetic SAGB evolution.

In the following, we discuss some explicit examples to illustrate the TP-SAGB evolution, and to further motivate the choice of our reference model and analyse its uncertainty. The first example is a star with an initial mass of  $9.1 M_{\odot}$ , with a He-core mass at the end of the second dredge-up of  $1.348 M_{\odot}$ .

During the evolution on the TP-SAGB the luminosity first increases

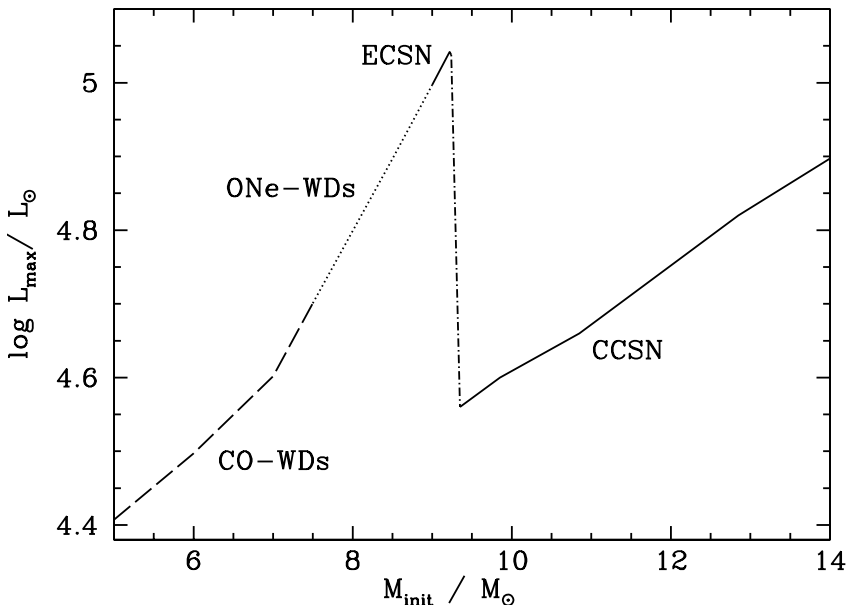


Figure 16. Maximum luminosity as function of the initial mass at the end of the evolution. Progenitors of CO white dwarfs reach luminosities up to  $\log L/L_{\odot} \sim 4.6$ , progenitors of ONe white dwarfs reach luminosities up to  $\log L/L_{\odot} \sim 5$ . Progenitors of ECSN are the most luminous, with  $\log L/L_{\odot} \geq 5$ , while progenitors of the least massive CCSN have pre-explosion luminosities of  $\log L/L_{\odot} \sim 4.6$ .

from  $\log L/L_{\odot} = 4.9$  to  $\log L/L_{\odot} = 5.02$ , and then drops slightly due to decreasing envelope mass which decreases the efficiency of hot-bottom burning. As a result, the inter-pulse core growth rate increases from  $3 \times 10^{-7} M_{\odot}/\text{yr}$  to  $1.5 \times 10^{-6} M_{\odot}/\text{yr}$ , but the effective core growth is significantly lower (by about factor 0.5) due to the effect of dredge-up. The mass loss rate increases from  $3 \times 10^{-5} M_{\odot}/\text{yr}$  to  $1 \times 10^{-4} M_{\odot}/\text{yr}$  (Fig. 18). In this model the SAGB ends after  $\sim 4.4 \times 10^4$  yr when the core reaches its Chandrasekhar mass. The remaining envelope has a mass of  $4.27 M_{\odot}$ .

For a 10% larger dredge-up efficiency the SAGB time increases to  $\sim 4.8 \times 10^4$  yr, and the remaining envelope decreases to  $3.82 M_{\odot}$ . For a 10% smaller dredge-up efficiency the SAGB decreases to  $\sim 4.0 \times 10^4$  yr, and the final envelope mass increases to  $4.61 M_{\odot}$ . For the case of no dredge-up the SAGB time is  $\sim 2.4 \times 10^4$  yr and the final envelope mass is  $6.1 M_{\odot}$ .

Using the mass loss prescription of VW93 and the parameterized

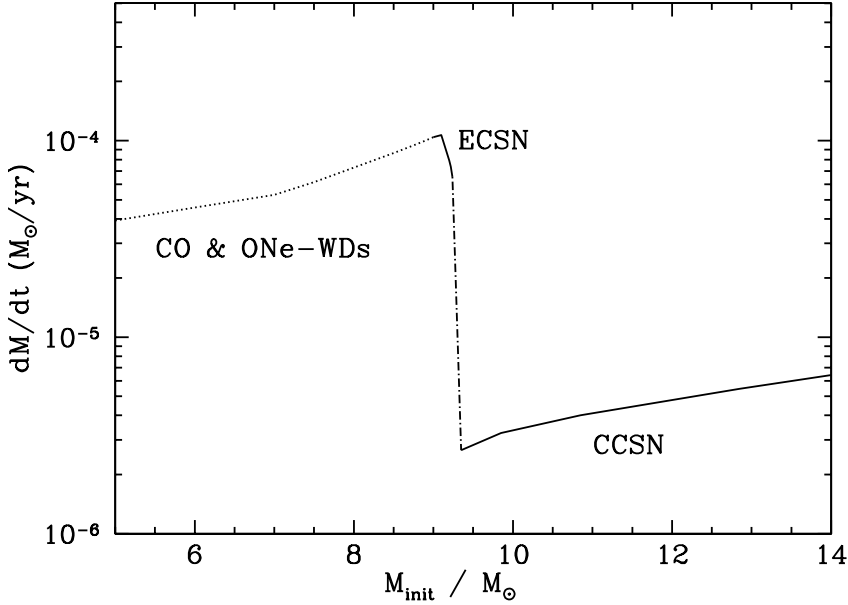


Figure 17. Mass loss rates according to Lo5 as function of initial mass, for the models shown in Fig 16.

dredge-up, the result is only different in the mass loss history, resulting in a smaller final mass. The main reason is that this mass loss prescription accounts for the superwind phase for TP-AGB stars, which gives a significantly different evolution of the envelope. The TP-AGB phase starts with low mass loss but makes a transition to the superwind phase after 1000 yr with mass loss rates around  $1 \times 10^{-4} M_{\odot}/\text{yr}$ , decreasing slowly due to the waning luminosity (Fig. 18, Upper Panel). After  $4.7 \times 10^4$  yr, the core reaches its Chandrasekhar mass with a final envelope mass of  $2.43 M_{\odot}$ .

An initially  $8.8 M_{\odot}$  star with the same mass loss and dredge-up (Fig. 19) becomes an ONe WD. The He-core mass at the beginning of the SAGB is  $1.296 M_{\odot}$ . During the SAGB evolution the luminosity increases to  $\log L/L_{\odot} = 4.95$ , then decreases due to mass loss. Assuming the Lo5 mass loss rate, the envelope is lost after  $\sim 1 \times 10^5$  yr. The mass loss rate increases steadily during the TP-AGB phase, but as the star reaches a surface temperature of 2500K (Sect. 2.5.2) we assume a constant mass loss rate of  $\dot{M} = 1 \times 10^{-4} M_{\odot}/\text{yr}$  during the last phase of the evolution. This is consistent with the observations of Lo5 who find only one star with a higher mass loss rate. The remaining ONe core has a mass of  $1.338 M_{\odot}$ . Repeating this calculation with the mass loss rate of VW93

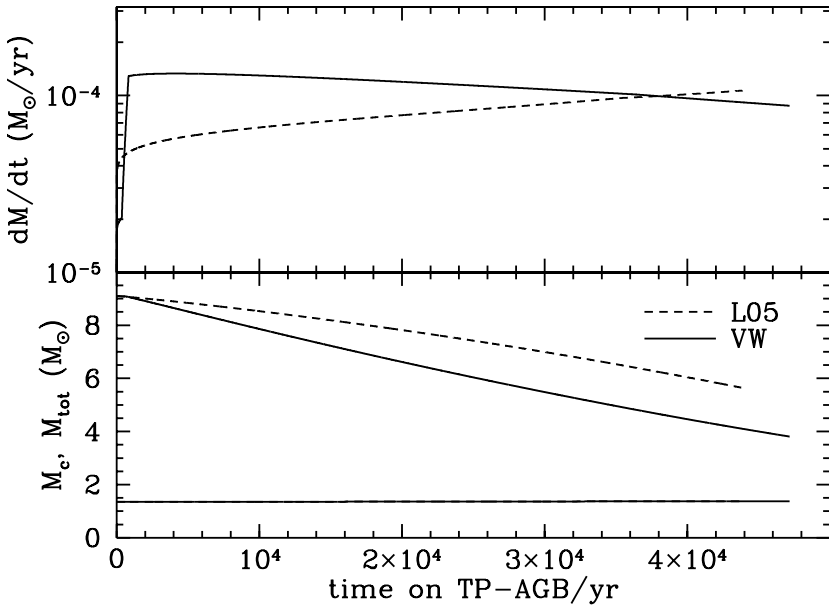


Figure 18. Synthetic AGB mass evolution for an initial mass of  $9.1 M_{\odot}$ . Upper panel: mass loss rate for two cases (L05 and VW93, § 2.5.2); the superwind regime in the VW93 mass loss prescription sets in at 1000yr right at the beginning of the AGB phase. Lower panel: evolution of the core and the total stellar mass.

does not show large differences (Fig. 19).

## 2.7 CONCLUDING REMARKS

We show that both the upper initial mass for SAGB stars and the maximum initial mass for ECSN sensitively depend on the assumptions for mixing during core H- and He-burning. EVOL models which include core overshooting, and which are consistent with the observed width of the main sequence, predict a smaller maximum initial mass for SAGB stars. Rotation would act similar to overshooting during the core burning phases. The STERN models include neither rotation nor overshooting, and the maximum initial mass for SAGB and ECSNe is larger by up to  $2.5 M_{\odot}$ . Equally important is the treatment of semiconvection during He-core burning.

On the other hand, the lower initial mass limit for ECSN is determined by the stellar properties on the AGB or SAGB. Most important are the third dredge-up efficiency, the mass loss rate, and the hot-bottom

Table 4. Final core and envelope masses for different initial masses. The first three columns give the initial conditions of the models. Models marked with an asterisk are calculated until the end of the second dredge-up with EVOL (Table 1), the other models are interpolated assuming a linear relation between the initial mass and the core mass at the end of the second dredge-up. The fourth and the fifth column give the final core and envelope mass for two different mass loss prescriptions (§ 2.5.2) and for a parameterized dredge-up efficiency (§ 2.5.2). The sixth and seventh column give the final core and envelope mass for a dredge-up efficiency of zero. In case a column contains “WD” or “NS”, the remnant is respectively a white dwarf or a neutron star. All masses are in units of a solar mass.

| $M_{\text{tot}}$ | initial conditions |                  | final conditions param. $\lambda$ |                  |                |                  | final conditions $\lambda = 0$ |                  |                |                  |
|------------------|--------------------|------------------|-----------------------------------|------------------|----------------|------------------|--------------------------------|------------------|----------------|------------------|
|                  | $M_{\text{c}}$     | $M_{\text{env}}$ | Lo5                               |                  | VW 93          |                  | Lo5                            |                  | VW 93          |                  |
|                  |                    |                  | $M_{\text{c}}$                    | $M_{\text{env}}$ | $M_{\text{c}}$ | $M_{\text{env}}$ | $M_{\text{c}}$                 | $M_{\text{env}}$ | $M_{\text{c}}$ | $M_{\text{env}}$ |
| 6.5000*          | 0.9900             | 5.5100           | 1.0039                            | WD               | 1.0060         | WD               | 1.0816                         | WD               | 1.0887         | WD               |
| 7.5000*          | 1.0700             | 6.4300           | 1.0886                            | WD               | 1.0903         | WD               | 1.1734                         | WD               | 1.1739         | WD               |
| 8.5000*          | 1.2440             | 7.2560           | 1.2809                            | WD               | 1.2761         | WD               | 1.3358                         | WD               | 1.3255         | WD               |
| 8.7500           | 1.2875             | 7.4625           | 1.3282                            | WD               | 1.3223         | WD               | NS                             | 0.2075           | 1.3654         | WD               |
| 8.8000           | 1.2962             | 7.5038           | 1.3376                            | WD               | 1.3316         | WD               | NS                             | 1.3774           | 1.3736         | WD               |
| 8.9000           | 1.3136             | 7.5864           | 1.3563                            | WD               | 1.3504         | WD               | NS                             | 3.2631           | NS             | 1.4514           |
| 9.0000           | 1.3310             | 7.6690           | NS                                | 0.0221           | 1.3693         | WD               | NS                             | 4.7723           | NS             | 3.0680           |
| 9.1000           | 1.3484             | 7.7516           | NS                                | 4.2672           | NS             | 2.4311           | NS                             | 6.0628           | NS             | 4.7208           |
| 9.2000           | 1.3658             | 7.8342           | NS                                | 6.7800           | NS             | 5.7643           | NS                             | 7.2711           | NS             | 6.6314           |
| 9.2500           | 1.3745             | 7.8755           | NS                                | 7.8321           | NS             | 7.7731           | NS                             | 7.8481           | NS             | 7.8138           |

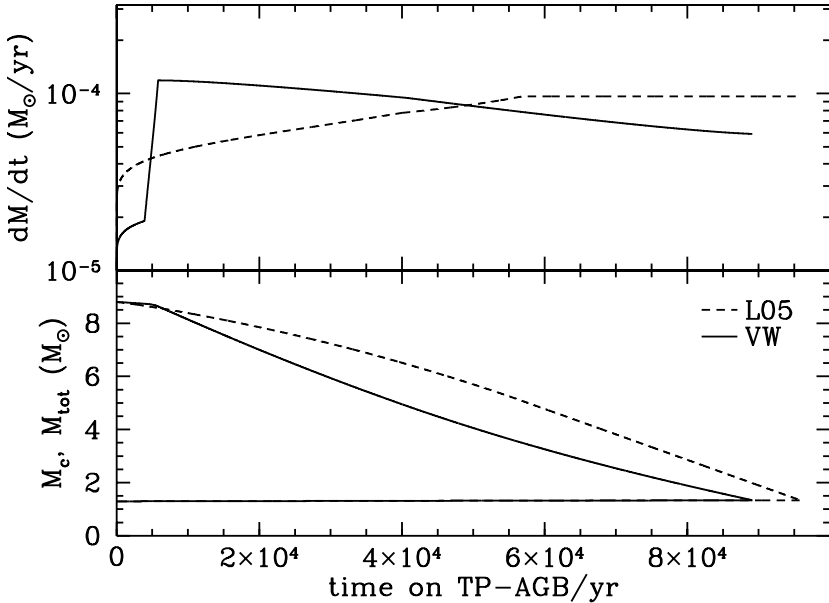


Figure 19. Similar to Figure 18 but for a  $8.8 M_{\odot}$  star. The core does not reach the Chandrasekhar mass but loses its envelope and becomes a massive ONe white dwarf.

burning efficiency and its dependence on the adopted convection theory for the envelope. In general, larger mass loss, larger dredge-up efficiency and large hot-bottom efficiency all decrease the initial mass range for ECSN, or even suppress the ECSN channel. In order to increase the accuracy of the transition initial mass between ECSN and CCSNe and of the lower mass limit for ECSNe, these classical issues of stellar evolution need to be improved specifically for the initial mass range of 6 to  $12 M_{\odot}$ .

Whereas we have discussed here the SAGB stars with C-ignition and formation of ONe cores as the most likely progenitors of an ECSN class of supernova, it is theoretically possible that initially less massive stars that develop CO cores could increase their core size on the TP-AGB up to the Chandrasekhar mass resulting in a supernova explosion. Despite the uncertainties still involved we can rule out this possibility for solar metallicity. There are two main reasons that prevent these  $\text{SN}_{1.5}$  from occurring: First, the mass loss would have to be much lower than observed. Second, models predict that the third dredge-up is larger for massive AGB stars with initial mass between 4 and  $7 M_{\odot}$  than for SAGB stars (Fig. 10; Karakas et al. 2002). This makes it even

more unlikely for massive AGB stars to significantly grow their cores.

We did not take into account mass loss until the beginning of the thermally pulsing phase. If mass loss were applied during the main sequence and up to the TP-AGB, less than half a solar mass would have been lost (Siess 2006, their Table 5). This may shift the quoted initial masses to a slightly higher value.

We note that there is large disagreement between the different studies on the dredge-up efficiency in SAGB stars (Ritossa et al. 1996; Doherty & Lattanzio 2006; Siess & Pumo 2006). Whereas Ritossa et al. (1996) and Siess & Pumo (2006) find negligible amounts of dredge-up, Doherty & Lattanzio (2006) find very efficient dredge-up with  $\lambda \sim 0.7$ . In our synthetic model we adopted a parameterized prescription (Fig. 10) that is based on state-of-the-art full stellar evolution calculations. To test the effect of dredge-up we also considered a case with no dredge-up. Clearly, the third dredge-up in SAGB stars needs to be studied in more detail. It is closely related to the mixing conditions at the bottom of the convective boundary. This is a hydrodynamic situation which requires multi-dimensional simulation which is complicated by the fact that for these extremely massive cores the dredge-up seems to be hot (Herwig 2004a), i.e., any small amount of H that could be mixed across the convective boundary will instantly burn violently with all the associated feedback on the evolution of the convective instability in that region.

It is presently not known whether ECSN from SAGB stars contribute to the  $r$ -process pattern in the universe. Explosions from stars in this mass range have been investigated as promising site for the astrophysical  $r$ -process (Wheeler et al. 1998; Sumiyoshi et al. 2001; Wanajo et al. 2003), based on the work of Hillebrandt et al. (1984) who exploded a ONe core model from Nomoto (1984a, 1987a). Other groups were not able to confirm the  $r$ -process contribution due to the low entropy (e.g., Burrows & Lattimer 1985; Baron et al. 1987; Mayle & Wilson 1988; Bethe & Wilson 1985). Kitaura et al. (2006) ruled out this possibility based on updated physics and two different nuclear equations of state.

In any case, our study outlines that ECSN from SAGB stars are likely to occur, if only at a level of a few per cent of the Type II supernova rate in the local universe. However, at low metallicity, the key physical ingredients to the evolution of thermally pulsing SAGB stars may change. In particular, the stellar wind mass loss rate may be lower, which might open the ECSN channel appreciably, and may even allow Type 1.5 supernovae. This issue will be discussed in a forthcoming paper.





SUPERNOVAE FROM MASSIVE METAL-POOR AGB STARS

---

A. J. T. Poelarends, N. Langer, F. Herwig, A. Heger

*submitted to Astrophysical Journal*

**ABSTRACT** We investigate possible supernova channels from massive asymptotic giant branch (AGB) stars. Poelarends et al. (2007, further on Po7, in this thesis Chapter 2) showed that, at solar metallicity, about 4%, and at most 20% of all supernovae are so called electron-capture SNe (ECSNe) produced by Super-AGB (SAGB) stars. Here, we investigate how this channel widens for lower metallicity where stellar winds may be weaker, and under which conditions carbon deflagration supernovae from AGB stars (so called SN Type 1.5) occur. To this end, a grid of low- $Z$  stellar evolution models is computed until the onset of thermal pulses. Beyond, we employ the synthetic SAGB model of Po7, extended to low metallicity stellar evolution. Using six different combinations of model parameters, we study the effects of dredge-up and mass loss on the TP-SAGB evolution. For our fiducial parameter set, we find the ECSN initial mass range widening from  $0.25 M_{\odot}$  at solar metallicity to almost  $2 M_{\odot}$  at  $\log Z/Z_{\odot} = -3$ . A corresponding shift of the minimum initial mass for ECSN from  $9 M_{\odot}$  ( $Z = Z_{\odot}$ ) to  $6.3 M_{\odot}$  ( $\log Z/Z_{\odot} = -3$ ) implies a doubling of the total supernova rate, with an ECSN fraction of about 50%. Our model predicts Type 1.5 SNe, but only for metallicities lower than about  $\log Z/Z_{\odot} = -3$ . We investigate the dependance of these results on our assumptions on mass loss and dredge-up during the TP-SAGB stage. We discuss observational consequences of metal-poor SNe from AGB stars, in particular their relevance to understand observed  $s$ - and  $r$ -enhancements in extremely metal-poor stars in our Galaxy, and the large number of neutron stars found in Galactic globular cluster.

### 3.1 INTRODUCTION

Stellar evolution in the transition region between white dwarf and neutron star formation is complicated by two different competitions. The stellar core is at the verge of significant electron degeneracy, and at the borderline between cooling and heating. And at the same time, the core growth through shell burning leads the core mass towards the Chandrasekhar mass while the envelope is rapidly evaporating through a strong stellar wind. The transition region is populated by so called Super-AGB (SAGB) stars, i.e. stars which do develop a highly degenerate core only after central carbon burning and which undergo thermal pulses. For rapid mass loss, the core can not grow to the Chandrasekhar mass, and an ONe white dwarf is produced. For low mass loss rates, the Chandrasekhar mass will be reached before the envelope is completely lost, and electron captures will lead to the collapse of the ONe core and an ensuing electron capture supernova (ECSN, [Nomoto 1984a](#); [Eldridge & Tout 2004c](#); [Ritossa et al. 1999](#); [Siess & Pumo 2006](#); [Poelarends et al. 2007](#)).

The lower end for the initial mass range for Super-AGB (SAGB) stars is given by the onset of non-explosive carbon burning, and the upper end by the onset of neon burning. Stars that ignite neon burning are too massive to become SAGB stars, undergo the advanced burning stages beyond carbon burning and form an iron core, which eventually collapses and gives rise to a normal core collapse supernova. SAGB stars instead experience the second dredge-up after the end of core He-burning, which is characteristic for the intermediate mass AGB stars as well. At this point and throughout the following early SAGB phase, carbon burning transforms the C/O core into an ONe core ([Nomoto 1984a, 1987a,b](#); [Ritossa et al. 1996](#); [Iben et al. 1997](#); [Garcia-Berro et al. 1997](#); [Ritossa et al. 1999](#)). Since the temperature is not high enough to start neon burning the electron degeneracy in the core increases and the SAGB star resembles a configuration very similar to the most massive C/O core AGB stars. The degenerate core is surrounded by the He-shell and H-envelope, and as in the AGB stars this double-shell burning on a degenerate core is unstable and leads eventually to thermonuclear He-shell flashes ([Yoon et al. 2004](#)). If the core mass can increase sufficiently, these SAGB stars will explode as a electron capture supernova due to electron captures on  $^{24}\text{Mg}$  and  $^{20}\text{Ne}$  ([Miyaji et al. 1980a](#); [Miyaji & Nomoto 1987](#); [Hashimoto et al. 1993](#)).

Initial studies concentrated on the evolution of the cores of SAGB stars at solar metallicity [Nomoto \(1984a, 1987a,b\)](#). According to these models, stars with helium cores between  $2.0$  and  $2.5 M_{\odot}$  form ONeMg cores and explode as core-collapse supernova. [Ritossa et al. \(1996\)](#); [Garcia-Berro et al. \(1997\)](#); [Iben et al. \(1997\)](#) and [Ritossa et al. \(1999\)](#) and more recently [Eldridge & Tout \(2004c\)](#); [Siess \(2006\)](#) and [Siess & Pumo](#)

(2006) studied different phases of the evolution of these stars in greater detail and found that SAGB stars resemble a similar configuration on the TPSAGB as their low mass counterparts. Eldridge & Tout (2004c) and Siess & Pumo (2006) investigated the effect of metallicity on the transitions from CO to ONe cores and the minimum supernova mass, but did not follow the subsequent evolution on the TPSAGB.

A detailed grid of intermediate TPAGB models with masses between 2 and  $6 M_{\odot}$  at  $Z = 10^{-4}$  was computed by Herwig (2004a,b). He finds very efficient dredge-up, which prevents further core growth on the AGB. Other studies, such as Girardi et al. (2000); Bono et al. (2000) computed whole grids of models for different metallicities, but also with a focus on the intermediate mass range. Gil-Pons et al. (2005) studied a  $9 M_{\odot}$  model at  $Z = 0$  and found very little deviations from their  $Z = 0.02$  model in terms of core mass and thermal pulse characteristics.

In this paper we identify the processes that influence the core growth of SAGB stars and our detailed stellar evolution sequences through synthetic SAGB calculations. The situation at extremely low and zero metallicity is considered as well. Our results are based on calculations with three different stellar evolution codes to obtain a understanding of the robustness of our findings. In Sect. 3.2 we give an overview of the stellar evolution codes and the synthetic model we use for modelling on the thermally pulsing AGB. Section 3.3 discusses the pre-AGB evolution and its dependence on the second dredge-up and metallicity. Section 3.4 discusses the assumptions and different input variations in our synthetic model. In Section 3.5 the results are presented. A summary and discussion of our results are provided in Section 3.7.

### 3.2 MODELS, DETAILED AND SYNTHETIC

We calculated four sequences of detailed models, three as a function of mass and one of metallicity. The first sequence was already presented in a previous paper (Poelarends et al. 2007, hereafter P07) and deals with stellar models of solar metallicity ranging from  $6.5 M_{\odot}$  to  $13.0 M_{\odot}$ . For a detailed discussion we refer the reader to P07. The second sequence as a function of the mass is calculated with a metallicity of  $Z = 10^{-4}$ . The mass range we consider for this set of models is  $6.0 M_{\odot}$  to  $11.0 M_{\odot}$ . The third sequence (KEPLER and STERN) are models with  $Z = 0$ . A fourth sequence of models (only with STERN) was calculated along the metallicity axis, with metallicities ranging from  $Z = 10^{-5}$  to  $Z = 0.02$ . The mass of the models in this sequence was set to  $9.0 M_{\odot}$ .

We evolved all models, starting from the zero age main sequence (ZAMS), until the completion of the second dredge-up (2DUP), which marks the end of the early asymptotic giant branch (EAGB) evolution. This gives the mass of the core, and mass and chemical composition of the envelope as a function of initial mass and metallicity, which we

use as input for the subsequent synthetic evolution on the thermally pulsing AGB. Since the computation of detailed models on the thermally pulsing AGB (TP-AGB) is computationally very intensive, we model this phase of the evolution with a synthetic code (see 3.2.2). This is possible since the behavior of AGB stars reaches a limit cycle after a few pulses (Ritossa et al. 1996).

### 3.2.1 Detailed evolutionary models

We used three stellar evolution codes, e.g. STERN (Langer 1998; Heger et al. 2000), EVOL (Blöcker 1995; Herwig 2000) and KEPLER (Weaver et al. 1978), to study the effects of different physics and numerical treatment. For a detailed discussion of the differences in input physics we refer to Po7, here we briefly highlight the differences and similarities.

All three codes use the OPAL opacities (Iglesias & Rogers 1996), and are equipped a nuclear network with all relevant reactions. For our investigation the most important difference between the codes is the treatment of thermally induced internal mixing. As discussed in Po7, these affect the He-core mass after central He-burning, and thereby the final evolution fate of the stellar model. STERN and KEPLER use the Ledoux-criterion to determine convective instability, and take isemiconvection into account. In EVOL convective boundaries are determined by the Schwarzschild criterion and mixing beyond the convective boundary is included by performing exponential-diffusive extra-mixing (Herwig et al. 1997; Herwig 2000).

Mass loss is not taken into account, since stars in the considered mass range lose very little mass during the early phases of their evolution, especially for the low metallicities considered here. Also rotation is not taken into account, which for the STERN models results in core masses that are probably too small (cf. Po7). EVOL and KEPLER give larger core masses mainly due to the inclusion of overshooting, which is calibrated to reproduce the observed width of the main sequence (EVOL) or fast semi-convection (KEPLER).

### 3.2.2 Synthetic code

Our synthetic models are based on those of Izzard et al. (2004) and fitted to the solar metallicity STERN models, as described in Po7. To take the effects of lower metallicity into account we adapted the algorithm.

- The luminosity,  $L$ , as described in Po7, depends explicitly on the metallicity  $Z$  and accounts well for the higher luminosity at lower metallicity (cf. Fig. 21).
- The radius,  $R$ , as described in Po7, does not explicitly depend on the metallicity  $Z$ . However, our models show that the increase

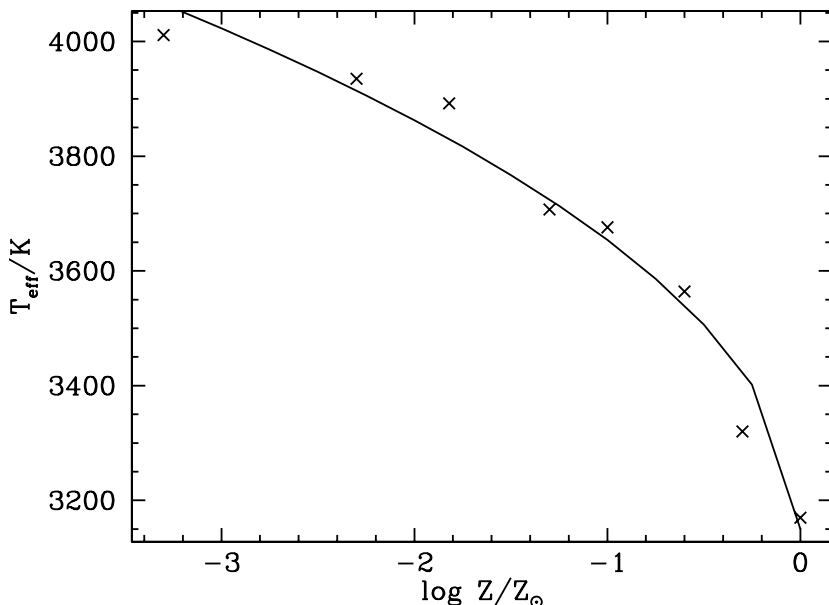


Figure 20. Effective temperature at the first thermal pulse as a function of metallicity for  $M = 9 M_{\odot}$  models computed with STERN. The line is a fit to the data (crosses) and is used to derive the effective temperature during the TP-AGB evolution.

in luminosity at lower metallicity is accompanied by a increase in effective temperature (e.g. about 1000 K difference between  $Z = 0$  and  $Z = 10^{-5}$  at the beginning of the TPSAGB), and a slight decrease in radius ( $\sim 10\%$  at  $\log Z/Z_{\odot} = -1.7$  and  $\sim 20\%$  at  $\log Z/Z_{\odot} = -3.5$ ). Since we use  $r$  instead of the radius – the effective temperature in our mass loss recipe, we choose to use the Po7 fit to the radius, and apply a modification for the temperature to account for the higher effective surface temperature at lower metallicities. This modification fits the data well (cf. Fig. 20) and is given by

$$T_{\text{eff}}(Z) = T_{\text{eff}}(Z = Z_{\odot}) \times \left( 1 + 0.16 \sqrt{\left| \log \left( \frac{Z}{Z_{\odot}} \right) \right|} \right) \quad (3.1)$$

- The parametrization of the core growth and hot bottom burning is taken from Po7. The value of  $Q$  depends on the hydrogen

abundance of the envelope, which is taken into account via

$$\begin{aligned} Y &= 0.24 + 2Z \\ X &= 1 - Y - Z \end{aligned} \quad (3.2)$$

The effects of envelope enrichment due to first and/or second dredge-up are only followed in helium, since the enrichment in metals is only 0.15 dex for  $Z = 10^{-5}$ .

- To parametrize the efficiency of the third dredge-up we include the fits of [Karakas et al. \(2002\)](#) in our synthetic code and linearly interpolate their exponents to lower metallicities. We are aware of the fact that these fits are only calibrated in a metallicity range from solar to  $Z = 0.004$  but the dependence on  $Z$  is very weak and we lack reliable models for lower metallicities (also in the literature) to fit our synthetic models to. We included a second option for the efficiency of the third dredge-up, which is  $\lambda = 0$ , i.e. no dredge-up for all metallicities.
- We include two different mass loss prescriptions in our synthetic models, i.e., the mass loss rate by [van Loon et al. \(2005\)](#) (hereafter vL), which is in terms of observations the best supported mass loss rate at the moment for this type of stars, and is thus our standard mass loss rate. We choose to use the RSG rate (instead of the combined AGB/RSG or AGB rate) since most of our TPSAGB stars have a luminosity that exceeds  $\log L/L_{\odot} \sim 4.9$ . The second mass loss rate we included in our code is [Vassiliadis & Wood \(1993\)](#), hereafter VW93 – we use their equation 5). Variation of the mass loss rate with the metallicity is taken into account with

$$\dot{M}(Z) = \dot{M}(Z = Z_{\odot}) \times \sqrt{Z/Z_{\odot}} \quad (3.3)$$

Our synthetic model is fitted to detailed models at solar metallicity but can be applied, with the modifications described above, to lower metallicities. However, we limit ourselves to metallicities between  $Z = Z_{\odot}$  and  $Z = 10^{-5}$ , and do not extend our synthetic models to zero metallicity.

### 3.3 EVOLUTION TO THE AGB

In comparison with the P07 calculations for solar metallicity, some basic properties of the models differ at lower metallicity. Figure 21 shows the evolution of a  $9M_{\odot}$  model in the HRD from the ZAMS to the asymptotic giant branch (AGB) for solar metallicity and  $Z = 10^{-4}$ . The model with  $Z = 10^{-4}$  is hotter and more luminous than the model with

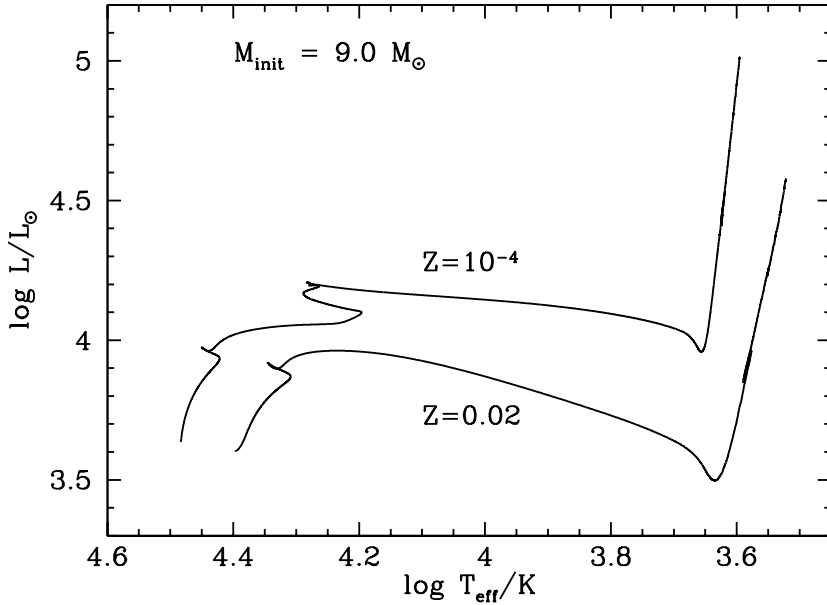


Figure 21. Evolutionary tracks (STERN) for a solar metallicity (solid line) and  $Z = 10^{-4}$  (dashed line) model of  $9.0 M_{\odot}$ . The model with  $Z = 10^{-4}$  is hotter and more luminous (caused by a combination of both a bigger core and a lower opacity) than the model with  $Z = 0.02$ .

solar metallicity during the entire evolution. The RGB and the location of the Hayashi-line is moved to the blue, in agreement with Schaller et al. (1992). As shown in Figure 22 the central conditions differ as well. The solar metallicity model has a smaller helium core and lower central temperature than the model with  $Z = 10^{-4}$ . These conditions causes the  $Z = 10^{-4}$  model to ignite carbon off center, subsequently followed by a series of inward growing flames that eventually reach the center and convert the whole interior of the star to an ONeMg core, which is not the case for the solar metallicity model. While this model develops some off center carbon ignition, the temperatures are not high enough to sustain the flames to move all the way to the center of the star, hence a CO core is left behind.

### 3.3.1 Core masses at the end of the early AGB

Figure 23 shows the helium core masses just before and just after the second dredge-up as function of the initial mass for three different metallicities. The core masses for the  $Z = 0.02$  sequence are discussed

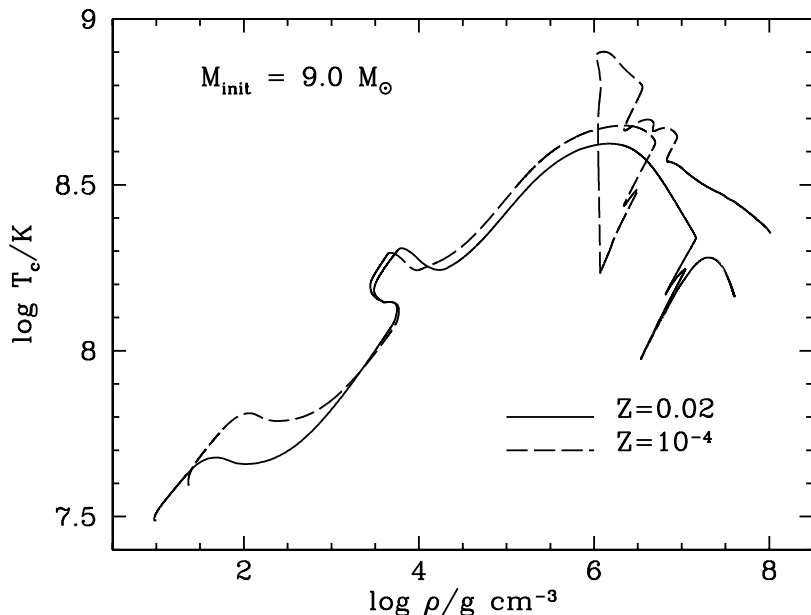


Figure 22. Evolutionary tracks (STERN) for the cores of the two models (see Fig 21). The models with  $Z = 10^{-4}$  has a more massive core, hence develops extensive carbon burning, while the  $Z = 0.02$  model only has minor carbon burning that does not reach the center of the star and consequently does not convert the entire core in a ONeMg core.

in detail in the previous paper, therefore we will concentrate on the discussion of the  $Z = 10^{-4}$  and  $Z = 0$  models and the differences with the  $Z = 0.02$  models. Our discussion will focus on two different transition masses that define the SAGB, e.g. the minimum mass for carbon ignition  $M_{\text{up}}$  and the maximum mass for which dredge-up occurs  $M_{\text{ccsn}}$ , which is also the minimum mass for stars that go through advanced burning stages, like neon, oxygen and silicon, and eventually explode as a core collapse supernova.

#### *The dependence of $M_{\text{up}}$ on metallicity*

The dependence of  $M_{\text{up}}$  on metallicity has already been discussed by a number of authors (Becker 1981; Tornambe & Chieffi 1986; Castellani et al. 1990; Cassisi & Castellani 1993; Bono et al. 2000; Girardi et al. 2000). Girardi et al. (2000) find – with a moderate amount of overshooting – that  $M_{\text{up}}$  has a value between 5 and  $6M_{\odot}$  for stars with  $-0.4 < \log Z/Z_{\odot} < 0.2$ , and between 4.5 and  $5M_{\odot}$  for  $\log Z/Z_{\odot} < -0.40$ . A recent study by Siess & Pumo (2006) finds however much higher values



for  $M_{\text{up}}$  ranging from  $\sim 9 M_{\odot}$  for  $Z = 0.02$  to values between 7 and  $8 M_{\odot}$  for  $-3.3 < \log Z / Z_{\odot} < -0.6$ .

In our models we also find different values for  $M_{\text{up}}$ , which is mainly due to the different convection criteria and whether we apply overshooting. For the EVOL/KEPLER models we find  $M_{\text{up}} \sim 7.5 M_{\odot}$  ( $Z = 0.02$ ) decreasing to  $M_{\text{up}} \sim 6 M_{\odot}$  for  $Z = 10^{-4}$ . The STERN models have significantly higher values for  $M_{\text{up}}$ , e.g.  $M_{\text{up}} \sim 9.0 M_{\odot}$  for  $Z = 0.02$  and  $M_{\text{up}} \sim 8.0 M_{\odot}$  for  $Z = 10^{-4}$ .

#### *The dependence of $M_{\text{ccsn}}$ on metallicity*

As described in the previous paper, the main reason why stars enter the thermally pulsing AGB (TPAGB) is the depth of the second dredge-up, which significantly reduces the helium core. If the second dredge-up stalls at the boundary of the helium core, the star can continue its evolution with subsequent burning phases, form an iron core which eventually encounters iron core collapse. On the other hand, if convection is strong enough to overcome the chemical barrier between the envelope and the core, the second dredge-up continues all the way down, until it reaches the helium burning shell. This deep second dredge-up reduces the mass of the helium core to below the Chandrasekhar mass. This different behavior of the second dredge-up gives a sharp bifurcation in the subsequent evolution of the star. The maximum initial mass for which second dredge-up operates is  $M_{\text{ccsn}}$ .

The transition for which stars do not develop a deep second dredge-up and continue their evolution to advanced burning stages and eventually a core collapse supernova behaves in a similar way as  $M_{\text{up}}$ , e.g. for  $Z = 0.02$   $M_{\text{ccsn}} \sim 9.25 M_{\odot}$  (EVOL & KEPLER) or  $M_{\text{ccsn}} \sim 12.4 M_{\odot}$  (STERN) and moves down with lower metallicities. This value changes for different evolutionary codes because of different convection prescriptions, but the basic pattern remains the same, i.e. a sharp transition for stars with and without a deep second dredge-up and an almost linear relation between the initial mass and the maximum and final helium core masses.

The only difference with respect to the pre- and post-second dredge-up core masses are the KEPLER models for  $Z = 0$  that show a reverse trend as shown in the lower panel of Figure 23. They are in agreement with the STERN  $Z = 0$  models, but those show only smaller pre-second dredge-up helium core masses, while the post-second dredge-up core mass is similar to the  $Z = 10^{-4}$  models. This reverse trend in pre-second dredge-up core mass is also shown in the  $\log Z / Z_{\odot} < -2.0$  models in Figure 24.

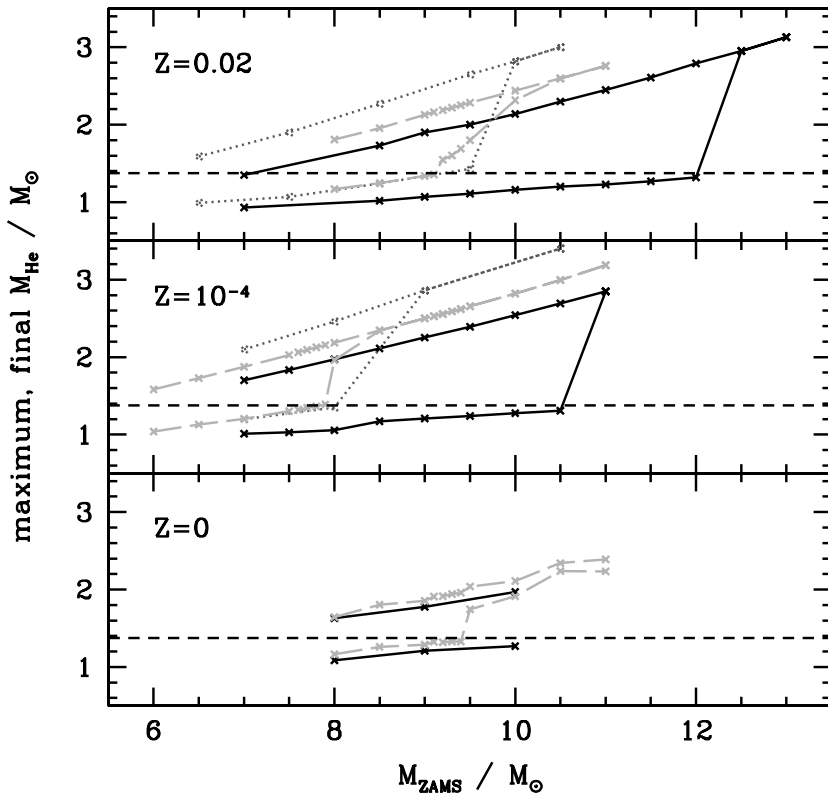


Figure 23. Maximum (upper line) and final (lower line) pre TP-AGB helium core masses for  $Z = 0.02$ ,  $Z = 10^{-4}$  and  $Z = 0$  as a function of the initial mass. The models have been calculated with three different codes (see text). The dotted (grey) line gives the results with the KEPLER code, the dashed (lightgrey) line represents EVOL data and the solid (black) line gives results obtained with STERN. The maximum helium core mass is reached before the onset of the second dredge-up. The difference between a deep second dredge-up and a 'not so deep' second dredge-up gives the difference between stars that evolve to respectively the TP-AGB or the RGB (with all the advanced burning stages until Fe). The used codes give different initial masses until which initial mass the deep second dredge-up does occur. The light dashed horizontal line gives the critical mass for the final helium core for which the star may experience an electron-capture supernova. Note that the core of the star still can grow during the TP-AGB and thus can reach the electron capture limit.

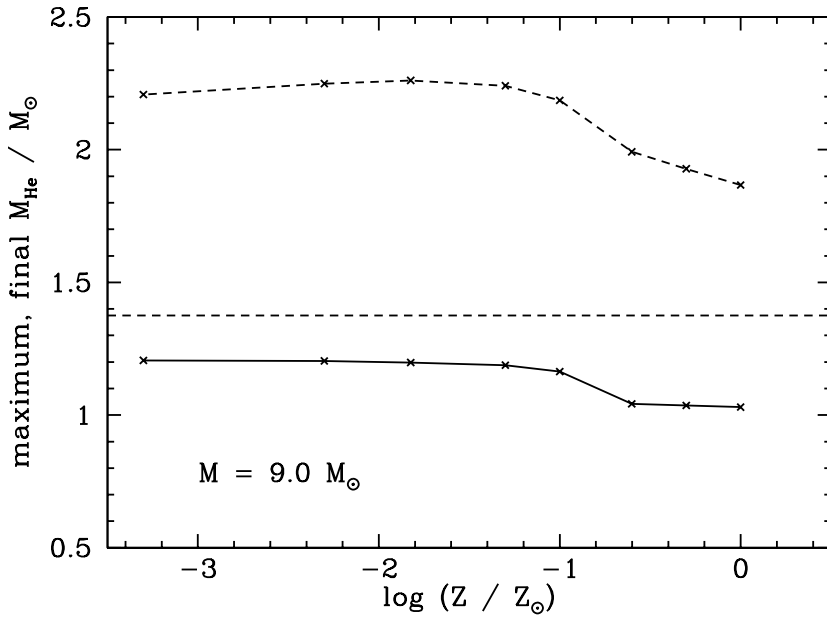


Figure 24. Maximum (dashed line) and final (solid line) pre TP-AGB helium core masses for a  $9M_{\odot}$  model as a function of the initial metallicity. The light dashed horizontal line gives the critical mass for the final helium core for which the star may experience an electron-capture supernova.

### 3.3.2 Pre-TPAGB core masses

To study the effect of metallicity on the core masses in greater detail and to allow for a interpolation over a wide range of initial masses and initial metallicities, we evolved with STERN a set of 8 stars, with a mass of  $9.0 M_{\odot}$ , from ZAMS to early AGB (EAGB) with different metallicities, starting from  $Z = 10^{-5}$  to  $Z = 0.02$ . The effect of the metallicity on the maximum and final helium core masses is shown in Figure 24 and is not difficult to understand: As the metallicity decreases, the opacities are lower, the stars are more luminous and hence develop larger cores (c.f. [Cassisi & Castellani 1993](#); [Siess & Pumo 2006](#)).

Using the results from these three studies, a sequence in mass with  $Z = 0.02$  (EVOL), another sequence in mass with  $Z = 10^{-4}$  (EVOL) and a sequence in metallicity with  $M = 9.0 M_{\odot}$  (STERN – which translates very well into a EVOL or KEPLER sequence of  $M = 7.3 M_{\odot}$ ), we were able to construct a diagram which shows the core masses just after the second dredge-up for a much larger grid. To construct this diagram,

we used the characteristic linear behavior of the pre- and post-2DUP core mass as a function of the initial mass and used the sequence along the metallicity axis to determine the offset for the core mass. An interpolation technique was used to create a dense grid along all axes, resulting in 80 grid points along the mass axis ( $3.0 < M/M_{\odot} < 11.0$ ) and 41 grid points along the metallicity axis ( $-4.0 < \log Z/Z_{\odot} < 0.0$ ).

The resulting diagram with the post second dredge-up core masses, which is almost identical to the core mass at the first thermal pulse, is shown in Figure 25. The diagram is divided into three regions, which show the carbon oxygen cores ( $M_c < 1.06 M_{\odot}$ ), the oxygen neon cores ( $1.06 < M_c/M_{\odot} < 1.375$ ) and the cores that are massive enough to explode as a classical core collapse supernova ( $M_c > 1.375$ , Woosley & Weaver 1995). The effect of the metallicity on the core mass is significant and the figure shows the almost linear behavior of the core mass with the initial mass over the entire metallicity range. The contour lines show lines of constant core mass. The variation of  $M_{\text{up}}$  with metallicity is shown as the border between models with a CO core and models with a ONe core.

Using the same technique we also constructed similar data sets for the pre-2DUP core mass, the envelope mass and the post-2DUP envelope composition, which significantly differ in hydrogen and helium abundance due to the enrichment of the envelope by the first and/or second dredge-up episodes.

### 3.4 EVOLUTION ON THE TPAGB

We used the results of the previous section (i.e. core mass as a function of the initial mass and metallicity, envelope mass and the hydrogen abundance of the envelope) as input for the synthetic code to calculate the evolution through the TP-AGB phase.

#### 3.4.1 *Input variations*

Two effects are parametrized in the code, the mass loss rate and the efficiency of the third dredge-up. They are important for the evolution of these stars but are uncertain. Using the synthetic code we study the effects of this uncertain input physics and try to put some constraints on this phase of the evolution.

#### *Mass loss rate*

The mass loss rate for massive AGB stars is quite uncertain (Habing 1996). Commonly used mass loss recipes are Vassiliadis & Wood (1993) and Bloeker (1995), but both are derived for low mass AGB stars and can hardly be extrapolated to the massive AGB star mass range. Some

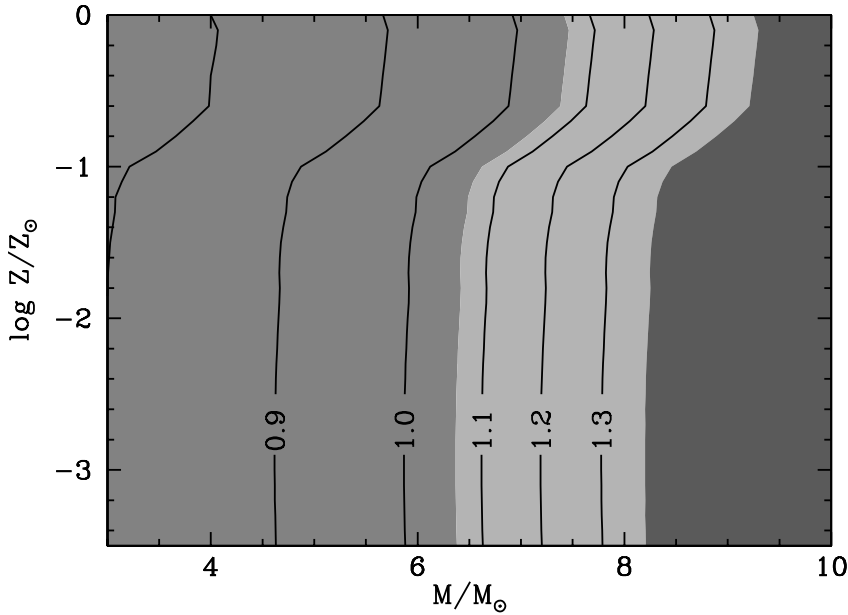


Figure 25. Diagram which shows the post second dredge-up core masses as a function of the initial mass and the metallicity. The contour lines show lines of constant core mass. The diagram is divided into three regions, which show the carbon oxygen cores ( $M_c < 1.06 M_\odot$ ), the oxygen neon cores ( $1.06 < M_c / M_\odot < 1.375$ ) and the cores that are massive enough to explode as a classical core collapse supernova ( $M_c > 1.375$ ). The effect of the metallicity on the core mass is clearly seen as well as the almost linear behavior of the core mass with the initial mass over the entire range in mass and metallicity.

progress has been made by [van Loon et al. \(2005, vL\)](#) who derived the mass loss for stars in this mass range based on observations of dust-enshrouded oxygen-rich, M-type AGB stars and red supergiants from the large Magellanic cloud and the galaxy. It is a function of the luminosity ( $L$ ) and the temperature ( $T$ ). This mass loss rate is not explicitly dependent on the metallicity, although they observed both the galaxy as the LMC. They were able to reproduce the observed data for the LMC and the galaxy with this single formula, without taking into account the difference in metallicity between the two samples. Note that they give three different formulae in their paper, e.g. one fitted to a sample of AGB stars with  $\log L/L_\odot < 4.9$ , one fitted to a sample of RSG with  $\log L/L_\odot > 4.9$  and one combined formula for both AGB and RSG. We choose to use the RSG formula, since most of the models we are interested in have at the beginning of the TPSAGB

already a luminosity larger than  $\log L/L_{\odot} = 4.9$ . We use this empirical mass loss rate as our standard rate. To study the effects of a complete different mass loss rate on our results, we also used the mass loss rate by [Vassiliadis & Wood \(1993, hereafter VW\)](#).

Both mass loss rates, e.g. vL and VW, do not have an explicit dependence on the metallicity. However, [Bowen & Willson \(1991\)](#) and [Zijlstra \(2004\)](#) argue that dust-driven mass loss breaks down at  $Z = 0.1Z_{\odot}$ , and thus that mass loss rates for low metallicity stars will be radiation driven and may be significantly lower than for stars of solar metallicity. Whether this assumption is correct for those stars is not clear (see for a review [van Loon 2005](#)), as these stars are thought to be oxygen rich which prevents the formation of carbon dominated dust, but since these stars can evolve to quite low temperatures, molecular opacities will come into play. Evidence for a much lower mass loss rate at  $[\text{Fe}/\text{H}] < -1$  comes from the deficiency of planetary nebulae in metal poor dwarf galaxies ([Zijlstra 2004, 2006](#)).

To study the effect of radiation driven wind, we did two studies, one for each mass loss rate, where we use a scaling with metallicity over the whole metallicity range that is commonly used for radiation driven winds (eq. 3.3).

#### *Thermal pulses and third dredge-up*

Another uncertainty is the phenomenon of thermal pulses and the adherent third dredge-up ([Doherty & Lattanzio 2006](#); [Siess 2006](#); [Poelarends et al. 2006](#)). When this third dredge-up occurs, it influences both the growth of the core and the metallicity of the envelope, which in turn could affect dust formation and the mass loss rate. No or almost negligible third dredge-up and a low mass loss rate would imply probably a wide channel for ECSN and even the possibility of SN1.5, the thermonuclear explosion of carbon oxygen cores. Very efficient third dredge-up and a high mass loss rate would imply a very narrow channel for electron capture supernovae.

Almost nothing is known about the efficiency of the third dredge-up in this mass range, especially for low metallicities. [Herwig \(2004a,b\)](#) studied the properties of dredge-up and envelope burning in very metal poor stars ( $Z = 10^{-4}$ ) with masses between 2 and  $6 M_{\odot}$ . He finds very efficient dredge-up, with  $\lambda > 1$  for the majority of the thermal pulses, and characteristics of a so-called “hot” dredge-up, corrosive convective H-shell burning that penetrates deep into the intershell and sometimes even the core. This *hot* dredge-up is more effective at higher core masses, which is relevant for this study.

To account for these different options, we use similar input as in P07, e.g. a lambda parametrization according to [Karakas et al. \(2002\)](#), extrapolated to higher masses and lower metallicities, and a lambda

Table 5. Summary of the scenarios.

|      | Massloss |    | $\lambda$ parametrization |               | Additional<br>Z-scaling |
|------|----------|----|---------------------------|---------------|-------------------------|
|      | vL       | VW | Karakas (mod.)            | $\lambda = 0$ |                         |
| vL   | x        |    | x                         |               |                         |
| vLZ  | x        |    | x                         |               | x                       |
| vLZo | x        |    |                           | x             | x                       |
| vLo  | x        |    |                           | x             |                         |
| VW   |          | x  | x                         |               |                         |
| VWZ  |          | x  | x                         |               | x                       |

value of zero for all initial masses and all initial metallicities.

We refer in the rest of this paper to these models as vL (standard models: with parametrized dredge-up and mass loss according to [van Loon et al. 2005](#)), vLZ (same as before but with the Z-scaling of eq. 3.3), vLZo (same as before, with Z-scaling and  $\lambda = 0$ ) and vLo (as standard but with  $\lambda = 0$ ). And for the mass loss rate according to [Vassiliadis & Wood \(1993\)](#): VW and VWZ (with parametrized dredge-up and resp. without and with the Z-scaling). This is also summarized in Table 5.

### 3.4.2 Evolution of the core toward WD or SN

Although we do not follow the evolution of the core, e.g. the degeneracy, the central temperature and the central density, we have two basic assumptions that we list below:

- A star that enters the TPAGB with a carbon oxygen core, retains a carbon oxygen core to the end of its evolution, although its core can exceed  $1.06 M_{\odot}$ , which is the threshold for carbon ignition. This scenario is sketched in Figure 26 (line A) which shows a cooling core, due to neutrino losses, that, although more massive than  $1.06 M_{\odot}$  is too cool to ignite carbon (dashed line). It is well possible that the temperature inversion is removed, which means that the central temperature is the highest temperature inside the star and the lines of maximum temperature (line B) and central temperature merge, as is shown in the figure. [Zijlstra \(2004\)](#) argued that, following the suggestion of [Iben & Renzini \(1983\)](#), at low metallicities the carbon oxygen core might be able to grow to the Chandrasekhar mass without igniting neon. When the Chandrasekhar mass is reached, carbon will ignite in a strongly degenerate core, causing a thermonuclear explosion similar to a

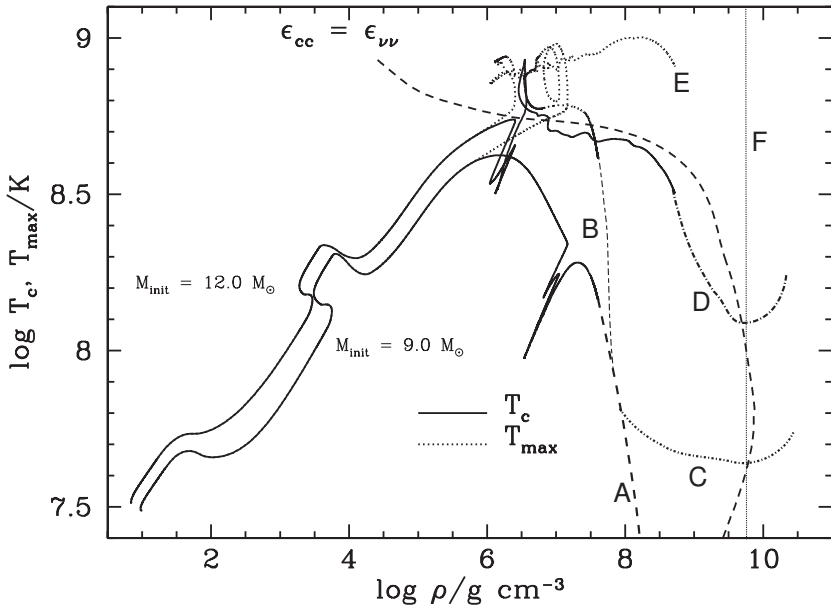


Figure 26. Possible evolutionary scenarios in the  $\rho_c - T_c$  diagram for  $Z = 0.02$ . The evolutionary paths of a  $9M_\odot$  and a  $12M_\odot$  star are plotted, both calculated with the STERN code. The solid lines represent the central conditions, the dotted lines represent the conditions at maximum temperature (if a temperature inversion is present). Masses are indicated. The line where energy gain due to carbon burning equals the energy loss due to neutrino cooling is indicated with a dashed line. As can be seen, the  $9M_\odot$  star has two weak carbon flashes, which do not reach the core, the  $12M_\odot$  star has extensive carbon burning which does reach the core. The possible evolution beyond the detailed models is indicated by a couple of lines (A, B, C and D) which is discussed in the text. The vertical line marked 'F' indicates the density at which electron captures on  $^{20}\text{Ne}$  start, causing a reduction of the pressure inside the core, which leads to a collapse.

Type Ia. [Iben & Renzini \(1983\)](#) called this type of explosion a Type 1.5, and the evolution in the  $\rho_c - T_c$  diagram is sketched with line C.

- The other assumption is similar to the previous one, but then for a neon oxygen core that grows more massive than the neon burning threshold ( $1.375M_\odot$ , [Nomoto 1983](#)). As shown in Figure 26, the maximum temperature inside the star – this is not at the center due to a temperature inversion – drops after carbon burning (line



E), and we assume this will continue, so that neon ignition is prevented, although it approaches the neon burning threshold in mass. We further assume that while the core grows, density increases (line D) and reaches the density for which electron captures on  $^{20}\text{Ne}$  and  $^{24}\text{Mg}$  (see next paragraph) come into play (line F), causing the core to collapse, subsequently followed by a supernova explosion (Nomoto et al. 1979; Miyaji et al. 1980a,b; Nomoto 1981, 1982, 1983, 1984a,b, 1985; Miyaji & Nomoto 1987; Nomoto 1987a; Hillebrandt et al. 1984; Wanajo et al. 2003; Kitaura et al. 2006; Wanajo 2005).

In a recent paper Gutiérrez et al. (2005) cast some doubt on this scenario. Previous calculations of the gravitational collapse of oxygen neon cores (Gutiérrez et al. 1996; Miyaji et al. 1980a,b) required a high abundance of  $^{24}\text{Mg}$  which does not occur in recent SAGB models (Ritossa et al. 1996; Siess 2006). Interestingly they found that relatively small abundances of unburnt carbon ( $X(^{12}\text{C}) \sim 0.015$ ) in the core could trigger a thermonuclear explosion at relatively low density ( $\sim 1 \times 10^9 \text{gcm}^{-3}$ ). Our SAGB models show a Mg abundance by mass of at most 7% and a carbon abundance of at most 4%, in which case the effect of electron captures on  $^{24}\text{Mg}$  would be insignificant (however, electron captures on  $^{20}\text{Ne}$  would still give rise to an ECSN) but the ignition of the residual carbon could well lead to a thermonuclear explosion before this stage is ever reached (line D).

### 3.5 RESULTS

Figure 27 shows the outcome of the evolution in the mass metallicity plane for our preferred model (vLZ), and Figure 28 shows the outcome of the evolution for all applied combinations of mass loss prescriptions and third dredge-up parametrization. The grey part of each diagram shows massive carbon oxygen white dwarf, the lightgrey part massive neon oxygen white dwarf, the white part the models that evolve into an electron capture supernova and the darkgrey part shows the models that are assumed to go through advanced burning stages before they collapse and explode.

#### 3.5.1 Mass loss

Figure 27 and Fig. 28A and B show models (vL and vLZ) that are evolved with van Loon's mass loss rate and a lambda parametrization according to Karakas et al. (2002), but with a different behavior for the dependence of the mass loss with metallicity. Panel 28A, where the mass loss does not explicitly scale with the metallicity (vL), shows that only the most massive neon oxygen cores are able to reach densities

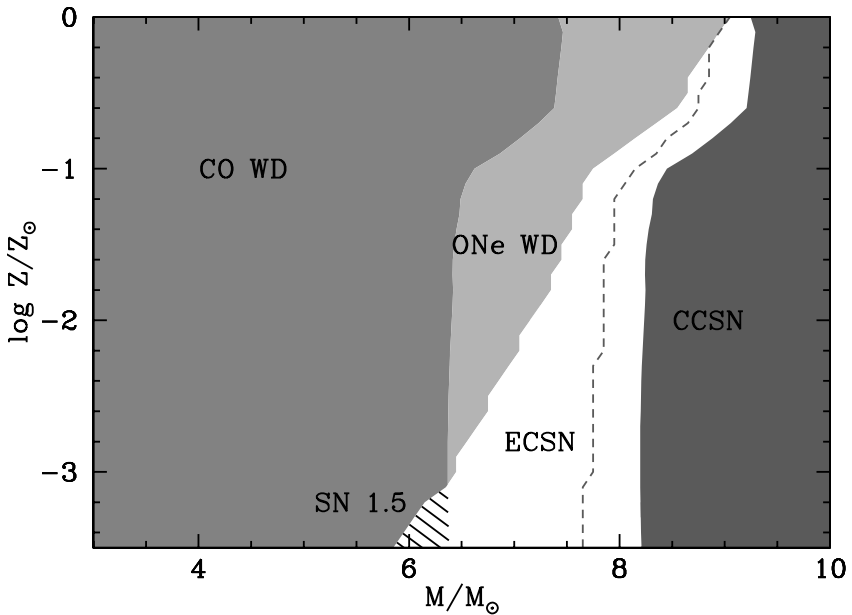


Figure 27. Final outcome of the evolution of the preferred model (vLZ) as a function of the initial mass and the metallicity calculated with the synthetic code, using the vL mass loss rate with a parametrized dredge-up efficiency and with a metallicity dependence of the mass loss. The diagram is divided into four regions, which show the carbon oxygen cores (CO WD, grey;  $M_{c,\text{init}} < 1.06 M_{\odot}$ ), the oxygen neon cores (ONe WD, lightgrey;  $1.06 < M_{c,\text{init}} / M_{\odot} < 1.375$ ), the cores that exploded as an electron capture supernova (ECSN, white) and the cores that are massive enough to explode as a classical core collapse supernova (CCSN, darkgrey;  $M_{c,\text{init}} > 1.375$ ). The shaded region indicates the SN1.5 range. The minimum ECSN mass for the same scenario but without the metallicity scaling in the stellar wind (vL) is shown with a dashed line.

high enough for electron captures on  $^{20}\text{Ne}$  and  $^{24}\text{Mg}$ , and that the mass range for which this occurs remains small over the whole metallicity range ( $\sim 0.25 - 0.5 M_{\odot}$ ). The rest of the neon oxygen cores form massive neon oxygen white dwarf as indicated by the contour lines which show the final mass. The situation in Panel 28B (vLZ) is different because the mass loss rate decreases for lower metallicities caused by the square root scaling. The window for electron capture supernovae increases with low metallicities, until at  $\log Z / Z_{\odot} = 10^{-3}$  all neon oxygen cores are able to grow to reach the Chandrasekhar mass. In this scenario with decreasing metallicity we see less and less neon oxygen white

dwarfs and increasing numbers of supernovae from this mass range. For metallicities lower than  $\log Z / Z_{\odot} = -3$  the most massive CO cores are able to explode as a SN<sub>1.5</sub>.

The results for VW and VWZ are almost similar to vL and vLZ as can be seen in Figure 28. Panels E and F can be directly compared to respectively Panels A and B. Panel E shows a very narrow range for ECSN, which gets even more narrow at lower metallicities, due to the high luminosities that are reached.

### 3.5.2 Dredge-up

Comparing Figure 28 Panel A with Panel C (vLo) gives us an idea what the effect is of the third dredge-up when no mass loss scaling with metallicity is applied. In these scenario's van Loon's mass loss rate is used. Panel A shows a parametrization of  $\lambda$  according to Karakas et al. (2002) and Panel B show a scenario with  $\lambda = 0$ . The range in which electron capture supernovae can occur with very inefficient dredge-up ( $\lambda = 0$ ) is wider than for the non-zero  $\lambda$  case over the whole metallicity range. The reason that it significantly widens for lower metallicities is that the core is able to grow very efficient because there is no dredge-up, hence stars with initially lower mass are able to reach the Chandrasekhar mass. For metallicities lower than  $\log Z / Z_{\odot} = -2.5$  the most massive CO cores are able to explode as a SN<sub>1.5</sub>.

When we compare vLZ (Panel B) with the scenario in Panel D (vLZo), where we also apply the scaling of the mass loss rate with metallicity but assume that there is no third dredge-up, so that the core growth is very efficient, the number of ECSN increases strongly, and this scenario gives rise to a significant number of SN<sub>1.5</sub>, degenerate carbon oxygen cores that reach the Chandrasekhar mass, while still surrounded by a hydrogen envelope. In this scenario, massive neon oxygen white dwarf will only be formed in environments with metallicities between solar and  $\log Z / Z_{\odot} = -0.6$ .

### 3.5.3 TP-SAGB tip luminosity

A key observational quantity is the luminosity at the tip of the TP-AGB. Figure 29 shows for our set of synthetic models the luminosities at the tip of the TPSAGB in a diagram as a function of the initial mass and initial metallicity. With increasing initial mass, the luminosity increases as expected, and our models show an increase in luminosity with decreasing mass, which is partly due to the more massive cores. Compared to a stellar population of solar metallicity, a population of very low metallicity will thus have more luminous TPAGB stars (c.f. Bowen & Willson 1991; Zijlstra 2004). Note that the most massive TP-SAGB stars, those which will explode as an ECSN, are more luminous

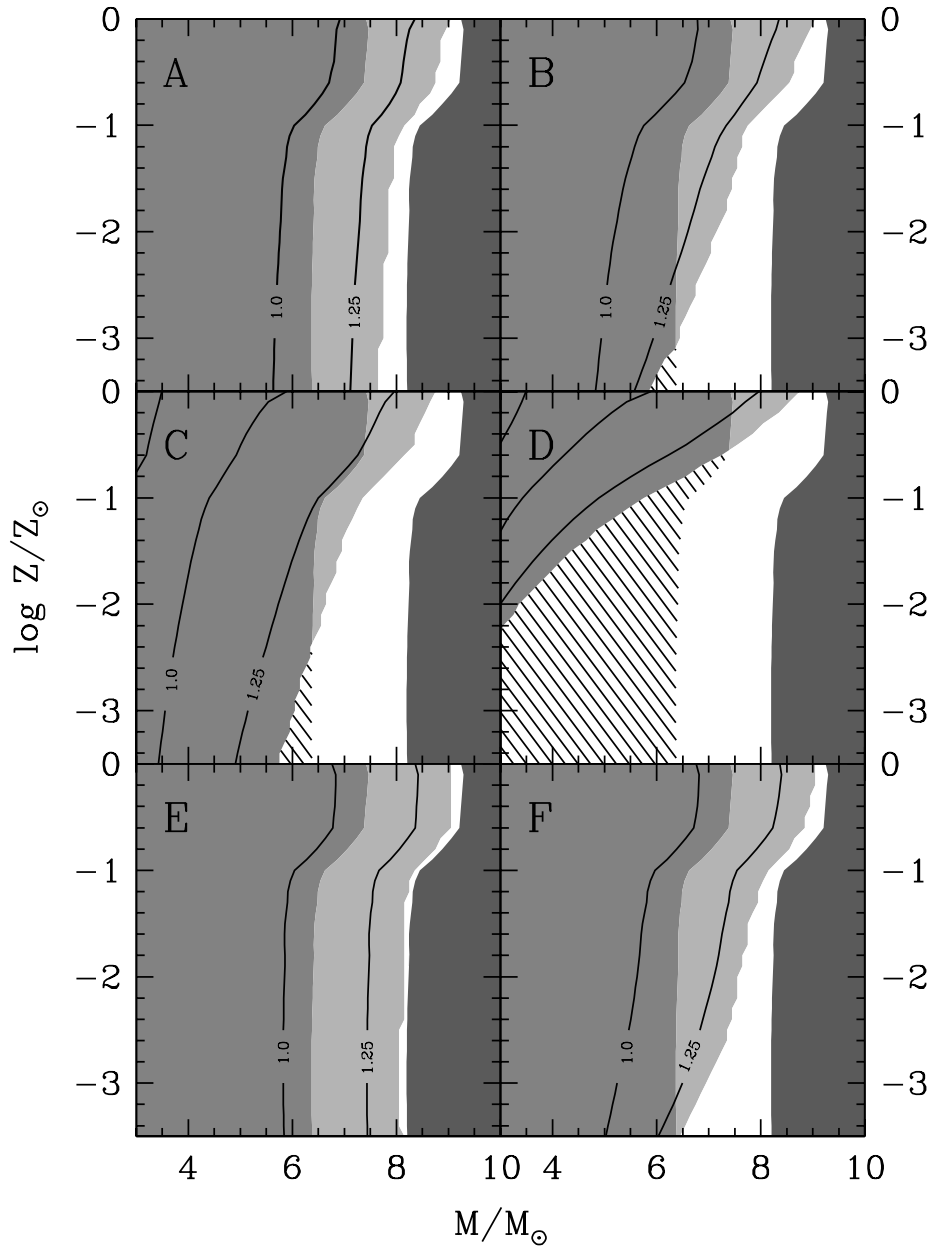
Figure 28. (*Opposite page:*) Diagram which shows the final outcome of the evolution as a function of the initial mass and the metallicity calculated with the synthetic code, using the vL mass loss rate with a parametrized dredge-up efficiency (Panels A & B) and resp. without and with a metallicity dependence of the mass loss (vL – Panel A, vLZ – Panel B) and with no dredge-up (lower two panels) and resp. with or without a metallicity dependence of the mass loss (vLZo – Panel C, vLo – Panel D). Panel E & F show the scenario with VW mass loss rate, the parametrized dredge-up and respectively without and with a metallicity dependence of the mass loss. The contour lines show lines of the final White Dwarf mass ( $M_{\text{fin}} = 0.75, 1.0$  and  $1.25 M_{\odot}$ ). The diagram is divided into four regions, which show the carbon oxygen cores (grey;  $M_{\text{c,init}} < 1.06 M_{\odot}$ ), the oxygen neon cores (lightgrey;  $1.06 < M_{\text{c,init}} / M_{\odot} < 1.375$ ), the cores that exploded as an electron capture supernova (white) and the cores that are massive enough to explode as a classical core collapse supernova (darkgrey;  $M_{\text{c,init}} > 1.375$ ). The shaded region in Panel B, C and D indicates the SN1.5 range.

than CCSN, just at the other side of the “second dredge-up boundary” (c.f. Eldridge & Tout 2004a,b, and Figure 16 in Chapter 2)

#### 3.5.4 Initial-final mass relation and envelope mass at explosion

Figure 30 shows the final mass at the end of the TP-SAGB evolution as a function of initial mass and metallicity. All stars that evolve to a white dwarf have final masses below  $1.375 M_{\odot}$ . Stars that explode as ECSN show a large variety of pre-supernova masses. Panel A shows that for the very narrow mass range in which ECSN can occur, the final envelope mass varies from almost negligible for the least massive ECSN, to very massive envelopes that hardly suffered any mass loss on the TPSAGB, for the most massive ECSN. Panel B shows that the SN1.5 that can occur in the mass range between  $6$  and  $6.5 M_{\odot}$  for  $\log Z / Z_{\odot} < -3$ , are expected to have envelope masses between  $0 M_{\odot}$  and  $4.5 M_{\odot}$ . This implies a dense shell of circum stellar material (CSM) surrounding the star – which is lost during the TPSAGB phase – with a mass between  $0$  and  $4.5 M_{\odot}$ . The same values for the final envelope mass are expected from Panel C, while Panel D gives  $7 M_{\odot}$  as the maximum envelope mass for SN Type 1.5. Expected envelope masses for ECSN are rather high in this scenario, especially for low metallicities, while all final masses can be expected in solar or nearly solar metallicities. The results with VW mass loss rate resemble basically the results obtained by applying vL.

Figure 31 shows how the shape of the initial-final mass relation changes with metallicity for our preferred model (vLZ). At lower metallicity the relation between the initial and final mass is much shallower than for higher metallicities, which gives rise to a large variety of pre-



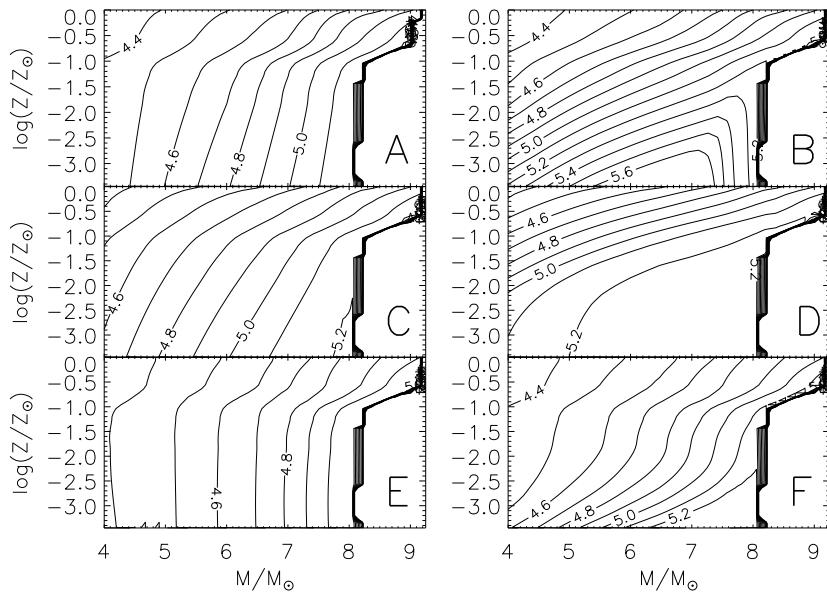


Figure 29. Diagram which shows the maximum luminosity on the TPSAGB as a function of the initial mass and the metallicity, calculated with the synthetic code, using the  $vL$  mass loss rate with a parametrized dredge-up efficiency (Panels A & B) and resp. without and with a metallicity dependence of the mass loss ( $vL$  – Panel A,  $vLZ$  – Panel B) and with no dredge-up (lower two panels) and resp. with or without a metallicity dependence of the mass loss ( $vLZo$  – Panel C,  $vLo$  – Panel D). Panel E & F show the scenario with VW mass loss rate, the parametrized dredge-up and respectively without and with a metallicity dependence of the mass loss. The part to the right that does not contain data are the models that explode as a core-collapse supernova.

supernova masses in a wide initial mass range. The initial-final mass relation is much steeper for higher metallicities.

Table 6 summarizes the relative numbers of CO and ONe white dwarf and of ECSN and CCSN for the different TPSAGB scenarios investigated. Regardless of which scenario, the CO white dwarfs always dominate the sample of white dwarfs, leaving only room for at most 2.5% ONe white dwarfs. At the other side of the mass spectrum, the CCSN dominate over ECSN, most clearly at solar metallicity, and less, but still dominant at lower metallicity. Interesting, but probably not realistic, is the  $vLZo$  scenario which produces significant numbers of SN1.5; up to 15% of all CO white dwarf at  $\log Z/Z_{\odot} = -3.0$  would be able to explode as a supernova.

Table 6. Summary of the models. The first and second column list the mass loss rate and the metallicity, the third and fourth column list the percentages of C/O white dwarf and ONe white dwarfs (with a lower limit at  $1 M_{\odot}$ ). The fifth, sixth and seventh column list the percentages of SN<sub>1.5</sub>, ECSN and CCSN. A Salpeter IMF is assumed. Entries marked with an asterisk give the percentage of CO white dwarf that were not able to explode as a SN<sub>1.5</sub>. Our fiducial model (vLZ) is set in *italic*.

|            | log $Z / Z_{\odot}$ | WD     |      | SN                |       |       |
|------------|---------------------|--------|------|-------------------|-------|-------|
|            |                     | C/O    | ONe  | SN <sub>1.5</sub> | ECSN  | CCSN  |
| <i>vLZ</i> | 0.00                | 98.30  | 1.70 | 0.00              | 2.84  | 97.16 |
|            | -1.00               | 98.35  | 1.65 | 0.00              | 12.94 | 87.06 |
|            | -2.00               | 98.72  | 1.28 | 0.00              | 20.35 | 79.65 |
|            | -3.00               | 99.76  | 0.24 | 0.00              | 32.07 | 67.93 |
| vL         | 0.00                | 98.30  | 1.70 | 0.00              | 2.84  | 97.16 |
|            | -1.00               | 97.93  | 2.07 | 0.00              | 5.13  | 94.87 |
|            | -2.00               | 97.86  | 2.14 | 0.00              | 6.88  | 93.12 |
|            | -3.00               | 97.90  | 2.10 | 0.00              | 8.15  | 91.85 |
| vLo        | 0.00                | 98.54  | 1.46 | 0.00              | 8.53  | 91.47 |
|            | -1.00               | 98.84  | 1.16 | 0.00              | 20.35 | 79.65 |
|            | -2.00               | 99.48  | 0.52 | 0.00              | 29.23 | 70.77 |
|            | -3.00               | 99.47  | 0.00 | 6.61              | 32.02 | 61.37 |
| vLZo       | 0.00                | 98.54  | 1.46 | 0.00              | 8.53  | 91.47 |
|            | -1.00               | 98.34* | 0.00 | 19.05             | 27.23 | 53.72 |
|            | -2.00               | 88.01* | 0.00 | 61.64             | 13.11 | 25.24 |
|            | -3.00               | 84.23* | 0.00 | 67.66             | 11.09 | 21.25 |
| VW         | 0.00                | 98.30  | 1.70 | 0.00              | 2.84  | 97.16 |
|            | -1.00               | 97.73  | 2.27 | 0.00              | 1.05  | 98.95 |
|            | -2.00               | 97.55  | 2.45 | 0.00              | 0.70  | 99.30 |
|            | -3.00               | 97.58  | 2.42 | 0.00              | 2.01  | 97.99 |
| VWZ        | 0.00                | 98.30  | 1.70 | 0.00              | 2.84  | 97.16 |
|            | -1.00               | 97.93  | 2.07 | 0.00              | 5.13  | 94.87 |
|            | -2.00               | 98.20  | 1.80 | 0.00              | 12.81 | 87.19 |
|            | -3.00               | 98.94  | 1.06 | 0.00              | 23.37 | 76.63 |

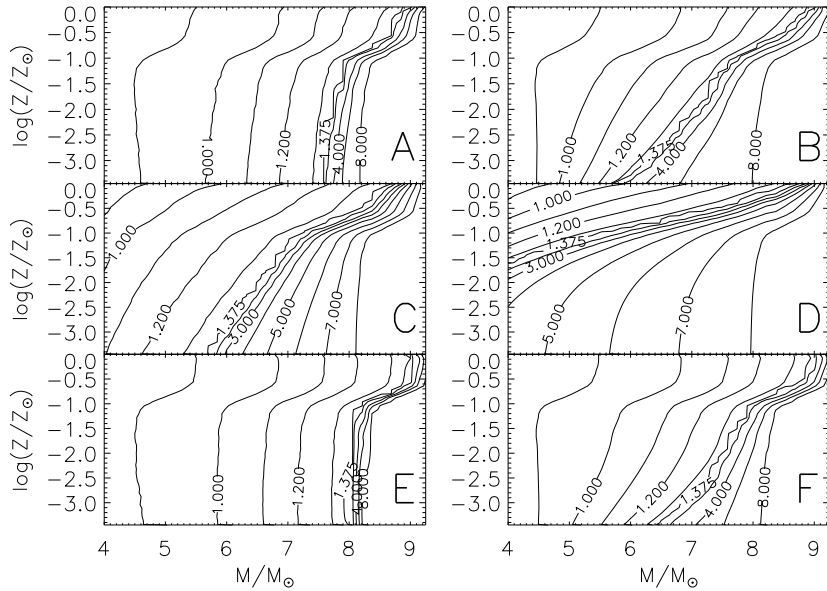


Figure 30. Diagram which shows the final mass as a function of the initial mass and the metallicity, calculated with the synthetic code. The naming of the panels is equal to Figures 28 and 29. Contour lines are drawn for 0.9, 1.0, 1.1, 1.2, 1.3, 1.375, 2, 3, 4, 5, 6, 7 and  $8 M_{\odot}$ .

### 3.5.5 *Supernova rate*

The effect of the different scenarios on the supernova rate is showed in Figure 32. Assuming a Salpeter initial mass function with  $\alpha = -2.35$ , the percentage of stars exploding as electron capture supernova on the TPSAGB, compared to the total number of supernovae is shown in the left panel. Our standard model shows a percentage that does not exceed 10%, while vLZ reaches 75%, of which some are supernovae of Type 1.5 and other electron capture supernovae of Type II. This scenario, which gives similar numbers to what Zijlstra (2004) predicted, can be ruled out, since we would observe a lot of these supernovae at not all to low metallicity and the imprints of the nucleosynthesis would be clearly visible, which are both not the case. The VW scenario gives lower supernova rates than our standard model, the rest is higher. All scenarios that have a metallicity dependence in the mass loss rate follow almost the same trend, starting at low supernova rates for solar metallicity, and rising for lower metallicities, roughly to values between 30% and 40%. If the mass loss rate at a metallicity of  $[\text{Fe}/\text{H}] < -1.0$  is significantly reduced (c.f. Bowen & Willson 1991; Zijlstra 2006), we can



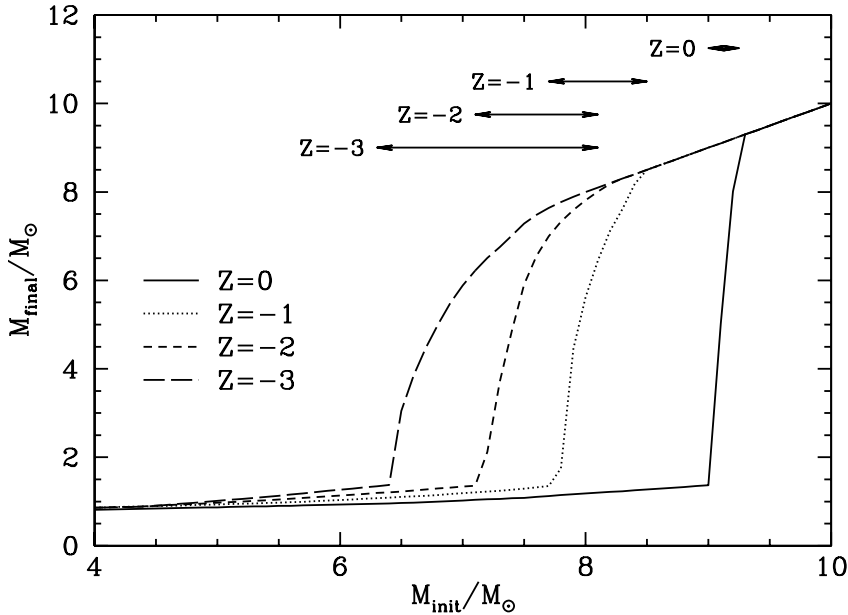


Figure 31. Initial final mass relation according the preferred model (vLZ) at four different metallicities ( $\log Z/Z_{\odot} = 0, -1, -2, -3$ ). The mass range over which ECSN occur for is indicated by arrows.

expect almost half of the supernovae we see at low metallicity to be an ECSN or SN<sub>1.5</sub>.

### 3.6 OBSERVATIONAL IMPLICATIONS

The results obtained above imply that the evolution of stars in the mass range  $5\text{--}10 M_{\odot}$  may proceed very differently at low metallicity, compared to the currently observable evolution of such stars in the Milky Way. This may complement the picture of more massive stars evolving very differently from their high metallicity counterparts: Due to a weakening of the winds of hot stars at low metallicity (Vink & de Koter 2005), mass loss induced angular momentum loss is avoided, and the stars may retain their initial angular momentum. Yoon & Langer (2005) and Yoon et al. (2007) found that the most rapidly rotating metal poor massive stars may evolve quasi-chemically homogeneous, with the consequence that such stars may form black hole when their initial mass is larger than  $\sim 10 M_{\odot}$ . In this respect, the models presented here only correspond to probably more numerous low metallicity stars which are not born with extreme rotation.

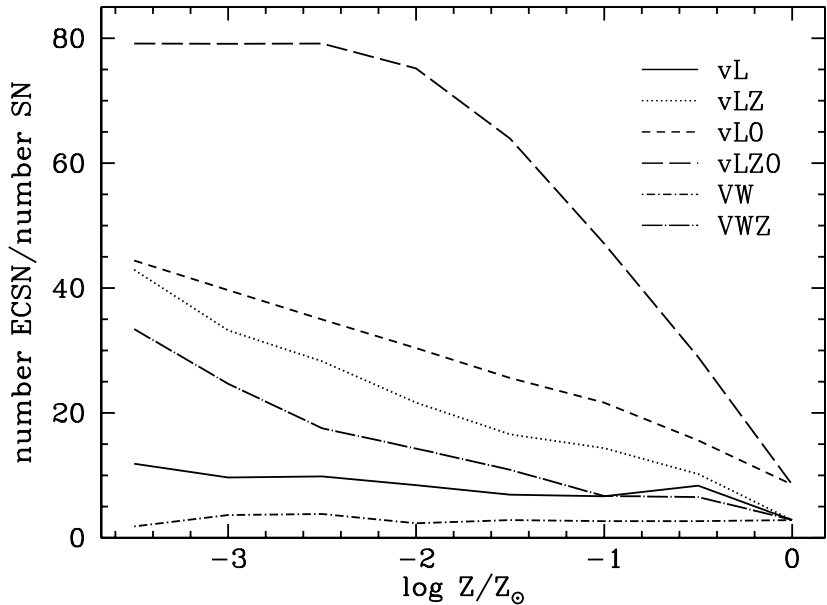


Figure 32. Number of ECSN over the total number of SN  $\times 100$  as a function of the initial metallicity for the different scenarios outlined in the text.

While the very rapidly rotating massive metal poor stars may give rise to long gamma-ray bursts (Yoon et al. 2007) — which can be observed out to very large redshift —, direct observations of the metal-poor stars modeled here are very difficult for metallicities smaller than that of the SMC (about  $Z_{\odot}/5$ ). In fact, in the local universe, the number of massive stars with a metallicity of  $Z_{\odot}/10$  is down by two orders of magnitude, that with  $Z_{\odot}/100$  by four orders of magnitude, compared to solar metallicity stars (Langer & Norman 2006). Thus, e.g., direct observations of low metallicity ECSNe are not very likely. However, due to their potentially large number at low metallicity, the ECSNe may have left traces which are observable today.

### 3.6.1 Neutron stars in globular clusters

Typically, when a neutron star is born in a supernova in the local universe, it obtains a natal kick which leads to a space velocity in excess of  $100\text{--}200 \text{ km s}^{-1}$  (Arzoumanian et al. 2002). However, it has been argued by Podsiadlowski et al. (2004) that ECSNe might produce neutron stars with a low kick velocity. Although somewhat speculative, this hypothesis, in the light of the results of this paper, would imply that

at low metallicity, a large fraction of neutron stars — for  $\log Z/Z_{\odot} \lesssim -3$  even the majority — might be born with a low kick velocity.

This scenario may have implications for the problem of neutron star retention in Galactic globular clusters. The large number of neutron stars found in these clusters (cf. [Pooley et al. 2003](#)) appears difficult to reconcile with standard population synthesis calculation ([Pfahl et al. 2002a](#)), even though [Podsiadlowski et al. \(2004\)](#) discuss that an enhanced number of ECSNe in close binary systems might alleviate this problem.

Most Galactic globular clusters have metallicities in the range  $-0.5 > \log Z/Z_{\odot} > -2.5$ . Assuming low kicks from ECSNe, our fiducial model predicts about 20% of all neutron stars to produce low kicks at  $\log Z/Z_{\odot} = -1.5$ , and about 30% at  $\log Z/Z_{\odot} = -2.5$  (cf. [Fig. 27](#)). To compare these numbers with the number of neutron stars found in globular clusters is complex, as it involves considerations of the dynamical evolution of these clusters and massive close binary evolution (e.g., [Kuranov & Postnov 2006](#)). However, such large numbers of low-kick neutron stars potentially produced by low- $Z$  ECSNe might significantly increase the number of predicted neutron stars in globular clusters.

### 3.6.2 *Polluted metal poor stars*

While it may be difficult to directly observe metal-poor SAGB stars, it is likely that their nucleosynthesis products are observable in low mass binary companions which are still observable today — analogous to the class of Barium-stars in our Galaxy (e.g., [Allen & Barbay 2006](#)). Indeed, the analysis of extremely metal poor stars is thought to contain the key to understand the variety of nucleosynthesis events during the early evolution of the Milky Way (see [Beers & Christlieb 2005](#) and [Jonsson et al. 2006](#) for a review).

There are attempts in the literature to connect the models presented above with extremely metal-poor stars which are enriched with  $r$ - and  $s$ -rich matter. In a close binary system, the  $s$ -process material would be produced during the thermal pulses by the SAGB star, and transferred to the companion by its stellar wind. The  $r$ -process material might be produced in the explosion of the SAGB star, if it evolves into an ECSN ([Wanajo et al. 2006](#)). Indeed, ECSNe ([Wanajo et al. 2003](#)), or more broadly stars with initial masses of the order of  $10 M_{\odot}$  ([Ishimaru et al. 2004](#)) have been suggested as  $r$ -process site. The efficiency of accreting matter from the exploding star onto the companion may be low ([Marietta et al. 2000](#)), but the expected low explosion energy ([Kitaura et al. 2006](#)) may help to overcome this problem.

Many of the observed  $r$ - and  $s$ -rich metal-poor stars are highly enriched in carbon. To accommodate this in the scenario outlined above might require that hot-bottom burning is avoided during the initial TP-SAGB evolution, as hot-bottom burning is expected to convert most

of the carbon, which is injected into the stellar envelope by the 3rd dredge-up, into nitrogen. The currently available models are not detailed enough to tell whether this is indeed possible or not. In Type 1.5 supernovae, on the other hand, a carbon enrichment is more easily possible, since the explosive carbon burning is expected to be incomplete. Whether or not such supernovae would produce any  $r$ -process material, however, is currently debated.

### 3.6.3 *Peculiar supernovae*

As argued by Po7, it is tempting, but not yet conclusive, to identify subluminous Type IIP supernovae with ECSNe. Here, we want to briefly discuss the possibility to observe Type 1.5 supernovae, which our models predict to occur at low metallicity. In principle, Type 1.5 supernovae are expected to resemble Type II supernovae during maximum light due to their hydrogen-rich envelope, but contain a core which is practically a Type Ia supernova, i.e. an CO white dwarf disrupted by explosive carbon burning.

A recently discovered rare variety of Type Ia SNe has been suggested to be connected with exploding massive AGB star. These supernova variety comprises four events: SN 2005gj, SN 2002ic, SN 1997cy and SN 1999E (cf. Hamuy et al. 2003; Deng et al. 2004; Chugai et al. 2004; Chugai & Yungelson 2004). These events show evidence for strong interaction of the supernova ejecta with a dense, hydrogen-rich circumstellar envelope. Hamuy et al. (2003) discusses two options for the origin of the CSM: mass loss by a supergiant in a binary scenario for SN Ia (cf. Livio & Riess 2003) or the mass loss by a single supergiant in the SN<sub>1.5</sub> scenario (Iben & Renzini 1983; Zijlstra 2004; Chugai et al. 2004; Tsujimoto & Shigeyama 2006).

In a discussion, Chugai et al. (2004) argue that a SN<sub>1.5</sub> scenario can account for most of the observable characteristics. At first they note that it is highly remarkable that two of the peculiar supernovae (SN 2002ic and SN 1997ic, out of the three known at that time) exploded in dwarf galaxies, which are characterized by low metallicity. Based on an analysis of the abundances they derive an upper limit for the metallicity of  $0.1 Z_{\odot}$ . Aldering et al. (2006) derive for SN 2005gj a three times higher metallicity of  $Z/Z_{\odot} < 0.3$ . The SN<sub>1.5</sub> scenario can also account for a dense CSM. Hamuy et al. (2003) argued that the amount of shock-heated CSM needed to reproduce the observed light curve of SN 2002ic is in the order of  $\sim 5 M_{\odot}$ , which is totally unexpected for SN Ia, but is in good agreement with our CSM predictions (see 3.5.4). On the other hand, the SN<sub>1.5</sub> scenario for these events requires that the stars lose their hydrogen-rich envelopes completely a few hundred years before the supernova explosion. Chugai & Yungelson (2004) argue that such a synchronisation might be achieved by the contraction of the CO

white dwarf as it approaches the Chandrasekhar limit.

The number of SN Ia with strong  $H\alpha$  emission is less than 1 per cent. If these explosions are caused by mass loss from a supergiant in a binary scenario, one would expect a higher fraction. SN1.5 however might be extremely rare at solar metallicity, but more prominent from low metallicity.

Finally, we want to point out that, while the contribution of the ECSNe to the Galactic chemical evolution is at most restricted to the  $r$ -process, Type 1.5 supernovae might be dominating the iron production during the epochs of their existence. As, if they can form, they come from the lowest mass supernova progenitors, their number may easily be very high due to the steepness of the stellar initial mass function, and thus dominate over the classical Type Ia supernovae (cf. Fig. 28 and Table 6).

### 3.7 DISCUSSION AND CONCLUSIONS

In this paper we presented our research on the progenitors of massive ONe white dwarfs, electron capture supernovae and Type 1.5 supernovae. An analysis of the general trends of supernova progenitors as function of metallicity was recently performed by [Eldridge & Tout \(2004c\)](#). Here, we focus on the white dwarf/neutron star formation limit, and cover the mass range between 6 and  $12.5 M_{\odot}$ , and metallicities ranging from solar to extremely metal poor, e.g.  $\log Z / Z_{\odot} \sim -3.5$ .

As concluded before (in P07), we find that the maximum initial mass for ECSN depends sensitively on the mixing assumptions for core H- and He-burning. Models like those computed with EVOL that include core overshooting, and that are consistent with the observed width of the main sequence, predict a smaller maximum mass for SAGB. Rotation would act similar on the core burning phase as overshooting. The STERN models calculated here include neither rotation nor overshooting, and accordingly the maximum mass for SAGB and ECSN is larger by up to  $2.5 M_{\odot}$ . Equally important are the treatment of semi-convection during He-core burning that effects the final core size and the ultimate fate of the star.

The lower mass for ECSN is exclusively determined by the stellar properties on the SAGB. The most important – and the most uncertain – are the efficiency of the third dredge-up, the efficiency of hot bottom burning and the mass loss during the TPAGB. Both a very in-efficient dredge-up or a low mass loss rate, can account for a significant fraction of ECSN, especially at lower metallicities. For metallicities below  $\log Z / Z_{\odot} \sim -2.5$  the occurrence of SN type 1.5 can not be excluded.

**ACKNOWLEDGMENTS** We are very grateful to Onno Pols and Maria Lugaro for useful discussions.



R. G. Izzard, A. J. T. Poelarends

*submitted to Astronomy & Astrophysics*

**ABSTRACT** Super Asymptotic Giant Branch (super-AGB) stars are those that undergo carbon burning followed by thermal pulses. They have a mass between about 8 and  $12.5M_{\odot}$ . More massive stars ignite neon and eventually core collapse, while lower mass stars do not ignite carbon. We use detailed models of super-AGB stars to construct a synthetic super-AGB model and calculate chemical yields. We investigate model uncertainties, particularly mass loss, convective overshooting and third dredge up, and quantify their effect on the yields. Our conclusion is that super-AGB stars are not important contributors to Galactic chemical evolution.

## 4.1 INTRODUCTION

The final stages of stellar evolution play a critical role in Galactic chemical evolution (GCE). The ejecta from dying stars form each successive stellar generation in an endless cycle of metal enrichment. Low- and intermediate- mass stars enrich their environment by ejection of their nuclear-processed stellar envelopes during the thermally pulsing asymptotic giant branch (TPAGB) phase when they alternate between shell hydrogen and helium burning. They leave a white dwarf remnant which is not hot enough to undergo further nuclear burning. In contrast, massive stars burn helium, carbon, neon, oxygen and silicon, leading to formation of an iron core which cannot burn further and instead collapses to a neutron star or black hole. The stellar envelope is ejected in a type II supernova. The mass boundary between the intermediate and massive stars is not known exactly and estimates range from  $7 M_{\odot}$  (Girardi et al. 2000) up to more than  $11 M_{\odot}$  (Ritossa et al. 1999), depending on the input physics, e.g. the choice of metallicity and convective overshooting.

The *super*-TPAGB (SAGB) stars live on the boundary between intermediate and massive stars. They are massive enough to ignite carbon but not massive enough to maintain nuclear burning beyond carbon (e.g. Siess 2006). They experience a second dredge up, which reduces their helium core mass, while massive stars do not. The core burns to an oxygen-neon mixture, on top of which lies a hydrogen-helium double burning shell that behaves like a lower mass TPAGB star with a carbon-oxygen core, (e.g. Iben & Renzini 1983). The burning shells increase the mass of the core in a series of thermal pulses and in the absence of any mass loss the oxygen-neon core may grow to about  $1.375 M_{\odot}$  (Nomoto 1987a) at which point electron capture on  $^{24}\text{Mg}$  causes the core to collapse to a neutron star. Detailed models of SAGB stars have been constructed by Garcia-Berro & Iben (1994); Ritossa et al. (1996); Garcia-Berro et al. (1997); Iben et al. (1997) and more recently by Eldridge & Tout (2004b) who consider SAGB stars as potentially-observable supernova progenitors.

The thermal pulse cycle in an SAGB star resembles a  $4 - 8 M_{\odot}$  TPAGB star, but with a shorter interpulse period and higher temperature at the base of the convective envelope. By virtue of their high mass, hot-bottom burning (HBB; e.g. Boothroyd et al. 1995), occurs at a very high temperature, often in excess of  $10^8$  K. The hydrogen-burning CNO, NeNa and MgAl cycles process the envelope and change the surface abundances. SAGB stars may be an important source of nitrogen, sodium and aluminium and perhaps play a part in the globular cluster Na – O anticorrelation mystery (Ventura & D’Antona 2005).

Mixture of material from the intershell region into the envelope, known as third dredge up, may occur in SAGB stars. Some models



suggest it does (e.g. (Herwig 2004a; Doherty & Lattanzio 2006) and the EVOL models used in section 4.2 and Poelarends et al. 2007), others that it does not (e.g. the STERN models presented in section 4.2, also Siess & Pumo 2006), or is inefficient (Ritossa et al. 1996). At present the occurrence of third dredge up in SAGB stars seems to depend on the choice of convective overshooting and numerical solution technique employed during the construction of the stellar models.

There are no detailed studies of chemical yields from SAGB stars, probably because detailed stellar models take a long time to make and suffer from the usual uncertainties due to mass loss, convective overshooting and third dredge up. A synthetic modelling technique, where stellar parameters such as luminosity, core mass and radius are fitted as simple functions from a few detailed models, enables us to explore the uncertain parameter space. In this paper we calculate the chemical yields of SAGB stars by modifying the algorithm of Izzard et al. (2004, I04) as updated by Izzard et al. (2006b, I06) and applying it to stars in the mass range  $8 \lesssim M/M_{\odot} \lesssim 13$ . We approximate stellar structural variables with formulae and interpolation tables, and use a simple model for HBB to follow the CNO, NeNa and MgAl cycles and surface abundances of the C, N, O, Ne, Na, Mg and Al isotopes. We extrapolate synthetic evolution, beyond the point when the detailed models fail, to the end of the SAGB phase. This is possible because the structure of AGB stars is such that after a number of pulses the evolution reaches a limit cycle (e.g. Ritossa et al. 1996).

In section 4.2 we describe our detailed models and synthetic algorithm. In section 4.3 we calculate the chemical yields from SAGB stars with varying mass loss rate, overshooting and third dredge up. We examine the relative effect on the chemical yield of a population of stars and compare to a canonical model which does not explicitly include SAGB stars with  $M > 8M_{\odot}$ . Section 4.4 discusses the implications of our results and some future directions for our research, after which we draw some conclusions.

## 4.2 MODELS, FULL AND SYNTHETIC

### 4.2.1 Full evolution models

Our full evolution models were constructed with the STERN code (Heger et al. 2000). We constructed models of mass 8.5, 9.0, 10.0, 11.5, 12.0 and  $12.3M_{\odot}$ , with metallicity  $Z = 0.02$ , no convective overshooting, no mass loss and no rotation. The 9-12  $M_{\odot}$  models ignite carbon (but not neon) and are the SAGB models we use as the basis of our synthetic model. The  $8.5M_{\odot}$  model does not ignite carbon.

The STERN code is a implicit pseudo-Lagrangian hydrodynamic code which solves all the basic equations for stellar evolution (Langer

et al. 1988; Langer 1991, 1998). The equation of state includes radiation, ionization, relativistic electron degeneracy and electron-positron pairs. Ions are treated as a Boltzmann gas (El Eid & Langer 1986) and the code uses opacity tables taken from OPAL (Iglesias & Rogers 1996), complemented with low-temperature opacities from Alexander & Ferguson (1994). The effects of  $\mu$ -barriers on convection is included by using the Ledoux criterion for convection and semiconvection (Langer et al. 1983).

Nuclear burning is traced by 35 isotopes and a network of 65 reactions, including the  $pp$  chains, CNO cycle and major helium, carbon, neon and oxygen burning reactions. The NeNa and MgAl cycles are solved separately with a 13 isotope network. The initial abundances are taken from Grevesse (1991).

To determine the effect of convective overshooting we use the overshooting models of Poelarends et al. (2007) which are constructed with the EVOL code (Blöcker 1995; Herwig 2004a). In EVOL convective boundaries are determined by the Schwarzschild criterion. Mixing beyond the convective boundary is formally taken into account by exponential-diffusive extra mixing (Herwig et al. 1997; Herwig 2000). The EVOL code allows the simultaneous, implicit solution of the nuclear network and the time-dependent mixing equations. This enables the code to follow fast burning and mixing events encountered during mixing of protons in the helium burning layer or during hot-bottom burning.

#### 4.2.2 Synthetic evolution models

Our synthetic models are based on those of Io6 who combined the synthetic single and binary stellar evolution code of Hurley et al. (2002, Ho2) with a synthetic prescription for nucleosynthesis. The code follows the TPAGB phase in detail, especially third dredge up and hot bottom burning, but runs in a just fraction of a second. The Ho2 models include convective overshooting, while Io6 include it except during the TPAGB phase, when the non-overshooting models of Karakas et al. (2002, Ko2) are used.

We have altered the Io6 prescription to explicitly deal with SAGB stars. First we alter the helium core mass to follow our STERN or EVOL models over the initial mass range  $7.5 \leq M_{\text{msun}} \leq 12.5$ :

- The helium core mass at the start of the early AGB phase,  $M_{\text{c,BAGB}}$ , is interpolated as a function of mass  $M$  according to our STERN or EVOL models (see Fig. 33). If  $M_{\text{c,BAGB}} < 1.9 M_{\odot}$  a CO core is formed and our synthetic stars follow the normal AGB evolution (as in Io4 & Io6). Otherwise, carbon ignition forms an oxygen-neon core. Neon ignition, and eventual core collapse, occurs when  $M_{\text{c,BAGB}} > 2.9 M_{\odot}$ , which is the condition that there is no second

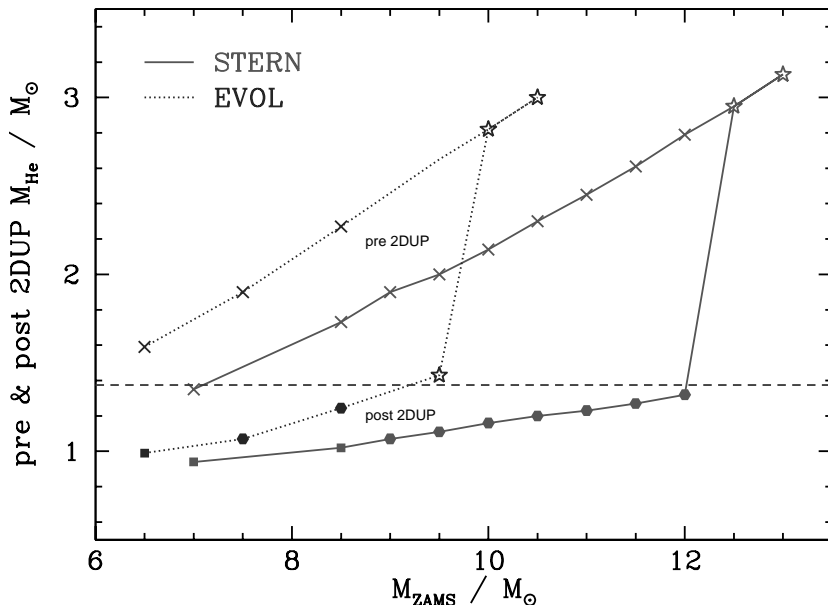


Figure 33. The hydrogen-exhausted core mass before and after second dredge up according to our STERN (solid line) and EVOL (dotted line) models as a function of initial stellar mass ( $M_{\text{ZAMS}}$ ). Because of convective overshooting, the EVOL core masses are larger for a given  $M_{\text{ZAMS}}$ . Second dredge up does not occur for helium core masses more massive than about  $2.9 M_{\odot}$ , corresponding to an initial mass of just over  $12 M_{\odot}$  with STERN and  $9 M_{\odot}$  with EVOL. The horizontal dashed line is the maximum mass of the carbon-oxygen or oxygen-neon core, beyond which it collapses to a neutron star. Squares denote carbon-oxygen cores, hexagons oxygen-neon cores and stars denote neon ignition (and subsequent supernova).

dredge up. Stars with helium core masses in the range  $1.9 \lesssim M_{\text{c,BAGB}}/M_{\odot} \lesssim 2.9$  ignite carbon, but do not ignite neon, so are our candidate SAGB stars. We use  $M_{\text{c,BAGB}}$  directly from a table of STERN or EVOL model results for masses in the range  $7 \leq M/M_{\odot} \leq 12.5$  (otherwise we use the Ho2 fit) and apply the above core mass limits in our synthetic code.

- The depth of second dredge-up determines the core mass at the first thermal pulse,  $M_{\text{c,1TP}}$ . It depends sensitively on the progenitor mass and model parameters. We linearly interpolate to find  $M_{\text{c,1TP}}$  as a function of  $M$  taken from our STERN or EVOL models. The EVOL models employ convective overshooting and are

considerably larger for a given  $M$  (Figure 33). For initial masses below  $7 M_{\odot}$  we extrapolate  $M_{c,1TP}$  from Ko2, which is in reasonable agreement with both EVOL and STERN.

Second, we develop a prescription for stars which have an SAGB phase i.e. stars with  $1.9 \lesssim M_{c,BAGB}/M_{\odot} \lesssim 2.9$  (corresponding to our STERN models with initial masses  $9 \leq M/M_{\odot} \leq 12$ ). For lower mass stars we use the Io4/Io6 prescription for the TPAGB phase while at higher mass we follow the Ho2/Io6 prescription for supernovae (see below for details).

- The luminosity formula of Io6 for TPAGB stars is re-fitted to our STERN models. In general the fits are excellent, but for  $M \geq 12 M_{\odot}$  our STERN models do not contain enough data points during the SAGB to be sure of a good fit so we extrapolate from the  $11.5 M_{\odot}$  model. The luminosity fit does not take into account the dips at each thermal pulse although these are taken into account when calculating the core growth (see below).
- The radius,  $R$ , is fitted to the STERN models with

$$\log_{10} R/R_{\odot} = -0.26 + 0.75 \log_{10} L/L_{\odot} - 0.41 \log_{10} M_{\text{env}}/M_{\odot} + 0.09 \log_{10}(M_{\text{env}}/M_{\text{env},1TP}), \quad (4.1)$$

where  $L$  is the luminosity,  $M_{\text{env}} = M - M_c$  is the convective envelope mass,  $M_c$  the helium core mass and  $M_{\text{env},1TP}$  is the envelope mass at the first thermal pulse.

- The helium-core growth rate,  $\dot{M}_c$ , is calculated from  $\dot{M}_c = QL$  where

$$Q = \min(1.43 \times 10^{-11}, 1.40 \times 10^{-11} + 4.17 \times 10^{-12}/X - 1.50 \times 10^{-12} M_{\text{env}}) \times f_{\text{DIP}} \quad (4.2)$$

is fitted directly to our STERN models,  $X$  is the envelope hydrogen abundance (by mass fraction) and

$$f_{\text{DIP}} = \max[0, \min(1, 0.51 - 0.04 M_{\text{env}})] \quad (4.3)$$

is a correction factor which takes into account luminosity dips at each thermal pulse.

- The interpulse period,  $\tau$ , is given by a simple fit to the core mass according to the STERN models, with a turn-on parameter for the first few pulses

$$\log(\tau/\text{years}) = 3.05 - 10.8 \log M_c - 17.0(\log M_c)^2 + (0.0169 - 8.13 \times 10^{-4} M) \times \min(20, N_{\text{TP}}). \quad (4.4)$$

- Surface isotopic abundances at the first thermal pulse, i.e. immediately following second dredge up, are taken directly from our STERN first thermal pulse model with corresponding  $M$ . In STERN models with  $M > 12 M_{\odot}$  some *dredge out* occurs, where carbon is mixed from the helium burned region to the surface (Ritossa et al. 1999; Siess 2006), but the change in surface abundances is very small.
- Our STERN models show no third dredge up, i.e. the ratio of mass dredged up at each thermal pulse to core mass growth – the third dredge up efficiency –  $\lambda$  is zero, however we can set  $\lambda$  to be non-zero in our synthetic model. The abundances of dredged-up material are taken from the intershell region of our 8.5, 9 and  $10 M_{\odot}$  STERN models. As an example, our  $9 M_{\odot}$  model has intershell abundances by mass fraction:  ${}^4\text{He} = 0.66$ ,  ${}^{12}\text{C} = 0.31$ ,  ${}^{16}\text{O} = 0.010$ ,  ${}^{22}\text{Ne} = 0.017$  and  ${}^{24}\text{Mg} = 2.4 \times 10^{-5}$ , which are similar to those of lower mass stars (e.g. Ko2). We modulate  $\lambda$  with a function of pulse number,  $1 - \exp(N_{\text{TP}}/N_{\text{cal}})$ , to simulate the turn on of dredge up over the first few pulses. Extrapolation of the Ko2 results to higher masses suggests  $N_{\text{cal}} \sim 5$ , and the results of Doherty & Lattanzio (2006) suggest a similar behaviour (for a  $9.5 M_{\odot}$  model) but after a short delay. The  $9.5 M_{\odot}$  EVOL model has a delay consisting of six weak pre-pulses, followed by one strong pulse and then normal thermal pulses (Poelarends et al. 2007). In our ignorance we set  $N_{\text{cal}} = 5$ .
- Our synthetic HBB model follows the CNO, NeNa and MgAl cycles. We fit the temperature and density at the base of the convective envelope to our STERN models,

$$\log T_{\text{BCE}} = g_T [(a + \phi\lambda) - b \exp(-N_{\text{TP}}/c)] , \quad (4.5)$$

$$\log \rho_{\text{BCE}} = g_{\rho} [d - e \exp(-N_{\text{TP}}/f)] , \quad (4.6)$$

where  $a(M) \dots f(M)$  are fitted for each  $M$  and then interpolated from tables as given in appendix 4.6.1 (note that  $a(M)$  is the peak temperature),  $N_{\text{TP}}$  is the number of thermal pulses,  $g_T$  and  $g_{\rho}$  are modulation factors which deal with mass loss (see below) and  $\phi$  is a correction factor (see below). Our STERN model temperatures are similar to, but not quite the same as, other models in the literature.

The  $9.5 M_{\odot}$  model of Doherty & Lattanzio (2006, DL06) and our  $9 M_{\odot}$  EVOL model are both hotter than the equivalent STERN model (see Fig. 34). Both these experience third dredge up with efficiencies of  $\lambda = 0.7$  and  $\lambda = 0.5$  respectively. We use a non-zero

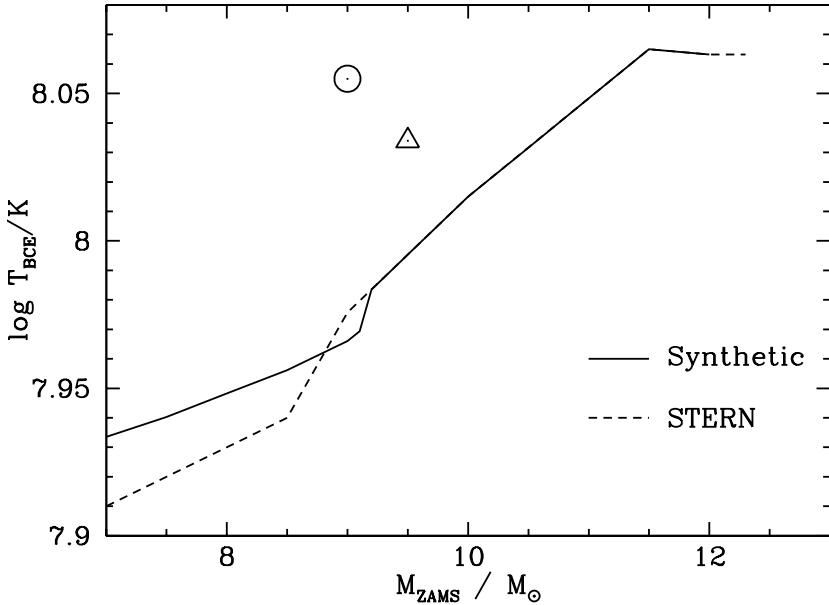


Figure 34. Peak log temperature at the base of the convective envelope as a function of initial mass ( $a(M)$  in equation 4.5). The solid line shows our synthetic model which is based on our non-overshooting STERN models for SAGB stars ( $M \gtrsim 9 M_{\odot}$ ) and the fit of Io6 for normal TPAGB stars with CO cores. The dashed line shows the equivalent STERN CO-core model temperatures. The triangle is the  $9.5 M_{\odot}$  model of [Doherty & Lattanzio \(2006\)](#) and the circle is our  $9 M_{\odot}$  EVOL model, both of which are hotter than our STERN models.

value of  $\phi$  to simulate an increase in  $T_{\text{BCE}}$  because of third dredge up, with  $\phi = 0.056$  or  $0.16$  to match DLo6 or EVOL.

- We use the same nuclear reaction rates as the STERN code.
- Our burning algorithm works by replacing the burn-mix-burn-mix... cycle in the convective envelope of an AGB star with a single burn-mix event (see e.g. Figure 1 of [Izzard et al. 2006a](#)). The envelope burn fraction and burn time are calibrated to our STERN models (see Io4 or Io6 for the calibration method). In general our calibrated synthetic model surface abundances agree well with our STERN models, however we have trouble fitting  $^{13}\text{C}$ . This is probably related to our crude single layer, single event approximation to HBB with a unique temperature and density, rather than a continuous process involving temperature and density gradients and convective mixing. On the other hand,

most of our synthetic isotopic abundances are fine, as shown in Figure 35, and we obtain a seven orders of magnitude speed increase over the STERN code. Without these approximations, which we think are reasonable and have been proven to work for intermediate mass AGB stars (I04,I06), the present study would be impossible.

- We ran one  $9 M_{\odot}$  STERN model set with an extreme mass-loss rate of  $10^{-3} M_{\odot} \text{ yr}^{-1}$  to determine how mass loss reduces  $T_{\text{BCE}}$  and  $\rho_{\text{BCE}}$ . The factors  $g_T$  and  $g_{\rho}$  are fitted as functions of  $M_{\text{env}}$  (see appendix 4.6.2 for details) to simulate the mass loss for this star and are then applied to all our synthetic stars. Our fitting formulae for  $L$  and  $R$  fit the model with mass loss surprisingly well, despite extrapolation into a regime where they are not strictly valid.
- Our STERN models do not include mass loss but our synthetic models can include mass loss before and during the SAGB phase. Prior to the SAGB we use either the mass loss prescription of Ho2 or no mass loss (to match our STERN models). During the SAGB phase we use one of: no mass loss, VW93<sup>1</sup> (Vassiliadis & Wood 1993, their Eq. 2), VW93<sup>2</sup> (their Eq. 5, which has a mass dependent term to delay the superwind for AGB stars with  $M \gtrsim 5 M_{\odot}$ ), Reimers (1975) with  $\eta = 1$  or  $\eta = 5$ , Blöcker & Schönberner (1991) with  $\eta = 0.1$  or van Loon et al. (2005, vLo5). When using the vLo5 rate we take the red supergiant rate for  $L > 10^5 L_{\odot}$ , otherwise the AGB rate, and cap  $T_{\text{eff}}$  at 4000 K to prevent the mass loss rate becoming very small during the transition to the white dwarf track.
- If the oxygen-neon core is not exposed by mass loss before it grows to  $1.37 M_{\odot}$ , it is converted into a neutron star and the envelope is ejected without further nuclear processing (e.g. Nomoto 1987a, Gutiérrez et al. 2005). Core-collapse supernovae in early AGB stars and massive helium stars are modelled by expelling the envelope and some of the CO core material with the yields of Chieffi & Limongi (2004)<sup>1</sup>. The remnant neutron star mass (the mass cut) is taken from the formula of Ho2, which gives typical neutron star masses around  $1.33 M_{\odot}$  from a  $10 M_{\odot}$ ,  $Z = 0.02$  progenitor. While the mass cut is a source of some uncertainty, a similar result ( $1.37 M_{\odot}$ ) is obtained with an alternate prescription due to Belczynski et al. (2002).
- Our *default* synthetic SAGB models use STERN non-overshooting core masses, no mass loss prior to the thermal pulses, vLo5 mass

<sup>1</sup> The unstable isotope  $^{26}\text{Al}$  is included in the  $^{26}\text{Mg}$  yield, so there is zero yield of  $^{26}\text{Al}$  from our core-collapse supernovae.

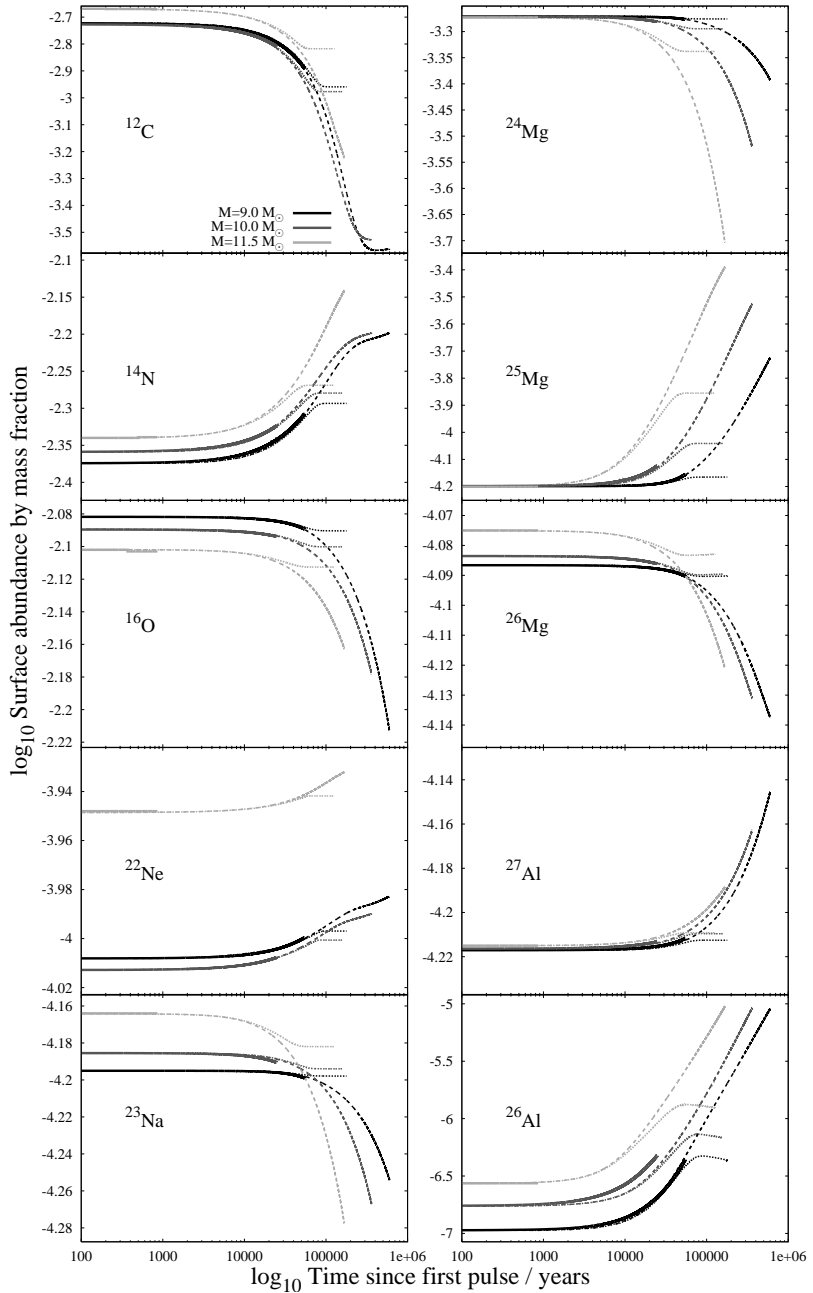


Figure 35. Log surface abundances (by mass fraction) vs time on the SAGB for our detailed STERN models (solid lines), our synthetic models with no mass loss (dashed lines) and with the mass loss rate of [van Loon et al. \(2005\)](#), dotted lines) for  $M = 9, 10$  and  $11.5 M_{\odot}$ . The solid and dashed lines should, and do, agree well. Synthetic evolution is terminated if the core mass reaches  $1.37 M_{\odot}$  or if the envelope is expelled.



loss during the thermally pulsing phase and no third dredge up ( $\lambda = \phi = 0$ ).

### 4.3 RESULTS

In this section we present the chemical yields from our synthetic model SAGB stars. We define the yield of an isotope as the mass ejected by a single star of a given mass. The results are presented in tables 7 to 16 and Figure 36.

We examine in turn each source of uncertainty in the yields: the HBB prescription, third dredge up, mass loss prescription, overshooting and the loss of type-II SNe in populations with SAGB stars. We then calculate yields for GCE and compare them to canonical yields.

#### 4.3.1 Hot bottom burning

Hot bottom burning in our massive-SAGB models converts carbon and oxygen into  $^{14}\text{N}$ ,  $^{23}\text{Na}$  and  $^{24}\text{Mg}$  into  $^{25,26}\text{Mg}$  and magnesium into  $^{26,27}\text{Al}$ . The abundance of  $^{20}\text{Ne}$  hardly changes and a small amount of  $^{22}\text{Ne}$  is created.

The success of our synthetic HBB calibration is shown in Fig. 35 in which we show the surface abundance changes as a function of time for our synthetic models with and without mass loss compared to our STERN model abundances. The corresponding ejected masses are given in tables 7 and 8 for no mass loss and vLo5 mass loss respectively and are also shown in Fig. 36, squares  $\square$  and filled circles  $\bullet$  respectively. Without mass loss there is a significant change in the envelope abundances due to HBB:

- Up to 85% of  $^{12}\text{C}$  and 25% of  $^{16}\text{O}$  in the convective envelope are converted into  $^{14}\text{N}$ , which increases by up to 40%.
- Sodium is decreased by up to one fifth.
- Surface  $^{24}\text{Mg}$  is reduced by up to 60%, with a corresponding factor of five increase in  $^{25}\text{Mg}$ .
- The unstable isotope  $^{26}\text{Al}$  increases by an order of magnitude or more (its formation rate is very sensitive to temperature).
- $^{26}\text{Mg}$  and  $^{27}\text{Al}$  change little.

Mass loss during the SAGB phase reduces  $M_{\text{env}}$  and hence the efficiency of HBB. Figure 35 shows the result of applying the vLo5 mass loss, with corresponding yields in table 8. The yield of nitrogen drops considerably relative to the constant mass models, while that of carbon increases. There is little change in the heavier isotopes, although  $^{25}\text{Mg}$

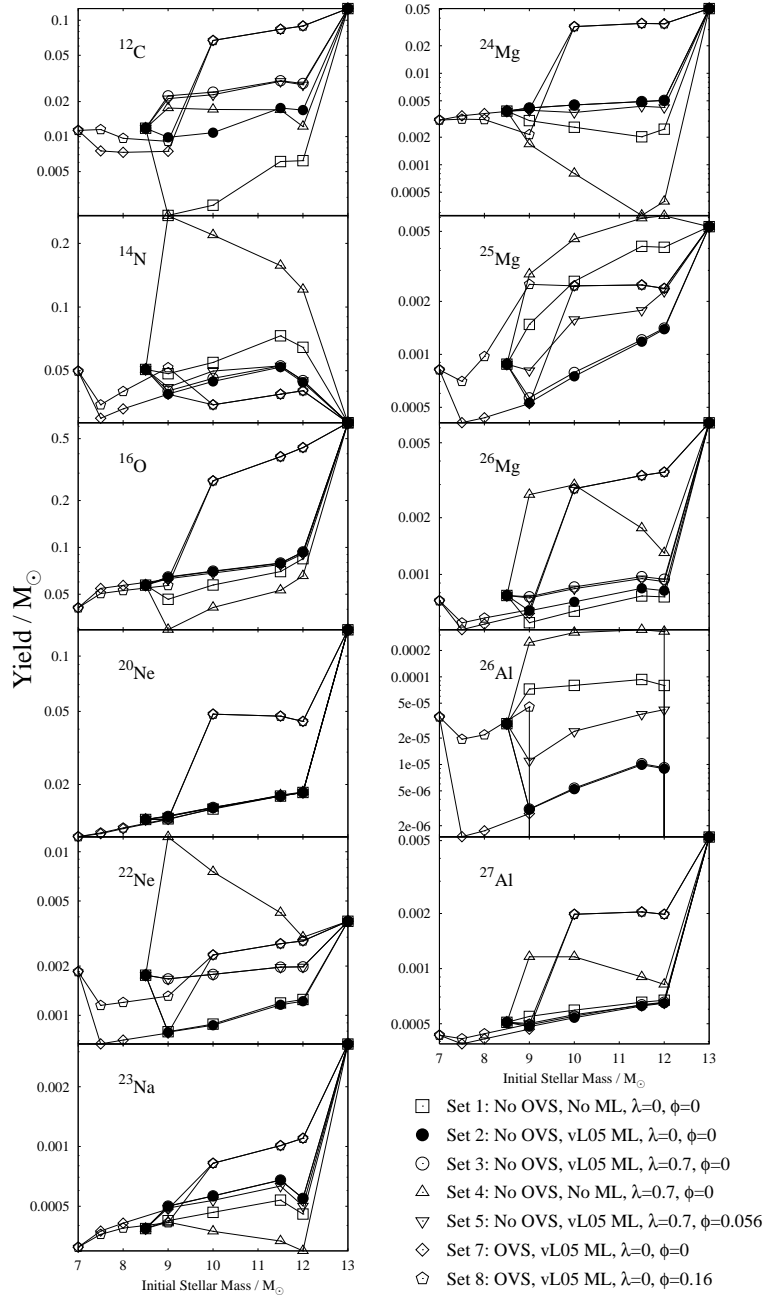


Figure 36. Isotopic yields as a function of initial mass from our synthetic models with differing input physics: OVS is overshooting, vL05 ML indicates the mass loss prescription of [van Loon et al. \(2005\)](#),  $\lambda$  is the dredge up efficiency and  $\phi$  is the temperature enhancement factor of equation 4.5. The 13  $M_{\odot}$  stars explode as type II supernovae without a SAGB phase, so have the same yield for each model set.

Table 7. Mass ejected per isotope (chemical yield) from our synthetic models with no overshooting or mass loss. The  $8.5 M_{\odot}$  has a CO core and is never an SAGB star, so follows the prescription of Io6, hence its higher  $^{12}\text{C}$  yield. The  $13 M_{\odot}$  model ignites neon, so does not have thermal pulses and goes on to explode in a type II supernova. All other models ( $9\text{--}12 M_{\odot}$ ) end as electron capture supernovae.

| $M/M_{\odot}$ | $^{12}\text{C}$ | $^{14}\text{N}$ | $^{16}\text{O}$ | $^{20}\text{Ne}$ | $^{22}\text{Ne}$ | $^{23}\text{Na}$ | $^{24}\text{Mg}$ | $^{25}\text{Mg}$ | $^{26}\text{Mg}$ | $^{26}\text{Al}$      | $^{27}\text{Al}$ |
|---------------|-----------------|-----------------|-----------------|------------------|------------------|------------------|------------------|------------------|------------------|-----------------------|------------------|
| 8.5           | 0.0118          | 0.0507          | 0.0572          | 0.0129           | 0.00176          | 0.000386         | 0.00386          | 0.00088          | 0.000773         | $2.92 \times 10^{-5}$ | 0.000509         |
| 9             | 0.0021          | 0.0484          | 0.0464          | 0.013            | 0.000794         | 0.000423         | 0.00304          | 0.00148          | 0.000554         | $7.26 \times 10^{-5}$ | 0.000548         |
| 10            | 0.00257         | 0.0547          | 0.0573          | 0.0147           | 0.000884         | 0.000466         | 0.00257          | 0.0026           | 0.000638         | $7.99 \times 10^{-5}$ | 0.000593         |
| 11.5          | 0.0061          | 0.0731          | 0.0699          | 0.0173           | 0.00119          | 0.000537         | 0.00202          | 0.00411          | 0.000768         | $9.33 \times 10^{-5}$ | 0.000655         |
| 12            | 0.00621         | 0.0645          | 0.0846          | 0.0181           | 0.00125          | 0.000457         | 0.00245          | 0.00406          | 0.00076          | $7.97 \times 10^{-5}$ | 0.000672         |
| 13            | 0.126           | 0.0284          | 0.632           | 0.139            | 0.00376          | 0.00328          | 0.051            | 0.00532          | 0.00638          | 0                     | 0.00523          |

Table 8. Synthetic model yields for default models which have no overshooting, no mass loss prior to the AGB and the mass loss of [van Loon et al. \(2005\)](#) during the SAGB. The  $13 M_{\odot}$  star explodes in a core collapse supernova, the  $12 M_{\odot}$  star dies in an electron capture supernova, the  $11.5 M_{\odot}$  star loses its envelope by stellar wind mass loss. The  $8.5 M_{\odot}$  is never an SAGB star, but loses its envelope during the TPAGB phase (where we impose the VW93<sup>1</sup> mass loss as in Koz/104/106).

| $M/M_{\odot}$ | $^{12}\text{C}$ | $^{14}\text{N}$ | $^{16}\text{O}$ | $^{20}\text{Ne}$ | $^{22}\text{Ne}$ | $^{23}\text{Na}$ | $^{24}\text{Mg}$ | $^{25}\text{Mg}$ | $^{26}\text{Mg}$ | $^{26}\text{Al}$      | $^{27}\text{Al}$ |
|---------------|-----------------|-----------------|-----------------|------------------|------------------|------------------|------------------|------------------|------------------|-----------------------|------------------|
| 8.5           | 0.0118          | 0.0507          | 0.0572          | 0.0129           | 0.00176          | 0.000386         | 0.00386          | 0.00088          | 0.000773         | $2.92 \times 10^{-5}$ | 0.000509         |
| 9             | 0.00985         | 0.0388          | 0.0642          | 0.0134           | 0.000789         | 0.0005           | 0.00418          | 0.000531         | 0.000641         | $3.07 \times 10^{-6}$ | 0.000482         |
| 10            | 0.0108          | 0.0445          | 0.07            | 0.0149           | 0.00087          | 0.000563         | 0.0045           | 0.00075          | 0.000715         | $5.23 \times 10^{-6}$ | 0.000539         |
| 11.5          | 0.0176          | 0.052           | 0.079           | 0.0173           | 0.00116          | 0.000677         | 0.0049           | 0.00118          | 0.000844         | $9.91 \times 10^{-6}$ | 0.000625         |
| 12            | 0.0169          | 0.044           | 0.0933          | 0.0181           | 0.00122          | 0.000548         | 0.00505          | 0.00139          | 0.00082          | $8.95 \times 10^{-6}$ | 0.000647         |
| 13            | 0.126           | 0.0284          | 0.632           | 0.139            | 0.00376          | 0.00328          | 0.051            | 0.00532          | 0.00638          | 0                     | 0.00523          |

Table 9. As table 8 but with third dredge up efficiency  $\lambda = 0.7$ .

| $M/M_{\odot}$ | $^{12}\text{C}$ | $^{14}\text{N}$ | $^{16}\text{O}$ | $^{20}\text{Ne}$ | $^{22}\text{Ne}$ | $^{23}\text{Na}$ | $^{24}\text{Mg}$ | $^{25}\text{Mg}$ | $^{26}\text{Mg}$ | $^{26}\text{Al}$      | $^{27}\text{Al}$ |
|---------------|-----------------|-----------------|-----------------|------------------|------------------|------------------|------------------|------------------|------------------|-----------------------|------------------|
| 8.5           | 0.0118          | 0.0507          | 0.0572          | 0.0129           | 0.00176          | 0.000386         | 0.00386          | 0.00088          | 0.000773         | $2.92 \times 10^{-5}$ | 0.000509         |
| 9             | 0.0224          | 0.0401          | 0.0646          | 0.0134           | 0.00167          | 0.000501         | 0.00418          | 0.000566         | 0.000761         | $3.1 \times 10^{-6}$  | 0.000493         |
| 10            | 0.0241          | 0.046           | 0.0704          | 0.015            | 0.00178          | 0.000564         | 0.0045           | 0.000789         | 0.000858         | $5.37 \times 10^{-6}$ | 0.00055          |
| 11.5          | 0.0302          | 0.0527          | 0.0794          | 0.0173           | 0.00197          | 0.000678         | 0.00491          | 0.00121          | 0.000973         | $1.02 \times 10^{-5}$ | 0.000635         |
| 12            | 0.0286          | 0.0449          | 0.0936          | 0.0181           | 0.00198          | 0.000548         | 0.00506          | 0.00141          | 0.000943         | $9.19 \times 10^{-6}$ | 0.000655         |
| 13            | 0.126           | 0.0284          | 0.632           | 0.139            | 0.00376          | 0.00328          | 0.051            | 0.00532          | 0.00638          | 0                     | 0.00523          |

and  $^{26}\text{Al}$  are still enhanced by up to 0.3 and 1 dex respectively. The other isotopes, in particular  $^{16}\text{O}$ ,  $^{20,22}\text{Ne}$ ,  $^{23}\text{Na}$ ,  $^{24}\text{Mg}$  and  $^{26}\text{Mg}$ , change very little due to HBB when mass loss is taken into account.

#### 4.3.2 *Third dredge-up*

We test two values for the dredge-up efficiency  $\lambda$ : zero (as found by Siess & Pumo 2006 and in our STERN models, also similar to the 7% found by Ritossa et al. 1996) and 0.7 (Doherty & Lattanzio 2006), both with the vLo5 mass loss rate. The yields for our  $\lambda = 0$  models are simply our default models, as shown in table 8 (or Fig. 36, filled circles ●), while table 9 shows the yields for  $\lambda = 0.7$  (or Fig. 36, open circles ○).

The only yield which are strongly affected is that of  $^{12}\text{C}$ , where an increase due to third dredge up over-compensates for destruction by the CN cycle. Some extra  $^{22}\text{Ne}$  and  $^{26}\text{Mg}$  is also produced.

In general, the SAGB phase is too brief for third dredge up to be important, even if  $\lambda \sim 0.7$ , when we use the vLo5 mass loss rate. We can increase the lifetime by turning off mass loss, as in table 10 (or Fig. 36  $\Delta$ ), which shows that most dredged-up carbon is CN-processed to give a large nitrogen yield. We do not consider that this case is very realistic because as  $\lambda$  approaches 1 there is no core growth and without mass loss the star can undergo HBB for a very long time – until it becomes a helium star. Our synthetic models certainly cannot cope in this case.

#### 4.3.3 *Third dredge-up and hot bottom burning combined*

The  $9.5 M_{\odot}$  model of Doherty & Lattanzio (2006) shows efficient third dredge up and consequently has a  $T_{\text{BCE}}$  during the SAGB. We test how this affects the chemical yields by setting  $\phi = 0.056$  to match the temperature increase in their model with  $\lambda = 0.7$ .

Table 11 (or Fig. 36  $\nabla$ ) shows the mass ejected for each isotope with this extra-hot bottom burning. There is little change compared to table 9 except an enhancement of  $^{25}\text{Mg}$  and  $^{26}\text{Al}$ . The effect of the temperature increase is limited by the short stellar lifetimes.

#### 4.3.4 *Mass loss rate uncertainty*

The mechanism by which mass is lost from AGB stars is poorly understood – especially for the relatively rare massive M-type AGB stars. As such we test many different mass-loss rate prescriptions and determine the effect on the chemical yields. Table 12 shows the TPAGB lifetimes and mass ejected as different isotopes for various mass-loss rates for our  $10 M_{\odot}$  models (with  $\lambda = 0$ ). In general, a strong mass-loss rate

Table 10. As table 9 with no mass loss.

| $M/M_{\odot}$ | $^{12}\text{C}$ | $^{14}\text{N}$ | $^{16}\text{O}$ | $^{20}\text{Ne}$ | $^{22}\text{Ne}$ | $^{23}\text{Na}$ | $^{24}\text{Mg}$ | $^{25}\text{Mg}$ | $^{26}\text{Mg}$ | $^{26}\text{Al}$      | $^{27}\text{Al}$ |
|---------------|-----------------|-----------------|-----------------|------------------|------------------|------------------|------------------|------------------|------------------|-----------------------|------------------|
| 8.5           | 0.0118          | 0.0507          | 0.0572          | 0.0129           | 0.00176          | 0.000386         | 0.00386          | 0.00088          | 0.000773         | $2.92 \times 10^{-5}$ | 0.000509         |
| 9             | 0.0176          | 0.27            | 0.0296          | 0.0129           | 0.0123           | 0.000416         | 0.00168          | 0.00285          | 0.00265          | 0.000246              | 0.00116          |
| 10            | 0.0171          | 0.219           | 0.0411          | 0.0148           | 0.00753          | 0.000374         | 0.000802         | 0.00452          | 0.00299          | 0.00032               | 0.00116          |
| 11.5          | 0.017           | 0.157           | 0.053           | 0.0175           | 0.00424          | 0.000334         | 0.000279         | 0.00594          | 0.00176          | 0.000344              | 0.0009           |
| 12            | 0.0122          | 0.121           | 0.0655          | 0.0182           | 0.003            | 0.000298         | 0.000396         | 0.00613          | 0.0013           | 0.000328              | 0.000819         |
| 13            | 0.126           | 0.0284          | 0.632           | 0.139            | 0.00376          | 0.00328          | 0.051            | 0.00532          | 0.00638          | 0                     | 0.00523          |

Table 11. As table 9 with  $\phi = 0.056$  simulate hotter bottom burning due to efficient third dredge up in SAGB stars .

| $M/M_{\odot}$ | $^{12}\text{C}$ | $^{14}\text{N}$ | $^{16}\text{O}$ | $^{20}\text{Ne}$ | $^{22}\text{Ne}$ | $^{23}\text{Na}$ | $^{24}\text{Mg}$ | $^{25}\text{Mg}$ | $^{26}\text{Mg}$ | $^{26}\text{Al}$      | $^{27}\text{Al}$ |
|---------------|-----------------|-----------------|-----------------|------------------|------------------|------------------|------------------|------------------|------------------|-----------------------|------------------|
| 8.5           | 0.0118          | 0.0507          | 0.0572          | 0.0129           | 0.00176          | 0.000386         | 0.00386          | 0.00088          | 0.000773         | $2.92 \times 10^{-5}$ | 0.000509         |
| 9             | 0.0212          | 0.0418          | 0.0629          | 0.0135           | 0.00167          | 0.00049          | 0.00394          | 0.000809         | 0.00075          | $1.1 \times 10^{-5}$  | 0.000502         |
| 10            | 0.0229          | 0.0498          | 0.0684          | 0.015            | 0.00178          | 0.000535         | 0.00373          | 0.00158          | 0.00084          | $2.39 \times 10^{-5}$ | 0.00056          |
| 11.5          | 0.0299          | 0.0527          | 0.0776          | 0.0174           | 0.00197          | 0.000632         | 0.00436          | 0.00178          | 0.00095          | $3.75 \times 10^{-5}$ | 0.000631         |
| 12            | 0.0279          | 0.045           | 0.0911          | 0.0181           | 0.00198          | 0.000502         | 0.00423          | 0.00228          | 0.000916         | $4.22 \times 10^{-5}$ | 0.000651         |
| 13            | 0.126           | 0.0284          | 0.632           | 0.139            | 0.00376          | 0.00328          | 0.051            | 0.00532          | 0.00638          | 0                     | 0.00523          |

Table 12. Time spent during the TPAGB phase ( $\tau$ , in units of  $10^5$  yrs) and yields from our non-overshooting,  $\lambda = 0$ ,  $10 M_{\odot}$  synthetic model with various mass-loss rate prescriptions (see section 4.2). Omitted isotopes change little. The latter two rows include mass loss prior to the SAGB, the others do not.

| $M/M_{\odot}$        | $\tau$ | $^{12}\text{C}$ | $^{14}\text{N}$ | $^{16}\text{O}$ | $^{20}\text{Ne}$ | $^{22}\text{Ne}$ | $^{23}\text{Na}$ | $^{24}\text{Mg}$ | $^{25}\text{Mg}$ | $^{26}\text{Mg}$ | $^{26}\text{Al}$      |
|----------------------|--------|-----------------|-----------------|-----------------|------------------|------------------|------------------|------------------|------------------|------------------|-----------------------|
| VW93 <sup>1</sup>    | 1.38   | 0.0131          | 0.042           | 0.0708          | 0.0149           | 0.000865         | 0.000569         | 0.00461          | 0.00064          | 0.000721         | $3.15 \times 10^{-6}$ |
| VW93 <sup>2</sup>    | 3.49   | 0.00314         | 0.0537          | 0.0598          | 0.0147           | 0.00088          | 0.000486         | 0.00296          | 0.00222          | 0.000652         | $5.89 \times 10^{-5}$ |
| Reimers $\eta = 1$   | 3.51   | 0.003           | 0.0539          | 0.0593          | 0.0147           | 0.000881         | 0.000482         | 0.00288          | 0.0023           | 0.000649         | $6.3 \times 10^{-5}$  |
| Reimers $\eta = 5$   | 3.87   | 0.00526         | 0.0504          | 0.0659          | 0.0147           | 0.000872         | 0.000533         | 0.00394          | 0.00124          | 0.000688         | $1.73 \times 10^{-5}$ |
| Blöcker $\eta = 0.1$ | 0.30   | 0.0151          | 0.04            | 0.0716          | 0.015            | 0.000862         | 0.000575         | 0.0047           | 0.000581         | 0.000727         | $2.04 \times 10^{-6}$ |
| VLo5                 | 1.58   | 0.0108          | 0.0445          | 0.07            | 0.0149           | 0.00087          | 0.000563         | 0.0045           | 0.00075          | 0.000715         | $5.23 \times 10^{-6}$ |
| None                 | 3.62   | 0.00257         | 0.0547          | 0.0574          | 0.0147           | 0.000883         | 0.000467         | 0.00259          | 0.00258          | 0.000639         | $7.89 \times 10^{-5}$ |
| Pre-AGB None         | 3.78   | 0.00363         | 0.0521          | 0.0585          | 0.0147           | 0.000903         | 0.000479         | 0.00336          | 0.00181          | 0.000643         | $6.45 \times 10^{-5}$ |
| Pre-AGB VLo5         | 1.53   | 0.0105          | 0.0433          | 0.0719          | 0.0149           | 0.000896         | 0.000552         | 0.00462          | 0.000649         | 0.000716         | $3.97 \times 10^{-6}$ |

such as VW93<sup>1</sup>, vLo5 or Blöcker with  $\eta = 0.1$ , leads to a short lifetime, little nuclear processing of the envelope and an ONeWD remnant. The VW93<sup>2</sup> and Reimers  $\eta = 1$  rates are slower so the yields resemble those when there is no mass loss (these stars suffer an electron capture SN leaving a NS remnant). Paradoxically, the SAGB lifetime for the Reimers  $\eta = 5$  model is longer with  $\eta = 1$ . This is because its luminosity drops as it initially loses mass, which in turn slows the core growth and the mass loss. It loses its envelope before its core reaches  $1.37M_{\odot}$  leaving an ONeWD. Such behaviour is indicative of the non-linear nature of TPAGB stars.

Mass loss prior to the AGB phase has often been ignored in previous works on AGB stars. With the prescription of Ho2 a  $10M_{\odot}$ ,  $Z = 0.02$  star loses  $0.57M_{\odot}$  of its envelope during the helium burning phase prior to the first thermal pulse. As shown in table 12 (the final two lines) mass loss slightly reduces the yields of isotopes produced by HBB, such as  $^{14}\text{N}$ , because  $\log T_{\text{BCE}}$  is roughly proportional to the mass  $M$ .

#### 4.3.5 Convective overshooting

Convective overshooting increases both  $M_{\text{c,BAGB}}$  and  $M_{\text{c,1TP}}$  for a given initial mass, as discussed in section 4.2.2.

Table 13 (or Fig. 36  $\diamond$ ) shows the chemical yields for the mass range 7 to  $10M_{\odot}$  when we take overshooting into account by using the EVOL fit to  $M_{\text{c,1TP}}$ . The  $7M_{\odot}$  model follows the Io6 prescription for the TPAGB as it does not ignite carbon, while the  $10M_{\odot}$  model explodes as a type-II supernova. The main difference between these yields and the non-overshooting yields is the mass range for HBB, which is smaller for overshooting models.

#### 4.3.6 Convective overshooting with third dredge-up

As mentioned in section 4.2.2 the EVOL models show efficient third dredge up. As in section 4.3.3 this leads to increased  $^{14}\text{N}$ ,  $^{22}\text{Ne}$ ,  $^{25}\text{Mg}$  and  $^{26}\text{Al}$  production, as shown in table 14 (and Fig. 36  $\diamond$ ).

#### 4.3.7 SNII-deficient yields

In this section we consider the canonical models of Io6 which show a type II explosion for  $M \gtrsim 8M_{\odot}$  and compare their yields to our synthetic SAGB model yields. For a range of masses the canonical models are SNII progenitors but undergo second dredge up in our synthetic models and are converted to SAGB stars. The yields of isotopes produced in type II supernovae, e.g.  $^{12}\text{C}$ ,  $^{16}\text{O}$ ,  $^{20}\text{Ne}$  and  $^{24}\text{Mg}$ , are reduced with respect to the canonical models as shown in table 15.



Table 13. As table 8 but with the convective overshooting  $M_{c,BAGB}$  and  $M_{c,ITP}$ . The  $M = 7 M_{\odot}$  model does not ignite carbon, the  $M = 10 M_{\odot}$  model ignites neon while intermediate masses are SAGB stars.

| $M/M_{\odot}$ | $^{12}\text{C}$ | $^{14}\text{N}$ | $^{16}\text{O}$ | $^{20}\text{Ne}$ | $^{22}\text{Ne}$ | $^{23}\text{Na}$ | $^{24}\text{Mg}$ | $^{25}\text{Mg}$ | $^{26}\text{Mg}$ | $^{26}\text{Al}$      | $^{27}\text{Al}$ |
|---------------|-----------------|-----------------|-----------------|------------------|------------------|------------------|------------------|------------------|------------------|-----------------------|------------------|
| 7             | 0.0113          | 0.0498          | 0.0409          | 0.0104           | 0.00185          | 0.000311         | 0.00308          | 0.000817         | 0.000725         | $3.49 \times 10^{-5}$ | 0.000433         |
| 7.5           | 0.00753         | 0.0298          | 0.0545          | 0.0108           | 0.000669         | 0.000375         | 0.00343          | 0.000409         | 0.000509         | $1.5 \times 10^{-6}$  | 0.000388         |
| 8             | 0.00732         | 0.033           | 0.057           | 0.0115           | 0.000706         | 0.000411         | 0.00363          | 0.000436         | 0.000545         | $1.75 \times 10^{-6}$ | 0.000413         |
| 9             | 0.00747         | 0.0387          | 0.0623          | 0.0129           | 0.000779         | 0.000484         | 0.00404          | 0.000525         | 0.000621         | $2.75 \times 10^{-6}$ | 0.000467         |
| 10            | 0.067           | 0.0345          | 0.268           | 0.0483           | 0.00234          | 0.000823         | 0.0324           | 0.00245          | 0.00285          | 0                     | 0.00198          |

Table 14. As table 13 but with third dredge up ( $\lambda = 0.5$ ) and extra-hot HBB ( $\phi = 0.16$ ).

| $M/M_{\odot}$ | $^{12}\text{C}$ | $^{14}\text{N}$ | $^{16}\text{O}$ | $^{20}\text{Ne}$ | $^{22}\text{Ne}$ | $^{23}\text{Na}$ | $^{24}\text{Mg}$ | $^{25}\text{Mg}$ | $^{26}\text{Mg}$ | $^{26}\text{Al}$      | $^{27}\text{Al}$ |
|---------------|-----------------|-----------------|-----------------|------------------|------------------|------------------|------------------|------------------|------------------|-----------------------|------------------|
| 7             | 0.0113          | 0.0498          | 0.0409          | 0.0104           | 0.00185          | 0.000311         | 0.00308          | 0.000817         | 0.000725         | $3.49 \times 10^{-5}$ | 0.000433         |
| 7.5           | 0.0115          | 0.0345          | 0.0505          | 0.0109           | 0.00115          | 0.000361         | 0.00315          | 0.000702         | 0.000553         | $1.94 \times 10^{-5}$ | 0.000414         |
| 8             | 0.00966         | 0.0399          | 0.0528          | 0.0116           | 0.0012           | 0.000388         | 0.00312          | 0.000973         | 0.000587         | $2.18 \times 10^{-5}$ | 0.000441         |
| 9             | 0.0091          | 0.0517          | 0.0569          | 0.013            | 0.00131          | 0.000413         | 0.00214          | 0.0025           | 0.000649         | $4.53 \times 10^{-5}$ | 0.000498         |
| 10            | 0.067           | 0.0345          | 0.268           | 0.0483           | 0.00234          | 0.000823         | 0.0324           | 0.00245          | 0.00285          | 0                     | 0.00198          |

Table 15. The difference between canonical yields of I06 and our synthetic SAGB yields. We use a pre-SAGB stellar wind according to Ho2, vLo5 mass loss for SAGB stars, set  $\lambda = 0$  and include overshooting for rows marked OVS. A value of zero indicates no difference, a positive value means relative destruction due to SAGB stars, a negative value means creation due to SAGB stars.

| $M/M_{\odot}$ | $^{12}\text{C}$ | $^{14}\text{N}$    | $^{16}\text{O}$ | $^{20}\text{Ne}$ | $^{22}\text{Ne}$     | $^{23}\text{Na}$      | $^{24}\text{Mg}$ | $^{25}\text{Mg}$ | $^{26}\text{Mg}$     | $^{26}\text{Al}$       |
|---------------|-----------------|--------------------|-----------------|------------------|----------------------|-----------------------|------------------|------------------|----------------------|------------------------|
| 8.5           | 0.0413          | -0.0194            | 0.077           | 0.0192           | 0.000145             | 0.000232              | 0.00717          | 0.000709         | 0.00125              | $-3.08 \times 10^{-5}$ |
| 8.5 OVS       | 0.045           | -0.00379           | 0.0739          | 0.0198           | 0.00115              | 0.000181              | 0.00715          | 0.00113          | 0.00144              | $-1.6 \times 10^{-6}$  |
| 9             | 0.0461          | -0.0198            | 0.149           | 0.0285           | 0.000307             | 0.000319              | 0.0209           | 0.00116          | 0.00169              | $-3.23 \times 10^{-5}$ |
| 9 OVS         | 0.0488          | -0.00377           | 0.147           | 0.0292           | 0.00126              | 0.000255              | 0.0209           | 0.00163          | 0.00186              | $-1.64 \times 10^{-6}$ |
| 10            | 0.0586          | -0.00912           | 0.203           | 0.0347           | 0.00149              | 0.000281              | 0.0289           | 0.00187          | 0.00221              | $-3.97 \times 10^{-6}$ |
| 10 OVS        | 0.00302         | $7 \times 10^{-5}$ | 0.0114          | 0.00201          | $7.4 \times 10^{-5}$ | $2.02 \times 10^{-5}$ | 0.00172          | 0.000112         | 0.00013              | 0                      |
| 11.5          | 0.0717          | -0.0121            | 0.322           | 0.028            | 0.00166              | 0.000384              | 0.0297           | 0.00139          | 0.00255              | $-6.86 \times 10^{-6}$ |
| 11.5 OVS      | 0.00342         | $9 \times 10^{-5}$ | 0.0358          | -0.00311         | $3.3 \times 10^{-5}$ | $4.110^{-5}$          | -0.00058         | -0.000119        | $6.6 \times 10^{-5}$ | 0                      |
| 12            | 0.0759          | -0.014             | 0.375           | 0.0243           | 0.00168              | 0.000435              | 0.0293           | 0.00108          | 0.00266              | $-8.52 \times 10^{-6}$ |
| 12 OVS        | 0.00349         | $10^{-4}$          | 0.0408          | -0.00309         | $4 \times 10^{-5}$   | $4.7 \times 10^{-5}$  | -0.00054         | -0.000118        | $8.8 \times 10^{-5}$ | 0                      |

The non-overshooting models show the greatest difference, up to a deficit of  $0.386 M_{\odot}$  in oxygen yield from a  $12 M_{\odot}$  star relative to the canonical model. The overshooting models exhibit a similar behaviour but over a smaller mass range, with little change relative to the canonical models for  $M \geq 10 M_{\odot}$ .

#### 4.3.8 Integrated yields

In order to determine if the SAGB – or not to SAGB – problem is important on a global scale, e.g. for GCE models, we calculate a set of integrated yields with the standard model parameters of Io6 and tested the various physical assumptions made in the previous sections. We define the integrated yield as the sum of the yields from a population of stars with initial masses  $0.1 \leq M/M_{\odot} \leq 80$  weighted by the initial mass function (IMF) of Kroupa et al. (1993). The mass loss prescription of Ho2 (with Ko2 during the TPAGB) is used unless otherwise stated.

The results are shown in table 16.

While the physical assumptions made about SAGB stars are important on a star to star basis, as shown in the previous sections, this is not the case for an integrated stellar yield:

- A. Introduction of an SAGB phase is at the expense of type II supernovae and decreases the integrated yield of  $^{12}\text{C}$ ,  $^{16}\text{O}$ ,  $^{20}\text{Ne}$ ,  $^{24}\text{Mg}$  etc. by typically less than 10%. Only the integrated yield of  $^{14}\text{N}$  increases, by less than 4%, in the non-overshooting models. The overshooting models make less  $^{14}\text{N}$  than the Io6 canonical models because they hot-bottom burn at a lower temperature than the extrapolation of the Io6 would suggest.<sup>2</sup>
- B. Introduction of convective overshooting reduces the mass range for SAGB formation and reduces the mass of SAGB stars. In this case the integrated yields are only slightly different to those of the canonical Io6 models.
- C. If we ignore mass loss prior to the SAGB phase, which means there is no mass loss at all in massive stars, the effect of the SAGB yield is swamped by an increase in supernova yields of oxygen and heavier isotopes and a decrease in carbon because the supernovae explode with more massive CO cores. This is not realistic.

<sup>2</sup> There are also subtle changes due to the difference between  $M_{\text{c,BAGB}}$  from the EVOL models and the Ho2 fit. This affects the mass of hydrogen burned,  $^{14}\text{N}$ -rich material in the intershell region in EAGB stars with  $10 \lesssim M/M_{\odot} \lesssim 12.5$ . This material is ejected during a supernova explosion, so the yield of  $^{14}\text{N}$  depends on  $M_{\text{c,BAGB}}$ . In our  $13 M_{\odot}$  models we use the Ho2  $M_{\text{c,BAGB}}$  so our synthetic models are identical to the Io6 canonical models.

Table 16. Integrated yields from a stellar population with various physical assumptions relative to the canonical yields of I06 (which have no SAGB phase for  $M > 8 M_{\odot}$ ). The yields of  $^{12}\text{C}$  and  $^{16}\text{O}$  are reduced while  $^{14}\text{N}$  slightly increases because of the inclusion of SAGB stars. When overshooting is taken into account (rows marked OVS) there is less effect due to SAGB stars because they form over a narrower mass range. The details of mass-loss, HBB or dredge-up prescription have a very minor effect. A value of 1.0 means the yield is the same as the canonical yield, less than 1.0 means less than the canonical yield and greater than 1.0 means greater than the canonical yield.

| Model                            | $^{12}\text{C}$ | $^{14}\text{N}$ | $^{16}\text{O}$ | $^{20}\text{Ne}$ | $^{22}\text{Ne}$ | $^{23}\text{Na}$ | $^{24}\text{Mg}$ | $^{25}\text{Mg}$ | $^{26}\text{Mg}$ | $^{26}\text{Al}$ | $^{27}\text{Al}$ |
|----------------------------------|-----------------|-----------------|-----------------|------------------|------------------|------------------|------------------|------------------|------------------|------------------|------------------|
| I06                              | 1.000           | 1.000           | 1.000           | 1.000            | 1.000            | 1.000            | 1.000            | 1.000            | 1.000            | 1.000            | 1.000            |
| VLo5                             | 0.963           | 1.016           | 0.932           | 0.960            | 0.979            | 0.984            | 0.872            | 0.945            | 0.935            | 1.130            | 0.956            |
| VLo5 $\lambda = 0.7$             | 0.968           | 1.018           | 0.933           | 0.960            | 0.988            | 0.984            | 0.872            | 0.946            | 0.937            | 1.130            | 0.957            |
| VLo5 OVS                         | 0.985           | 0.966           | 0.980           | 0.983            | 0.978            | 0.993            | 0.960            | 0.966            | 0.969            | 0.885            | 0.981            |
| VLo5 OVS $\lambda = 0.7$         | 0.989           | 0.967           | 0.980           | 0.984            | 0.986            | 0.993            | 0.960            | 0.967            | 0.971            | 0.886            | 0.982            |
| VW93 <sup>1</sup>                | 0.964           | 1.014           | 0.933           | 0.960            | 0.979            | 0.984            | 0.873            | 0.945            | 0.935            | 1.125            | 0.956            |
| VW93 <sup>2</sup>                | 0.960           | 1.035           | 0.930           | 0.960            | 0.980            | 0.982            | 0.868            | 0.977            | 0.934            | 1.396            | 0.957            |
| Reimers $\eta = 1$               | 0.960           | 1.036           | 0.930           | 0.960            | 0.980            | 0.982            | 0.868            | 0.979            | 0.934            | 1.423            | 0.957            |
| Reimers $\eta = 5$               | 0.961           | 1.029           | 0.932           | 0.960            | 0.980            | 0.983            | 0.870            | 0.963            | 0.934            | 1.234            | 0.957            |
| Blöcker $\eta = 0.1$             | 0.965           | 1.009           | 0.933           | 0.960            | 0.978            | 0.985            | 0.873            | 0.940            | 0.935            | 1.112            | 0.956            |
| no TPAGB $\dot{M} \lambda = 0.7$ | 0.964           | 1.235           | 0.927           | 0.960            | 1.045            | 0.979            | 0.861            | 1.028            | 0.965            | 2.674            | 0.966            |
| I06 No-Pre-AGB- $\dot{M}$        | 0.797           | 0.893           | 1.262           | 1.321            | 1.085            | 1.359            | 1.174            | 1.246            | 1.461            | 0.570            | 1.480            |
| No-Pre-AGB- $\dot{M}$ VLo5       | 0.763           | 0.902           | 1.200           | 1.281            | 1.063            | 1.343            | 1.054            | 1.194            | 1.399            | 0.675            | 1.438            |

- D. All other things being equal, the SAGB mass loss prescription alters the total integrated yield per isotope by typically a fraction of one per cent.
- E. Our main conclusions are only invalid when we turn off AGB mass loss and turn on strong dredge up. This combination is difficult to justify.

Compared to the I06 canonical yields our synthetic population with vL05 mass loss, overshooting and no dredge up shows variation by no more than 5% (except for the unstable  $^{26}\text{Al}$  which changes by 11%). This is small compared to uncertainties in GCE codes and their various input parameters and distributions (e.g. Romano et al. 2005).

#### 4.4 DISCUSSION

Our results suggest that SAGB stars are not important contributors to Galactic nucleosynthesis at solar metallicity. The bulk of element production is due to either lower-mass AGB stars or higher-mass stars which explode as type II or Ib/c supernovae. The main effect of introducing SAGB stars into our population models is the removal of the SNII ejecta contribution over a narrow mass range.

Our models also suggest the SAGB stars are not the likely source of abundance anticorrelations in globular clusters. None of our models show simultaneous creation of sodium and destruction of oxygen as required by globular cluster formation scenarios (e.g. Ventura & D'Antona 2005). Hot bottom burning activates the  $^{23}\text{Na}(p, \gamma)^{24}\text{Mg}$  reaction as well as the ON cycle, so both  $^{23}\text{Na}$  and  $^{16}\text{O}$  are destroyed. This is in contrast to the observed anticorrelations e.g. NGC2808 (with  $[\text{Fe}/\text{H}] \sim -1$ ) in which oxygen is depleted by 1.5 dex and sodium enhanced by about 1 dex (Carretta et al. 2006). Lowering the metallicity of our models to match NGC2808 will increase  $T_{\text{BCE}}$  and the  $^{23}\text{Na}(p, \gamma)^{24}\text{Mg}$  reaction rate, exacerbating the problem.

Nuclear reaction rates are uncertain, so we made a synthetic  $10 M_{\odot}$  model with the  $^{22}\text{Ne}(p, \gamma)^{23}\text{Na}$  rate increased by a factor of 2000 (Iliadis et al. 2001). If we turn off mass loss we find a modest 0.35dex increase in sodium and a 0.1dex decrease in oxygen. We can play further by switching on third dredge up. This introduces more  $^{22}\text{Ne}$ , hence  $^{23}\text{Na}$  by  $^{22}\text{Ne}(p, \gamma)^{23}\text{Na}$ , so with  $\lambda = 0.7$  and the increased reaction rate we can force sodium up by 1 dex. However, oxygen is reduced by only 0.2 dex. If we then increase the temperature in line with the overshooting models ( $\phi = 0.12$ ) we can destroy the oxygen, but this activates the  $^{23}\text{Na}(p, \gamma)^{24}\text{Mg}$  reaction which also destroys the sodium. This is all somewhat artificial, because third dredge up increases the C + N + O abundance, which is *not* observed in the globular clusters, and we turned off the mass loss to increase the time for which HBB is active.

Hence our SAGB models do not help to solve the globular cluster abundance anticorrelation problem no matter how hard we push our models.

This is not to say that SAGB stars are not interesting objects. They are the brightest AGB stars and should show some surface abundance changes due to HBB. If mass loss is not as rapid as predicted by vL05 or if we have underestimated  $T_{\text{BCE}}$  then these stars will produce a significant amount of the radioactive  $^{26}\text{Al}$  and associated gamma ray emission, which should be observable.

It is completely unknown if third dredge up occurs in these stars. Even if it does, the high mass-loss rate implied by vL05 limits the contribution of dredged-up material to Galactic abundances unless  $\lambda \sim 1$ . Given the already narrow mass range for SAGB formation, especially when overshooting is taken into account, it is unlikely that third dredge up is important for chemical yield calculations. Regarding the *s*-process, the intershell region of these stars is thin (less than  $10^{-3} M_{\odot}$ ) and the base of the envelope so hot that significant production of *s*-process isotopes is unlikely (Goriely & Siess 2004).

We have neglected to discuss the few massive SAGB stars which do *not* lose their envelope before their core collapses to a neutron star. Such stars are of lower mass than any other neutron star progenitor so are favoured by the IMF and may be a significant formation channel. In our synthetic models with mass loss (vL05 and Ho2) the initial mass range for this channel is  $12.1 - 12.5 M_{\odot}$  or, with overshooting core masses,  $9.0 - 9.6 M_{\odot}$ . There may be nucleosynthesis and expulsion of material during the collapse e.g. some *r*-processing (Wanajo et al. 2003), or there may not (Kitaura et al. 2006), or residual carbon burning (Gutiérrez et al. 2005). Some of our ONe cores have  $^{12}\text{C} = 4\%$  (by mass) which would ignite in a thermonuclear explosion before electron capture takes place. We leave this to a future investigation because we do not currently know the chemical yields from the resulting explosion.

We have not considered the presence of a binary companion to an SAGB star. A companion in a close orbit will lead to mass transfer of the AGB envelope and reduce the amount of nucleosynthesis by third dredge up and HBB (e.g. Izzard 2004). SAGB stars have radii up to  $1000 R_{\odot}$ , considerably larger than early-AGB stars of similar mass, so are more likely to interact with a companion. On the other hand, in wide binaries there might be significant accretion onto a companion star, which could lead to abundance anomalies.

#### 4.5 CONCLUSIONS

In the context of galactic chemical evolution, chemical yields from SAGB stars are not important. The main effect on global yields, at a level of a few per cent, is due to removal of SNII progenitors over a narrow mass

Table 17. Coefficients for the fits to  $T_{\text{BCE}}$  and  $\rho_{\text{BCE}}$ .

| $M/M_{\odot}$ | $a$   | $b$     | $c$    | $d$               | $e$   | $f$   |
|---------------|-------|---------|--------|-------------------|-------|-------|
| 7             | 7.910 | -0.271  | 4.613  | 4709              | -3089 | 8.996 |
| 8.5           | 7.940 | -0.0696 | 6.75   | 4670              | -758  | 7.055 |
| 9             | 7.976 | -0.0638 | 19.0   | 5161              | -946  | 52.2  |
| 10            | 8.015 | -0.0436 | 31.5   | $5.2 \times 10^3$ | -1000 | 200   |
| 11.5          | 8.065 | -0.0314 | 51.388 | $5.0 \times 10^3$ | -1000 | 200   |
| 12            | 8.063 | -0.0314 | 51.388 | $5.2 \times 10^3$ | -1000 | 200   |
| 12.3          | 8.063 | -0.0314 | 51.388 | $5.2 \times 10^3$ | -1000 | 200   |

range. These stars undergo thermal pulses and lose their envelopes by wind loss, leaving a white dwarf. Our SAGB models do not provide for a solution to the globular cluster abundance anticorrelation problems because HBB is too hot to simultaneously destroy oxygen and make sodium – instead our stars destroy sodium.

The yields of SAGB stars are uncertain due to, in order of importance, convective overshooting, mass loss and the efficiency of third dredge up.

If mass-loss rates are much lower than those expected from extrapolation of normal AGB or red supergiant rates, if there is deep third dredge up or deeper dredge out or if our results cannot be applied to lower metallicities, our conclusions may be premature. We are working to extend our detailed model set to lower metallicity where both hot bottom burning and third dredge up are more active.

**ACKNOWLEDGEMENTS** RGI wrote some of the code and did much of the required thinking while at *CIQuA*. Thanks to Evert Glebbeek and Onno Pols for reading the manuscript.

## 4.6 APPENDIX: FITTING DETAILS

### 4.6.1 $T_{\text{BCE}}$ factors

The factors  $a(M)$  to  $f(M)$  are given in table 17.

4.6.2 *Mass loss factors*

The factors of equations 4.5 and 4.6 are

$$\begin{aligned} g_T &= 1 - \exp[-(M_{\text{env}} - 0.94) / 0.753] , \\ g_\rho &= \frac{1.42 + 0.31(M_{\text{env}} + 1)}{1 + 0.025M_{\text{env}}^{-3.7}} . \end{aligned}$$



THE EFFECTS OF BINARY EVOLUTION ON THE  
DYNAMICS OF CORE COLLAPSE AND  
NEUTRON-STAR KICKS

---

Ph. Podsiadlowski, N. Langer, A. J. T. Poelarends,  
S. Rappaport, A. Heger, E. Pfahl

*Astrophysical Journal*, 2004, 612, 1044-1051

**ABSTRACT** We systematically examine how the presence in a binary affects the final core structure of a massive star and its consequences for the subsequent supernova explosion. Interactions with a companion star may change the final rate of rotation, the size of the helium core, the strength of carbon burning and the final iron core mass. Stars with initial masses larger than  $\sim 11 M_{\odot}$  that experience core collapse will generally have smaller iron cores at the point of explosion if they lost their envelopes due to a binary interaction during or soon after core hydrogen burning. Stars below  $\sim 11 M_{\odot}$ , on the other hand, can end up with larger helium and metal cores if they have a close companion, since the second dredge-up phase which reduces the helium core mass dramatically in single stars does not occur once the hydrogen envelope is lost. We find that the initially more massive stars in binary systems with masses in the range  $8 - 11 M_{\odot}$  are likely to undergo an electron-capture supernova, while single stars in the same mass range would end as ONeMg white dwarfs. We suggest that the core collapse in an electron-capture supernova (and possibly in the case of relatively small iron cores) leads to a prompt or fast explosion rather than a very slow, delayed neutrino-driven explosion and that this naturally produces neutron stars with low-velocity kicks. This leads to a dichotomous distribution of neutron star kicks, as inferred previously, where neutron stars in relatively close binaries attain low kick velocities. We illustrate the consequences of such a dichotomous kick scenario using binary population synthesis simulations and discuss its implications. This scenario has also important consequences for the minimum initial mass of a massive star that becomes a neutron star. For single stars the critical mass may be as high as  $10 - 12 M_{\odot}$ , while for close binaries, it may be as low as  $6 - 8 M_{\odot}$ . These critical masses depend on the treatment of convection, the amount of convective overshooting and the metallicity of the star and will generally be lower for larger amounts of convective overshooting and lower metallicity.

### 5.1 INTRODUCTION

For the last decade, it has generally been accepted that the high speeds inferred for isolated, normal radio pulsars imply that neutron stars (NSs) receive a large impulse, or “kick,” at birth. Measured proper motions for  $\simeq 100$  radio pulsars indicate typical kick speeds in excess of  $100 - 200 \text{ km s}^{-1}$  (Lyne & Lorimer 1994; Hansen & Phinney 1997; Cordes & Chernoff 1998; Arzoumanian et al. 2002), though the functional form of the underlying speed distribution is poorly constrained. The physical mechanism that causes this kick is presently unknown, but is presumably the result of some asymmetry in the core collapse or subsequent supernova (SN) explosion (see, e.g., Pfahl et al. (2002c) for discussion and references).

In apparent conflict with the high speeds of isolated radio pulsars, Pfahl et al. (2002c) identified a new class of high-mass X-ray binaries (HMXBs) wherein the neutron stars must have been born with relatively low kick speeds. These HMXBs are distinguished by their long orbital periods ( $P_{\text{orb}} > 30 \text{ d}$ ) and low eccentricities ( $e \lesssim 0.2$ ), with the prime example being X Per/4U 0352+309 ( $P_{\text{orb}} \simeq 250 \text{ d}$ ;  $e \simeq 0.1$ ). The orbits of these systems are sufficiently wide that tidal circularization is negligible, so that the observed eccentricities should reflect the conditions immediately after the SN explosion. Such low eccentricities essentially require that the neutron stars in these systems received low kick speeds of  $\lesssim 50 \text{ km s}^{-1}$ .

Further observational evidence that at least some neutron stars receive low kicks at birth is provided by the fact that a large number of neutron stars are found in globular clusters, where some massive globular clusters may contain more than  $\sim 1000$  neutron stars (Pfahl et al. 2002a). Since the central escape velocity is generally  $\lesssim 50 \text{ km s}^{-1}$ , essentially all of the neutron stars born in a globular cluster should escape from the cluster if they received a kick consistent with the kick distribution for single radio pulsars (for a detailed discussion of this so-called ‘neutron-star retention problem’ see Pfahl et al. 2002a). If all of these neutron stars were originally born in massive binaries, this would alleviate the problem somewhat, since in this case the momentum imparted to the neutron star would be shared by the total mass of the system, leading to a correspondingly smaller space velocity of the post-supernova binary (Brandt & Podsiadlowski 1995). However, while the membership in a binary increases the number of neutron stars that can remain bound in the cluster significantly, the effect may not be large enough to explain the observed numbers unless clusters were much more massive at an earlier epoch than they are today (Drukier 1996; Pfahl et al. 2002a).

To simultaneously account for the new class of HMXBs and the high speeds of radio pulsars, Pfahl et al. (2002c) suggested that neutron stars

originating from progenitors that are single or members of wide binaries receive the conventional large kicks, while neutron stars born in close binaries receive small kicks (also see [Katz 1975, 1983](#) and [Hartman 1997](#) for earlier more *ad hoc* suggestions of a significant population of neutron stars with small natal kicks). [Pfahl et al. \(2002c\)](#) further argued that the proposed dichotomy between high and low kick speeds, and its relation to the evolutionary history of the NS progenitor, might be associated with the rotation rate of the collapsing core. However, as we will show in this paper, the core structure itself (e.g., its mass and composition) depends strongly on whether a star evolves in a close binary or in isolation. This can produce differences in the actual supernova and may allow a prompt (or at least a fast) supernova explosion mechanism to be successful in some cases; this in turn may lead to relatively low supernova kicks.

The outline of this paper is the following: In § 2 we systematically discuss the differences in the core evolution for stars in close binaries and in single systems/wide binaries and discuss the implications for the core-collapse phase. In § 3 we develop a general scheme for forming neutron stars in different types of systems and the expected differences in kick velocity, associating them with individual known systems or classes of systems. In § 4 we discuss how this scheme can be tested both observationally and suggest how further progress can be made on the theoretical side.

## 5.2 BINARY EVOLUTION AND THE PRE-CORE-COLLAPSE CORE STRUCTURE OF MASSIVE STARS

It is often naively assumed that the evolution of helium cores is the same irrespective of whether the core is surrounded by a hydrogen envelope or not, and that the final core structure will be similar in the two cases. However, binary evolution may affect the final pre-supernova structure of a massive star in several fundamentally different ways: (1) the rate of rotation of the immediate pre-supernova core, (2) the size of the helium core, (3) the occurrence of a second dredge-up phase at the beginning of the asymptotic-giant branch (AGB), and (4) the C/O ratio at the end of helium burning which affects the strength of carbon burning and the final size of the iron core. These effects can dramatically change the condition of core collapse as first pointed out by [Brown et al. \(1999\)](#) and in particular [Brown et al. \(2001\)](#), who showed that the final iron cores of massive stars will be significantly smaller for stars that have lost their hydrogen-rich envelopes soon after the end of core hydrogen burning.

### *The role of rotation*

While massive stars are generally rapid rotators on the main sequence,

there are several efficient mechanisms by which they lose their angular momentum during their evolution. The final rotation rate of the core of a massive star depends on whether the star passed through a red-supergiant phase during which the core will be effectively braked by the hydrodynamic and magnetic coupling to the slowly rotating envelope (Spruit & Phinney 1998; Heger et al. 2004) and the wind mass loss during a subsequent Wolf-Rayet/helium-star phase, which can be very efficient in extracting angular momentum from a helium star (Heger & Woosley 2003) and slowing it down in the process. Pfahl et al. (2002c) argued that stars that lost their H-rich envelopes soon after the main-sequence phase (so-called early Case B mass transfer<sup>1</sup>) might avoid this phase where the core is effectively braked and may still be rapidly rotating at the time of core collapse.

However, whether the star can avoid spin-down also depends on whether mass transfer is dynamically stable or unstable. In the case of stable Case B Roche-lobe overflow, Langer et al. (2003) showed that, if the mass-losing star remains tidally locked to the orbit, this provides a very efficient method of slowing down the rotation rate of the mass-losing star. On the other hand, in the case of unstable mass transfer, leading to a common-envelope and spiral-in phase (Paczynski 1976), the spiral-in timescale is much shorter than any realistic synchronization timescale, and tidal locking would not be expected. In this case, the core of the mass-losing star could still be rapidly rotating after the ejection of the common envelope. This implies that the scenario suggested by Pfahl et al. (2002c) probably requires late case B mass transfer (i.e., dynamically unstable mass transfer that leads to a CE phase before the core has been spun down significantly).

Another situation which may lead to a rapidly rotating core is the complete slow merger of two massive stars, in particular if it occurs after helium core burning, as in models for the progenitor of SN 1987A (Ivanova & Podsiadlowski 2003) which predict a very rapidly rotating core for the immediate pre-supernova star (also see Joss & Becker 2003).

Finally we note that, if the exploding star is still accreting from a companion at the time of the supernova, one would also expect a rapidly rotating core (Langer et al. 2004).

As this discussion shows, binary interactions can significantly affect the final pre-supernova rotation rate of the core of a massive star, although the details can be rather involved and are not completely understood. In addition, what is even less clear at the present time is how this affects the physics of the core collapse itself and, in particular, the magnitude of the kick imparted to the newborn neutron star.

<sup>1</sup> It is common practice to distinguish among three evolutionary phases of the primary at the onset of mass transfer, following Kippenhahn & Weigert (1967) (see also Lauterborn 1970; Podsiadlowski et al. 1992). Case A evolution corresponds to core hydrogen burning, Case B refers to the shell hydrogen-burning phase, but prior to central helium ignition, and Case C evolution begins after helium has been depleted in the core.

### *The size of the helium core and the second dredge-up*

The final size of the helium core depends strongly on the evolution of the H-rich envelope. During core helium burning, the helium core ordinarily grows substantially because of hydrogen burning in a shell – often the dominant nuclear burning source – which adds fresh helium to the core. On the other hand, in a binary a star may lose its H-rich envelope before He burning (or early during the He-burning phase). In this case, the helium core can no longer grow and may in fact shrink because of the strong stellar wind expected in the subsequent Wolf-Rayet phase (e.g., [Woosley et al. 1995](#); [Wellstein & Langer 1999](#); [Wellstein et al. 2001](#); [Pols & Dewi 2002](#)). Therefore, the final mass of the helium core will often be lower for stars in close binaries than in single systems/wide binaries (see Fig. 37).

Another factor that strongly affects the mass of the final helium core is the occurrence of a second dredge-up phase. When stars up to  $\sim 11 M_{\odot}$  ascend the asymptotic giant branch, they generally experience a second dredge-up phase where the convective envelope penetrates deep into the H-exhausted core and dredges up a significant fraction of the helium core ([Iben 1974](#)). As a consequence, the size of the helium core can be dramatically reduced (by up to  $\sim 1.6 M_{\odot}$ ; see Fig. 37). However, the occurrence of the second dredge-up depends on the presence of a convective H-rich envelope. If the star loses its H-rich envelope before this phase, dredge-up does not occur. In this case, the final size of the helium core is larger for a star in a binary than its single counterpart (note that this is the opposite of what happens to their more massive counterparts). This is illustrated in Figure 37 which shows the final helium core mass as a function of initial main-sequence mass for single stars (thick solid curve; [Poelarends et al. 2007](#)) and for stars in binaries that lose their envelopes either in Case A or Case B mass transfer (based on the results of [Wellstein et al. 2001](#)). The almost discontinuous change of the final helium mass around  $12 M_{\odot}$  is a direct consequence of the fact that stars below this mass have experienced a second dredge-up phase, while stars above this mass do not or only dredge up a moderate amount of the helium core. Note that the final mass for these stars is less than the minimum mass for core collapse ( $\sim 1.4 M_{\odot}$ ). After the dredge-up phase, the helium core may grow again because of hydrogen shell burning, just as in a normal AGB star. Whether the core can reach the critical mass for core collapse depends on the timescale on which the star loses its envelope in a stellar wind or superwind. While this is somewhat uncertain, we estimate that for the models in Figure 37, single stars below  $\sim 12 M_{\odot}$  will not reach the critical mass for core collapse and will end their evolution as ONeMg white dwarfs. There may be a small mass range around this boundary where single stars reach the condition for core collapse.

In contrast, the shaded region between the dot-dashed thick lines

indicates the expected range of the final helium core mass for stars that lose their envelopes by binary interactions (in this case, the final core mass depends on the evolutionary phase and the core mass at the time of mass transfer).

In the past, [Nomoto \(1984a, 1987a\)](#) has argued that an electron-capture supernova is the expected fate for stars with main-sequence masses in the range of  $8-10 M_{\odot}$ . In his calculations, these stars developed helium cores in the range of  $M = 2.0-2.5 M_{\odot}$ <sup>2</sup> and never developed an iron core; in this case, the collapse is triggered by the electron capture on  $^{24}\text{Mg}$  and  $^{20}\text{Ne}$  ([Nomoto 1984a, 1987a](#)) (for a recent discussion see [Wanajo et al. 2003](#)). In [Figure 37](#), the light dashed horizontal lines indicate approximately the range of helium-core masses which can be expected to lead to an electron-capture supernova (based on the results of [Nomoto \(1984a, 1987a\)](#); also see [Habets 1986](#)). As [Figure 37](#) shows, because of the second dredge-up, the mass range for which single stars experience an electron-capture supernova may be very narrow if non-existent, while there is a large mass range for which it may occur for a star in a close binary. Indeed a binary channel may be the only place where it can occur.

#### *The C/O ratio and the strength of carbon burning*

Another more subtle effect is that the lack of a H-burning shell leads to a lower C/O ratio at the end of helium core burning which affects the strength of subsequent carbon burning and the final size of the iron core. This effect was first pointed out and explained by [Brown et al. \(2001\)](#) and can be understood as follows.

In the late phase of helium core burning, the alpha-capture reaction  $^{12}\text{C} + \alpha \rightarrow ^{16}\text{O}$ , which destroys carbon, tends to dominate over the carbon-producing triple- $\alpha$  reaction (because of the different functional dependence on the number density of  $\alpha$ -particles). As a consequence, carbon is systematically being destroyed in this late core-helium-burning phase (this switch occurs when the helium mass fraction falls below  $Y = 0.1-0.2$ ). In helium cores surrounded by a hydrogen-burning shell, both the hydrogen-exhausted core and the convective helium-burning core continue to increase during helium core burning.

<sup>2</sup> We note that in [Nomoto's](#) calculations, stars in the range of  $8-10 M_{\odot}$  either did not experience a second dredge-up phase or only during carbon shell burning. As a consequence, most of his models in this mass range, unlike ours, experienced a core-collapse supernova even in the case of single stars. We suspect that this difference can be attributed to the different opacities employed. The new OPAL opacities are significantly larger in the critical temperature range, which makes dredge-up more likely or occur earlier. We emphasize that this dredge-up behaviour is qualitatively found in all other recent, detailed studies of stars in this mass range ([Ritossa et al. 1996](#); [Garcia-Berro et al. 1997](#); [Iben et al. 1997](#); [Eldridge & Tout 2004c](#)). We note, however, that the range of initial masses which leads to helium cores in the range of  $2.0-2.5 M_{\odot}$  depends on some of the uncertainties in the stellar modelling, in particular the treatment of convection and convective overshooting (for further discussion of the uncertainties see § 2.2).

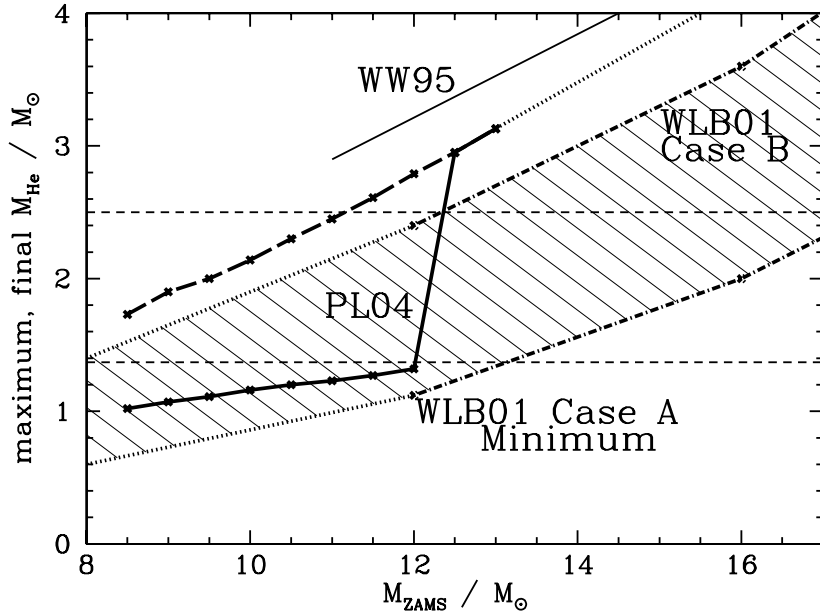


Figure 37. Final mass (thick solid line) and maximum mass (thick dashed line) of the helium core in single stars as a function of initial mass according to [Poelarends et al. \(2007\)](#) (PL04). For comparison, the final helium core masses from the calculations of [Woosley & Weaver \(1995\)](#) are indicated by a thin solid line. The final helium core masses of close binary models undergoing Case B mass transfer from [Wellstein et al. \(2001\)](#) (WLB01) are shown as the upper dot-dashed line, while those experiencing Case A mass transfer (WLB01) may lie anywhere between the lower dot-dashed line and the Case B line. The results from the binary calculations have been extrapolated for initial masses below  $12 M_{\odot}$  (dotted part). Note that the PL04 and WLB01 models have been computed with the same assumptions for convective mixing, while the WW95 models assumed a higher semiconvective mixing efficiency. The light dashed horizontal lines give the range for the final helium core mass for which the star may experience an electron-capture supernova. Note that the parameter range for which this may occur for a single star is very small.

This leads to the continued injection of fresh helium into the helium-burning core and prolongs the phase in which carbon is preferentially destroyed. This eventually produces a smaller carbon abundance at the end of core helium burning than would be the case for a naked helium core, where the convective core does not grow. This has drastic consequences for the subsequent carbon-burning phase if helium or carbon-oxygen cores of similar sizes are compared. For high carbon abundances (as expected for naked helium cores), the phase of convective carbon shell burning lasts longer, typically leading to smaller carbon-exhausted cores). This in turn produces smaller iron cores with steeper density gradients outside the iron core (Fryer et al. 2002; Heger et al. 2002). Thus, for the same initial size of the helium or carbon core, the higher carbon abundance in a star that lost its hydrogen-rich envelope before the central helium abundance dropped below  $\sim 10\%$  will result in a pre-supernova structure that more easily produces a successful supernova.

Brown et al. (2001) demonstrated that this dichotomy leads to much smaller iron cores for massive stars and that, as a consequence, even a  $60 M_{\odot}$  main-sequence star may produce a neutron star rather than a black hole if it has lost its envelope before its helium core-burning phase. In contrast, the minimum mass for black-hole formation for single stars may be as low as  $20 M_{\odot}$  (Fryer 1999; Fryer & Kalogera 2001).

In analogy to these results, it is reasonable to expect that there will be significant differences in the core properties even for massive stars with  $M \lesssim 20 M_{\odot}$ , possibly allowing for successful prompt (fast) supernova explosions (see e.g., Sumiyoshi et al. 2001 and § 2.1).

### 5.2.1 Prompt (fast) explosions and supernova kicks

At present, neither the mechanism that produces a successful core-collapse supernova nor the origin of supernova kicks is properly understood (see Janka et al. 2003; Fryer 2004 for detailed recent reviews, and also Fryer & Warren (2002, 2004). In one of the most popular explosion scenarios, it is the delayed heating by neutrinos that revives the outgoing supernova shock several 100 ms after it stalled in the initial core bounce (i.e., after many dynamical timescales). In this scenario, the origin of the supernova kick may be connected with asymmetries in this long phase where the explosion develops (e.g., due to the continued accretion onto the proto-neutron star or caused by the strong convection in the neutrino-heated region; e.g., Janka et al. 2003). In contrast, in a prompt supernova explosion, the initial bounce drives a successful supernova shock on the dynamical timescale of the proto-neutron star. The absence of a long phase where the explosion teeters at the brink of success could then be the cause for the absence of a large supernova



kick.

Such a scenario is supported by some of the most recent core-collapse simulations by [Scheck et al. \(2004\)](#), see, however, also [Fryer & Warren 2002, 2004](#) for a very different view). In the simulations by [Scheck et al. \(2004\)](#), a large supernova kick (up to and above  $500 \text{ km s}^{-1}$ ) is caused by asymmetries in the neutrino flux, which have their origin in low-order instabilities driven by the convective motion behind the stalled shock. An essential requirement in these simulations, which allows these convective instabilities to grow, is that the duration of the convective, stalled phase is longer than  $\sim 500 \text{ ms}$  (i.e., many convective turnover timescales). Such *slow* explosions are expected for fairly large iron cores. In contrast, for a small iron cores or in the case of electron-capture supernovae, the simulations by [Scheck et al. \(2004\)](#) suggest *fast* explosions where these convectively driven instabilities are unable to grow, leading to rather small kick velocities<sup>3</sup>.

It seems quite attractive to relate the dichotomy in the supernova kicks to the differences between a slow and a prompt (fast) supernova explosion. Whether a supernova explosion develops promptly or in a delayed manner depends mainly on the difference between the mass of the Fe-Ni core and the mass of the collapsing core (which in turn also depends on the initial entropy in the core), since this determines the amount of shock energy that is consumed in the nuclear dissociation of heavy elements (see [Hillebrandt et al. \(1984\)](#) for a detailed discussion and references; [Sumiyoshi et al. 2001](#)).

Electron-capture supernovae provide a particularly promising scenario for a prompt (fast) explosion, since the whole core collapses to nuclear densities; this makes it much easier for the shock to eject the envelope, preventing the growth of the instabilities that lead to large kicks. As our previous discussion shows, electron-capture supernovae may only (or mainly) occur in close binaries; in this case, neutron stars with low kicks may be (almost) exclusively produced in close binary systems (with orbital periods  $\lesssim$  a few 100 d).

### 5.2.2 *The minimum mass for core collapse*

An important related issue is the question of the minimum initial mass,  $M_{\text{min}}$ , of a star that leads to a core-collapse supernova in a single or binary system. It is commonly assumed that this minimum mass is around  $8 M_{\odot}$ , the minimum mass above which ignite carbon off-center (rather than explosively in the center) and form an ONeMg core ([Iben 1974](#)). If the ONeMg core is able to grow to reach the Chandrasekhar mass, it will collapse in an electron-capture supernova. However, if a

<sup>3</sup> Note that, unlike the case of a *prompt* explosion, the fast explosions in the simulations by [Scheck et al. \(2004\)](#) occur on a timescale long compared to the dynamical timescale of the proto-neutron star.

star experiences mass-transfer already on the main sequence, an initial star as massive as  $\sim 16 M_{\odot}$  may end its evolution as a white dwarf rather than experience core collapse<sup>4</sup>. On the other hand, as discussed above, stars below  $12 M_{\odot}$  may only experience core collapse if they have lost their envelopes by binary interactions after their main-sequence phase but before experiencing dredge-up on the AGB. This implies that the value of  $M_{\min}$  may be as high as  $12 M_{\odot}$  for single stars and as low as  $8 M_{\odot}$  for relatively close binaries.

The exact value for  $M_{\min}$  is quite sensitive to the treatment of convection and, in particular, the amount of convective overshooting, and the metallicity of the star. The value of  $M_{\min} = 12 M_{\odot}$  was obtained for models that used the Ledoux criterion for convection without convective overshooting. We estimate that using the Schwarzschild criterion would reduce  $M_{\min}$  to  $\sim 11 M_{\odot}$  if no convective overshooting is included, and to  $\sim 10 M_{\odot}$  if the recent empirical calibration of convective overshooting (Pols et al. 1997; Schroder et al. 1997) is adopted (also see Ritossa et al. 1999; Eldridge & Tout 2004c). Similarly, the minimum mass for off-center carbon ignition may be as low as  $\sim 6 M_{\odot}$  for models including convective overshooting (Han 2002, unpublished).

Han et al. (1994) also found that, for low-metallicity ( $Z = 0.001$ ) models without convective overshooting, the minimum mass for off-center carbon ignition was systematically lower ( $\sim 6 M_{\odot}$ ) than for solar metallicity ( $\sim 8 M_{\odot}$ ).

As these discussions illustrate, the initial mass range that leads to the formation of ONeMg white dwarfs, which also determines the minimum mass for stars that will experience core collapse, depends both on the details of binary interactions and on the stellar properties. Different treatments of convection are expected to lead to initial mass ranges ranging from  $[6,9] M_{\odot}$  to  $[9,12] M_{\odot}$ . In addition at low metallicity, these ranges should be systematically shifted towards lower masses (by perhaps  $2 M_{\odot}$  for  $Z = 0.001$ ; Han et al. 1994). Considering that this is an important parameter in galactic modelling, a thorough re-examination of this issue is urgently needed (Poelarends et al. 2007; Eldridge & Tout 2004c).

We emphasize that the exact values of this mass range do not affect the main arguments in this paper, since this only shifts the mass range in which an electron-capture supernova can be expected, but does not change the expected dichotomous behaviour.

---

<sup>4</sup> This occurs when the system experiences an additional RLOF phase after core He exhaustion (Case ABB mass transfer; Wellstein et al. 2001; Podsiadlowski et al. 2003) during a He red-supergiant (RSG) phase; strong mass loss during the He-RSG stage may lead to a similar outcome.

### 5.3 A DICHOTOMOUS KICK SCHEME

The scenario for NS kicks proposed herein has a significant impact on the theoretical production probabilities and distributions of orbital parameters of binary systems containing neutron stars. We illustrate this by means of a Monte Carlo binary population synthesis (BPS) calculation. Below we provide a brief description of the important elements of the code; further details may be found in Pfahl et al. (2002b,a,c, 2003). The BPS code follows a randomly generated sample of massive primordial binaries through the phase of mass transfer from the primary to the secondary.<sup>5</sup> The initial primary and secondary masses,  $M_{1i}$  and  $M_{2i}$ , are drawn from the respective distributions  $p(M_{1i}) \propto M_{1i}^{-2.5}$  and  $p(q_i) = 1$ , where  $q_i \equiv M_{2i}/M_{1i} < 1$  is the initial mass ratio. For simplicity, we assume circular orbits, and the initial orbital separation,  $a_i$ , is chosen from  $p(a_i) \propto a_i^{-1}$ .

Given some critical mass ratio, which we take to be  $q_c = 0.5$ , the mass transfer from the primary to the secondary is assumed to be stable if  $q_i > q_c$  and the envelope of the primary is mostly radiative when mass transfer begins (so-called Cases “A”, “early B”, and “early C”), and dynamically unstable if  $q_i < q_c$  or the primary has a convective envelope (Cases “late B” and “late C”). In any case, we assume that the entire hydrogen-rich envelope of the primary is removed during mass transfer, leaving only the primary’s hydrogen-depleted core.

For stable mass transfer, we suppose that the secondary accretes a fraction,  $\beta = 0.75$ , of material donated by the primary, and that the remaining mass escapes the system with a specific angular momentum that is  $\alpha = 1.5$  times the orbital angular momentum per unit reduced mass. The value of  $\alpha = 1.5$  is characteristic of mass loss through the L2 point, but the choice of  $\beta = 0.75$  is fairly arbitrary – although it is convenient, as it gives  $a_f/a_i \sim 1$ , where  $a_f$  is the final orbital separation. Dynamically unstable mass transfer results in a common-envelope phase, wherein the secondary spirals into the envelope of the primary. The common-envelope phase was treated in the same way as in Pfahl et al. (2002c). A fraction,  $\eta_{CE} \lesssim 1$ , of the initial orbital energy is available to unbind the common envelope from the system. If insufficient energy is available, the two stars will merge. Otherwise, the envelope of the primary is dispersed, the secondary emerges near the ZAMS without having accreted any significant amount of mass, and the orbital separation is  $\sim 100$  times smaller. A merger results in nearly every case where  $q_i < q_c$  and the primary’s envelope is radiative when mass transfer starts. A number of these evolutionary steps are illustrated in the top six panels of the schematic shown in Figure 39.

<sup>5</sup> Here “primary” and “secondary” refer to the initially more and less massive star, respectively.

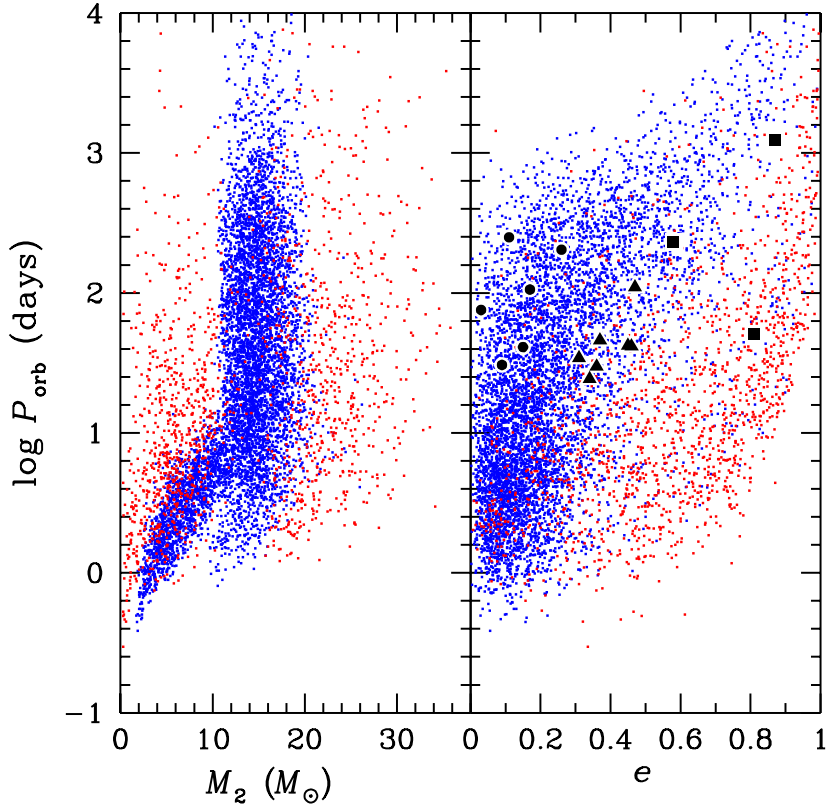


Figure 38. Results of a single HMXB binary population synthesis calculation that utilizes our proposed dichotomous kick scenario. Each red (blue) dot represents a system where the primary was (was not) highly evolved when it lost its hydrogen-rich envelope, and the exposed core evolved to collapse to form a neutron star with a subsequent large, conventional (small, unconventional) natal kick; see the text for details. Markers in the right panel indicate the observed wide, low-eccentricity HMXBs (*filled circles*), and the well-known eccentric HMXBs (*filled triangles*). The *filled squares* show the three radio pulsars with massive binary companions in eccentric orbits. We did not include observed systems with  $P_{\text{orb}} \lesssim 10$  days, since their orbital parameters are likely to have been altered by tidal circularization effects.

## Dichotomous Kick Scenario

Large Natal Kick    Small Natal Kick

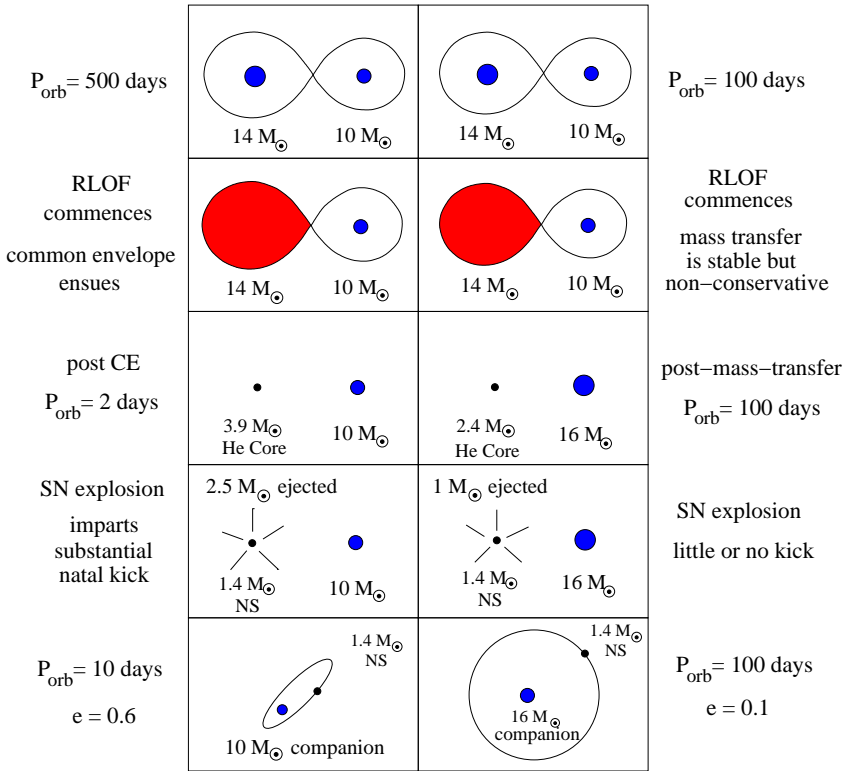


Figure 39. Illustrative binary evolution scenarios leading to the formation of high-mass X-ray binaries. In the left panel, the binary is sufficiently wide at the onset of mass transfer that the primary has a fully formed  $3.9 M_{\odot}$  He core. By contrast, in the right panel the primary’s envelope is lost while the He core is substantially lower in mass ( $2.4 M_{\odot}$ ). In the proposed dichotomous kick scenario the former case leads to a large natal kick, while the latter case results in a “prompt (fast)” supernova event and a smaller kick (see text).

Upon exhausting its remaining nuclear fuel, the exposed core of the primary explodes as a Type Ib or Ic SN. We assume that the supernova mass loss and natal NS kick are instantaneous, and that the orientations of the kicks are distributed isotropically. In light of the discussion above, the specific prescription adopted for NS kicks is as follows. Kick speeds are drawn from a Maxwellian distribution, with a mean that depends on the initial mass of the primary and its evolutionary state when it first fills its Roche lobe (see Fig. 39). If  $8 < M_{1i} < 14M_{\odot}$  and mass transfer begins before helium ignition in the primary’s core (Cases A and B), the mean kick speed takes a small value of  $30 \text{ km s}^{-1}$ , while in all other cases the mean is  $300 \text{ km s}^{-1}$ . The range of masses and the actual mean kick speeds used here are reasonable choices, but are somewhat arbitrary, and were chosen mainly for illustrative purposes.

The results of our BPS calculation are shown in Figure 38 in the  $P_{\text{orb}} - M_2$  and  $P_{\text{orb}} - e$  planes, where  $M_2$  is the mass of the secondary star, including the mass it has accreted from the primary, and  $e$  is the orbital eccentricity. Each small dot represents an incipient high-mass X-ray binary immediately after the supernova explosion that produces the neutron star. The red dots represent systems which experienced the nominal natal neutron star kicks (see also left column of Figure 39) while the blue dots are systems where the primary lost its envelope early enough so that the natal kicks were much smaller – in accord with the dichotomous kick scenario proposed herein (see right hand panel of Fig. 39).

The vertical blue strip in the  $P_{\text{orb}} - M_2$  plane of Fig. 38 results mostly from early Case B systems in which the primaries had largely radiative envelopes and start mass transfer before core He ignition. The resultant mass transfer is stable and the H-exhausted core evolves to a “prompt (fast)” SN explosion with a small natal kick. These systems generally acquire small eccentricities, especially for  $P_{\text{orb}}$  in the range of 10–100 days. These are presumably the systems that evolve to become the newly identified class of HMXBs with relatively wide, low-eccentricity orbits (e.g., X Per/4U 0352 + 30;  $\gamma$  Cas/MX 0053+604; XTE J0543-568; the filled circles in Fig. 38). For the systems of this type with still wider orbits, even the small natal kicks assumed here are sufficient to induce substantial eccentricities.

The blue “tail”-shaped region in the  $P_{\text{orb}} - M_2$  plane of Figure 38 results from late Case B systems commencing mass transfer when the primary had a large, convective envelope, but still before core He core ignition. These lead to common-envelope events and result in systems with short orbital periods (i.e.,  $P_{\text{orb}} < 10$  days; see e.g., Fig. 39). Since such short period systems would, in any case, be circularized by tidal friction, it may be difficult to distinguish these from their Case C cousins where the primaries were much more evolved at the start of mass transfer, and which received larger natal kicks. Systems in these

latter categories (late Case B and late Case C) presumably include many of the famous HMXBs such as Cen X-3, LMC X-4, 4U 0900-40, and SMC X-1, with current-epoch (approximately) circular orbits and short orbital periods. The red dots in Figure 38 are those receiving a large kick, where the primary was highly evolved at the onset of mass loss (Case C). These likely account for the class of eccentric HMXB systems with  $P_{\text{orb}}$  in the range of  $\sim 20 - 200$  days, e.g., 4U 0115+63, GX 301-2, 4U 1145-619, and EXO 2030+375 (Bildsten et al. 1997) (filled triangles in Fig. 38) and the three radio pulsars with massive companions in highly eccentric systems (filled squares in Fig. 38) PSR 1259-63 (Johnston et al. 1992), PSR J0045-7319 (Kaspi et al. 1994, 1996) and PSR J1740-3052 (Stairs et al. 2001).

Finally, we note that this dichotomous kick scenario helps the long-standing “retention problem” for neutron stars in globular clusters. In an earlier work (Pfahl et al. 2002a) we reported that our original dichotomous kick scenario yielded an enhancement factor of about 4 over the fraction of retained neutron stars without the appropriate subset of small kicks. We also pointed out (Pfahl et al. 2002a) that a dichotomous kick scenario would likely increase the theoretical formation rate of double neutron star systems by approximately an order of magnitude. Both of these enhancements are expected to be carried over to this newer kick scenario.

#### 5.4 DISCUSSION AND FUTURE WORK

As we have shown, the presence in a binary can dramatically affect the structure of the core of a massive star at the time of core collapse. Stars above  $\sim 11 M_{\odot}$  are generally expected to have smaller iron cores if they lose their envelopes in a close binaries. Stars in the range of  $8 - 11 M_{\odot}$  may explode in an electron-capture supernova if they are in a close binary, while single stars or stars in wide binaries will experience a second dredge-up phase and are more likely to end their evolution as ONeMg white dwarfs. We suggested that in the case of small iron cores or in the case of an electron-capture supernova, the supernova occurs through a prompt (fast) explosion rather than a delayed neutrino-driven explosion and argued that this is more likely to produce neutron stars with low kick velocities.

While speculative at the moment, this scenario has important observational implications and suggests the need for further theoretical studies. These include a systematic exploration of the late evolution of the cores of stars around  $10 M_{\odot}$ , both for stars evolved in isolation and in a close binary, the dependence on metallicity and the amount of convective overshooting (e.g., Poelarends et al. 2007; Eldridge & Tout 2004c), and a re-examination of the core-collapse phase for electron-capture supernovae and low-mass iron cores. One immediate prediction

of this scenario is that neutron stars that formed from ONeMg or low-mass iron cores should produce neutron stars of systematically lower mass ( $\sim 1.25 M_{\odot}$  for a typical equation of state<sup>6</sup>). [Wanajo et al. \(2003\)](#) suggested that prompt explosions are the site for the r-process; if some of this r-processed matter is captured by the companion stars, this may produce detectable chemical anomalies in neutron-star companions (e.g., X Per) similar to the case of the companion in Nova Scorpii ([Israelian et al. 1999](#); [Podsiadlowski et al. 2002](#)). Note also that, in this case, only small amounts of iron and other heavy elements are ejected in the supernova. If all neutron stars in globular clusters were to form through such a channel, one would not expect significant chemical pollution of the cluster with heavy elements from supernova ejecta ([Price & Podsiadlowski 1993](#)).

Our scenario also has important implications for the minimum mass for neutron-star formation; it suggests that only single stars more massive than  $\sim 10\text{--}12 M_{\odot}$  become neutron stars, while in binaries the mass may be as low as  $6\text{--}8 M_{\odot}$ . The exact values will depend both on the amount of convective overshooting and the metallicity of the population; larger amounts of overshooting and lower metallicity are both expected to shift these critical masses to lower values. The detection of both young, single massive white dwarfs and neutron stars in binaries in open clusters with a turnoff mass around  $10 M_{\odot}$  would provide direct evidence for such a dichotomy. Another promising method to observationally constrain the minimum mass for a core-collapse supernova is through the detection of the progenitors of Type II-P supernovae, stars that have not lost all of their H-rich envelopes at the time of the supernova explosion (see e.g., [Smartt et al. 2002](#)).

Finally, it is worth mentioning another channel which is likely to produce an electron-capture supernova and possibly a neutron star with a low kick if the basic picture described in this paper is correct: this involves the accretion-induced collapse (AIC) of a white dwarf to form a neutron star, either because an ONeMg white dwarf accreting from a companion star is pushed above the Chandrasekhar limiting mass ([Nomoto 1987b](#); [Nomoto & Kondo 1991](#)) or as the result of the merger of two CO white dwarfs which is also likely to lead to the formation of a neutron star rather than a Type Ia supernova ([Nomoto & Iben 1985](#)). In principle, AIC could produce single low-velocity neutron stars with a rate as high as  $3 \times 10^{-3} \text{ yr}^{-1}$  ([Han 1998](#); [Nelemans et al. 2001](#)).

---

<sup>6</sup> The pulsar that formed last in the recently discovered double-pulsar binary PSR J0737-3039 ([Burgay et al. 2003](#); [Lyne et al. 2004](#)) has a low mass of  $\sim 1.25 M_{\odot}$ , although at present it is not clear whether the formation of the second pulsar is consistent with a low-velocity kick.



ACKNOWLEDGMENTS We thank H.-Th. Janka and C. F. Fryer for very useful discussions.



## NEDERLANDSE SAMENVATTING

---

Als je op een heldere nacht naar boven kijkt, kun je er een paar duizend zien. Maar die paar duizend is maar een heel klein gedeelte van het totale aantal sterren dat bestaat. Om het nog onwerkelijker te maken: we weten niet eens hoeveel sterren er zijn; in ieder geval miljarden en waarschijnlijk wel iets van 100 miljard keer 100 miljard. Maar dat is maar een schatting...

Sterrenkunde is de wetenschap van de 'grote getallen.' De afstand tot onze zon is nog net in kilometers uit te drukken (150 miljoen kilometer), maar de afstand tot de dichtstbijstaande ster wordt al lastig (ongeveer 35 miljard kilometer). En ook de zon zelf, eigenlijk maar een middelmatig sterretje, is al erg groot en zwaar vergeleken bij wat we nog een beetje kunnen begrijpen naar aardse maatstaven. Sterrenkundigen hebben daarom een soort van eigen eenhedenstelsel ontwikkeld, met de zon als standaard.

*Sterrenkundige eenheden*

- $1 M_{\odot}$  staat voor 1 zonsmassa en is ongeveer  $2 \times 10^{30}$  kg, en dat is een 2 met dertig nulletjes erachter.
- $1 R_{\odot}$  staat voor 1 zonsstraal en is ongeveer 700.000 km.
- $1 L_{\odot}$  staat voor 1 zonslichtkracht en is ongeveer  $4 \times 10^{26}$  Watt, vergelijkbaar met 4 met 24 nulletjes 100 Watt lampen.

Zo worden de enorme getallen teruggebracht tot wat werkbaardere getallen.

Toch is het een vergissing om te denken dat sterrenkundigen alleen maar bezig zijn met grote dingen. Om iets groots als een ster te begrijpen, moet je juist heel veel weten over hoe het er op microscopisch niveau aan toe gaat. Het allerkleinste niveau waar sterrenkundigen zich mee bezig houden, is het niveau van atomen, die op hun beurt bestaan uit protonen (positief geladen deeltje), neutronen (neutraal, of ongeladen deeltje) en elektronen (negatief geladen deeltje). Juist deze kleine deeltjes, waarvan er miljarden zijn in een ster, zijn essentieel voor hoe een ster eruit ziet, wat hij allemaal meemaakt gedurende zijn leven, en hoe hij uiteindelijk 'doodgaat'. Sterrenkundigen die dit allemaal proberen te begrijpen houden zich bezig met sterevolutie.

*protonen,  
neutronen en  
elektronen*

*Sterevolutie*

### 6.1 DE EVOLUTIE VAN STERREN

Het begin van het leven van iedere ster is in een grote gaswolk. Hoe die gaswolk daar gekomen is voert te ver om hier in detail te bespreken

*Gaswolk*

– en veel daarvan is nog onduidelijk – maar oorzaken kunnen liggen in botsingen van sterrenstelsels of andere verstoringen, die ervoor zorgen dat er op één plek een behoorlijke hoeveelheid gas terecht is gekomen. Sommige van deze gaswolken zijn heel klein, maar anderen zijn heel groot en zwaar, zodat zich met gemak honderden, soms wel duizenden of miljoenen sterren uit zo'n gaswolk kunnen vormen.

*Instortende  
gaswolk*

Laten we eens kijken naar één zo'n gebiedje in een gaswolk. Door een of andere oorzaak wordt op een gegeven moment de dichtheid (aantal deeltjes per kubieke centimeter) in ons gebied iets hoger dan in de rest van de wolk. Door deze hogere dichtheid en dus 'ophoping' van massa (gewicht) gaat ons gebied andere deeltjes die in de buurt zitten aantrekken, waardoor ons gebied steeds zwaarder wordt, en op een gegeven moment onder zijn eigen gewicht gaat instorten. Alle deeltjes in de omgeving zullen worden aangetrokken door de zwaartekracht, en zich naar het gebied toe bewegen met de hoogste dichtheid. Hierdoor neemt de dichtheid nog verder toe, en ook de temperatuur gaat stijgen.

*Waterstoffusie*

Hoe hoger de temperatuur in het binnenste van dit stukje gaswolk wordt, hoe sneller de gasdeeltjes (protonen & neutronen) gaan bewegen. Eerst vliegen ze nog lekker langs elkaar heen, maar als de temperatuur en de dichtheid gaan stijgen, komen ze vaker met elkaar in botsing, maar ze kaatsen ieder een andere kant op alsof het een soort biljartspel is. Doordat er de kern van onze *proto-ster* zwaarder en zwaarder wordt, blijft de temperatuur stijgen, totdat hij hoog genoeg is om de gasdeeltjes niet alleen te laten botsen, maar ze zo hard te laten botsen, dat ze met elkaar versmelten, of om de wetenschappelijke term te gebruiken, ze fuseren. Een proton (waterstofdeeltje dat zijn elektron is verloren) en een neutron vormen samen een deuteriumdeeltje, en als twee deuteriumdeeltjes botsen en fuseren, wordt dit een heliumdeeltje. Het bijzondere van zo'n botsing is dat er bij die botsing (of fusie) energie vrijkomt, in de vorm van een lichtdeeltje. Als er één schaap over de dam is, volgen er meer. Overal waar de temperatuur hoog genoeg is – en dat zal vooral in het centrum van onze proto-ster zijn – beginnen protonen op elkaar te botsen en met elkaar te fuseren. En door al die reacties ontstaat er een soort stroom van licht die zich vanuit het centrum van de ster een weg naar buiten baant, waardoor de gaswolk gaat stralen. Een nieuwe ster is geboren!

*Levensduur zon*

Stel nu dat dit een ster is die vergelijkbaar is met onze zon. Hoeveel van zulke fusiereacties moeten er dan plaatsvinden per seconde om zo fel te kunnen stralen als de zon? Een snelle berekening laat zien dat  $1 L_{\odot} = 3.85 \times 10^{26} \text{ J/s} = 2.4 \times 10^{39} \text{ MeV/s}$ . Iedere fusiereactie levert 26.72 MeV op, en dat betekent dus dat er iedere seconde  $9 \times 10^{37} \times 4$  protonen worden omgezet in 1 helium deeltje. Hoelang zou de zon dit vol kunnen houden? Als we aannemen dat alleen de binnenste 10% van de zon meedoen met het botsings- en fusiefeest dan hebben we daar ongeveer  $0.1 M_{\odot} = 2 \times 10^{29} \text{ kg} = 1.2 \times 10^{56}$  deeltjes (1 deeltje – proton

of neutron – weegt ongeveer  $1.67 \times 10^{-27}$  kg). We delen dan het aantal deeltjes dat we op voorraad hebben, door het aantal deeltjes dat we per seconde verbruiken, en dan komen we uit op  $3.33 \times 10^{17}$  seconden, wat ongeveer gelijk is aan 10.5 miljard jaar. Zolang kan de zon dus doen met haar brandstof (onder alle aannames die we hebben gedaan)! De fase waarin dit proces (protonen worden omgezet in helium) plaatsvindt, noemen we de hoofdreeks. Omdat sterren die zwaarder zijn dan de zon veel meer licht produceren en dus sneller door hun brandstof heen zijn, zitten ze gemiddeld korter op de hoofdreeks dan lichtere sterren.

*Hoofdreeks*

Als de kern van onze ster volledig is omgezet in helium en er geen protonen meer over zijn, gaat de kern weer krimpen. Door dit krimpen gaan de temperatuur en dichtheid weer omhoog. Op een gegeven moment is de temperatuur hoog genoeg om te beginnen met de fusie van helium, waarbij drie heliumdeeltjes op elkaar botsen en fuseren tot één koolstofdeeltje. En langzamerhand wordt zo de kern van deze ster omgezet in koolstof en ook zuurstof (als er een heliumdeeltje fuseert met een koolstofdeelte). Als de ster zwaar genoeg is, kan dit proces (fusie → brandstof op → krimpen → temperatuur & dichtheid omhoog → temperatuur hoog genoeg voor volgende fusiereactie → fusie) zich nog een aantal keer herhalen. De ster gaat dan van heliumfusie over in koolstoffusie, waarna nog fusie volgen van neon, zuurstof en silicium. Omdat iedere volgende stap in deze keten steeds minder energie oplevert, zullen deze stappen zich ook steeds sneller achter elkaar voordoen. Zo duurt bijvoorbeeld heliumfusie in een gemiddelde ster nog een paar miljoen tot een miljard jaar, terwijl siliciumfusie – de laatste stap – in zware sterren maar een paar uren duurt.

*Heliumfusie*

*De kringloop van de overige fusiefases*

Niet alle sterren gaan door al deze fases heen. Om koolstof te kunnen fuseren moet een ster in ieder geval 7.5 keer zwaarder zijn dan de zon, en voor neon geldt een grens van ongeveer  $9.25 M_{\odot}$ . Sterren die nog zwaarder zijn, zullen niet alleen neon fuseren, maar ook alle andere fusiereacties achter elkaar doorlopen.

*De massa van een ster bepaald zijn uiteindelijke lot*

Hoe een ster evolueert, door welke fusieprocessen hij heengaat, en wat z'n uiteindelijke lot is, hangt dus voor een groot gedeelte af van hoe zwaar de ster is. Daarom maken sterrenkundigen een onderscheid tussen lichte sterren en zware sterren.

### 6.1.1 Lichte sterren

Lichte sterren zijn sterren die waterstoffusie, heliumfusie en misschien ook nog koolstoffusie hebben, maar daarna stopt het. Ondanks dat de kern weer begint te kringen, kan de temperatuur niet hoog genoeg meer worden om verder te gaan met de fusie van neon. Langzaam koelt de ster af en vormt een heel klein bolletje, ongeveer zo groot als de aarde, maar met een massa die ergens in de buurt van de zon zit. Daarom heen zitten nog twee dunne schillen. In de binnenste schil,

*Asymptotische  
reuzentak ster*

*Thermische puls*

*Exotische  
chemische  
reacties*

*Witte dwerg*

die direkt om het bolletje heenligt, wordt helium gefuseerd, en in een schil die net iets verder naar buiten zit, wordt waterstof gefuseerd. Door deze aparte opbouw van de ster, is hij heel groot en heel helder, maar relatief koel (ongeveer 3000 graden Celsius). Omdat de ster zo groot is, wordt hij een reus genoemd, en de naam die sterrenkundigen eraan hebben gegeven is *asymptotische reuzentak ster*, of in het engels asymptotic giant branch star, afgekort met AGB star, een afkorting die je veel tegen komt in dit proefschrift. In de heliumfusieschil, die dus bovenop de kern ligt, gebeuren allemaal spectaculaire dingen. De meeste tijd is de heliumfusie op een heel laag niveau, en wordt er, door de waterstofschild erboven – die rustig doorgaat met fuseren – een soort van heliumbuffer opgebouwd. Maar eens in de zoveel tijd treedt er een soort van kettingreactie op waardoor een groot deel van de pas opgebouwde heliumbuffer in één keer wordt omgezet in koolstof en zuurstof. In een korte tijd komt er hierdoor heel veel energie vrij – bijna 100 miljoen keer zoveel als de zon per seconde uitzendt – en een soort van schokgolf gaat door de bovenliggende lagen, die de hele opbouw van de ster gedurende korte tijd ontregeld. De ster wordt nog groter en helderder dan hij al was, maar uiteindelijk komt alles weer tot rust en lijkt het alsof er niks is gebeurd. Maar schijn bedriegt! Gedurende de puls (zo noemen we zo'n plotselinge fusiereactie en volgende opvlakking van de ster), maar ook in de periode daarna, zijn er allerlei bijzondere reacties op gang gekomen die allerlei exotische chemische elementen hebben gemaakt die je normaal niet zo snel in sterren vindt, elementen zoals borium en thorium, maar ook zilver, goud en lood die heel belangrijk zijn voor de chemische samenstelling en evolutie van het heelal. Maar daarover later meer. Gedurende deze fase wordt de mantel van de ster steeds kleiner, totdat hij helemaal weg is, en alleen de kern van de ster is overgebleven. Het enige wat deze kern nu nog kan doen is afkoelen, en we noemen zo'n ster een witte dwerg.

### 6.1.2 *Zware sterren*

In tegenstelling tot lichte sterren, kan de temperatuur in de kern van zware sterren wel hoog genoeg worden om alle fusiereacties te voltooien. Nadat de heliumkern is omgezet in een kern van koolstof en zuurstof, komt koolstof tot ontbranding en wordt de kern een neon-zuurstof kern. Neon kan daarna fuseren en laat een magnesium-zuurstof kern achter, waarna alle zuurstof wordt gefuseerd tot silicium. De laatste stap in deze keten is de fusie van silicium tot ijzer. Omdat deze laatste stappen steeds minder energie opleveren, volgens ze steeds sneller op elkaar. De stap van silicium tot ijzer is de laatste stap, omdat alle reacties voorbij ijzer energie kosten en geen energie meer opleveren, wat natuurlijk niet zo voordelig is voor de ster. Als eenmaal de kern

van de ster uit ijzer bestaat, en er dus geen verdere fusieprocessen meer mogelijk zijn die wel energie opleveren om de ster stabiel te houden, begint de ster in te storten. Er is niks meer dat de aantrekkende kracht van de zwaartekracht kan weerstaan en met enorme snelheden stort het gas, wat zich rondom de kern bevindt, naar beneden, naar het centrum. Daar loopt de druk zo hoog op, dat op een gegeven moment de ijzerkernen uit elkaar vallen in losse protonen, neutronen en elektronen, de protonen en elektronen samensmelten tot nog meer neutronen, totdat uiteindelijk de neutronen allemaal tegen elkaar aan komen te liggen en zo een keiharde bal vormen van ongeveer 10 kilometer groot, een zogenaamde neutronenster. Alle deeltjes die nu nog naar beneden vallen, komen hard in botsing met deze neutronenster en stuiteren terug omhoog, waardoor er enorme schokgolven zich een weg naar buiten banen door het gas wat er over is gebleven van de ster. De invallende beweging die het gas maakte, wordt gekeerd en alle gas wordt nu met enorme snelheden het heelal in geslingerd. De ster ontploft en veroorzaakt een lichtflits die we tot diep in het heelal kunnen waarnemen, en wat sterrenkundigen een supernova explosie noemen. Omdat tijdens de explosie de temperatuur tot ontzettend hoge waarden kan oplopen, worden er ook hier allerlei exotische chemische elementen gemaakt die niet tijdens de gewone evolutie van sterren ontstaan.

*Ijzerkern begint  
in te storten*

*Neutronenster*

*Supernova  
explosie*

### 6.1.3 Tussen lichte en zware sterren

Als je tot zover in dit verhaal gekomen bent, dan kun je nu de voor de hand liggende conclusie trekken dat er ergens een overgang moet zijn tussen lichte sterren en zware sterren. En dat klopt: die overgang is precies het onderwerp van dit proefschrift, omdat hierover nog heel veel onduidelijk is. Twee dingen spelen op deze overgang een belangrijke rol. De eerste is hoe snel de ster zijn mantel verliest, en de tweede is hoe snel de kern kan groeien. Als de ster zijn mantel verliest, voordat de kern – die ondertussen al z'n koolstof heeft omgezet in zuurstof en neon – een bepaalde kritische waarde heeft bereikt, dan wordt de ster een witte dwerg, net zoals alle andere lichte sterren. Als de kern echter eerder de kritische massa bereikt voordat de hele mantel is weggeblazen, dan zal de ster exploderen als een supernova, en lijken op een zware ster. Het lijkt een beetje op een race, een competitie tussen het groeien van de kern en het verliezen van de mantel. Het zijn dus een speciaal soort sterren op die overgang, omdat ze lijken op een lage massa ster – en dus aan het einde van hun leven net een AGB ster zijn met allemaal van die thermische pulsen – maar die toch, op een of andere manier, ontploffen als een supernova. Deze bijzondere sterren noemen we daarom Super-AGB sterren.

*Overgang  
tussen lichte en  
zware sterren*

*Super-AGB  
sterren*

Rondom deze overgang zijn er veel dingen die nog onduidelijk zijn, o.a. waar die overgang zich bevindt en hoe breed die overgang is,

hoeveel van zulke speciale sterren zijn er eigenlijk, hoe zien ze er uit, kunnen we ze zien, wat gebeurt er als ze exploderen, wat voor invloed hebben ze gehad op de evolutie van het heelal?

## 6.2 DE EVOLUTIE VAN HET HEELAL

Voordat ik ga uitleggen wat er in dit proefschrift allemaal staat, moet ik eerst iets anders vertellen over de evolutie van het heelal als geheel. De meeste sterrenkundigen denken dat het heelal ontstaan is in de oerknal of *Big Bang*, een grote explosie, waarin zowel ruimte en tijd, als alle natuurwetten zijn ontstaan. Hoewel er behoorlijk wat problemen zijn met deze theorie, heeft het ook een groot aantal succesen op zijn naam staan, en zijn er met behulp van deze theorie een heel aantal dingen in het huidige heelal goed te begrijpen. Daarom nemen bijna alle sterrenkundigen in het oerknalmodel hun uitgangspunt.

Eén van de dingen waar het oerknalmodel een heel goede verklaring voor kan geven is de vorming van chemische elementen en de hoeveelheden daarvan. Zo weten we uit metingen dat de zon bestaat uit ongeveer 70% waterstof, 28% helium en 2% andere chemische elementen, die we in de sterrenkunde voor het gemak "metalen" noemen, ookal zijn het niet allemaal metalen. Maar we weten ook uit waarnemingen, dat de hoeveelheid metalen vroeger een stuk lager is geweest dan de huidige 2%, en het oerknalmodel voorspelt dat dit na de oerknal zelf ongeveer 0% moet zijn geweest. Vanaf het begin van het heelal, tot het tijdstip waarop we nu leven, is er dus een toename geweest van metalen, en dit is precies wat we waarnemen. Zo kennen we bijvoorbeeld heel oude sterren, de zogenaamde 2de generatie sterren, die een veel lager percentage metalen hebben dan sterren die recenter gevormd zijn, sommige tot 100.000 keer zo weinig. Het percentage metalen, of kortweg de metalliciteit, vertelt je dus iets over hoe oud een ster is, en zo kan de metalliciteit worden gebruikt als een soort klok.

Het leuke is nu dat de toename van het percentage metalen in het heelal heel simpel te verklaren is met behulp van de elementen die sterren produceren tijdens en vooral aan het eind van hun leven. Want, zoals we al zagen, zet een ster gedurende de eerste fase van z'n leven waterstof om in helium, maar in latere fases worden zuurstof, neon en allerlei andere chemische elementen tot aan ijzer gemaakt. En in lichte sterren tijdens de fase van de pulsen, en in zware sterren tijdens de explosie, worden er nog veel meer – hoewel in niet al te grote hoeveelheden – exotische elementen gemaakt. Al deze chemische elementen zorgen ervoor, dat de hoeveelheid metalen toeneemt, als ze in het heelal terecht komen, bijvoorbeeld doordat de ster een groot gedeelte van z'n mantel verliest, of door de supernova explosie die de buitenlagen het heelal in slingert. Sterren zijn dus heel belangrijk voor de chemische evolutie van het heelal. En ondanks dat we al heel veel begrijpen over

*Oerknal*

*Vorming van  
chemische  
elementen*

*Hoeveelheid  
metalen neemt  
toe in de loop  
van de tijd*

*Sterren zijn  
belangrijke  
"vervuilers"*



hoe de chemische samenstelling van het heelal is veranderd, blijven er toch nog een aantal onopgeloste vragen over, en zeker de laatste jaren hebben heel veel sterrenkundigen erop gewezen dat het antwoord op deze vragen mogelijk ligt in het overgangsgedrag tussen lichte en zware sterren.

### 6.3 DIT PROEFSCHRIFT

Dit is dus de context voor dit onderzoek. Om dit onderzoek te kunnen doen heb ik heel veel gebruik gemaakt van computers en computerprogramma's. Eerst leg ik hieronder de methode uit die ik gevolgd heb, en daarna zal ik kort de inhoud van de verschillende hoofdstukken uitleggen.

#### 6.3.1 Methode

Van sterren weten we eigenlijk helemaal niks. Het enige wat we kunnen meten zijn de kleur en de helderheid van een ster, en soms, als hij in een dubbelster zit – twee sterren die rondjes om elkaar heendraaien – kunnen we ook nog berekenen hoe zwaar de ster is. That's it, daar moeten we het mee doen. Hoe kunnen we dan toch iets zeggen over hoe een ster eruit ziet en hoe hij gedurende zijn leven veranderd? Hoe weten we eigenlijk zeker dat een ster waterstof fuseert tot helium en of de temperatuur daarvoor wel hoog genoeg is?

Een van de fundamentele aannames in de sterrenkunde is dat de natuurwetten zoals we ze hier op aarde kennen, overal in het heelal precies hetzelfde doen. Een klein voorbeeldje: Als we hier iets los laten (bijvoorbeeld een pen) dan valt die pen naar beneden, of een klein beetje wetenschappelijker gezegd, de twee voorwerpen die in het spel zijn, de aarde en de pen, trekken elkaar aan en bewegen als gevolg daarvan naar elkaar toe. Omdat de aarde veel zwaarder is dan de pen, lijkt het alsof de pen naar de aarde toevalt. Als sterrenkundigen nemen we nu aan dat als we een aarde en een pen in een heel andere hoek van het heelal zouden aantreffen, ze zouden gehoorzamen aan precies dezelfde natuurwetten als hier op aarde. Ze zullen elkaar dus ook aantrekken, en ook daardoor de pen naar de aarde toe vallen. We nemen aan dat dit niet alleen voor een pen en de aarde geldt, maar ook voor sterren en alle natuurwetten die we kennen.

In de loop van de eeuwen hebben we door natuurkundig onderzoek een vrij compleet beeld op kunnen bouwen van hoe onze natuur in elkaar zit, en heel veel van die kennis, die vaak door allerlei proeven tot stand is gekomen, is verwoord in natuurwetten. Zo hebben we natuurwetten die de kracht tussen voorwerpen met massa beschrijven (de zwaartekracht), natuurwetten die de krachten tussen voorwerpen met lading (positieve en negatieve) beschrijven (elektro-magnetische

*Natuurwetten  
zijn overal  
hetzelfde*

*Experimenten  
en natuurwetten*

kracht), natuurwetten die het gedrag van gassen beschrijven, en zo zou ik nog even door kunnen gaan. Al die wetten beschrijven een gedeelte van de werkelijkheid, en kunnen we dus ook toepassen op sterren, en het leuke is dat we om sterren te kunnen begrijpen en na te kunnen maken in onze computers niet eens zo heel veel natuurwetten nodig hebben, sterker nog, met vijf (!) vergelijkingen kunnen we al een heel eind komen.

*Een ronde ster wordt voorgesteld als een lijntje van het centrum naar de rand*

**STEREVOLUTIECODE** Een sterevolutiecode is een heel groot computerprogramma waar die vijf belangrijkste vergelijkingen, nog een aantal natuurwetten en nog veel meer informatie is ingestopt. Omdat sterren rond zijn – of bijna rond – bouwen we de ster op uit allemaal bolletjes (of eigenlijk schillen) die allemaal om elkaar heen liggen, alsof het een ui is. Iedere schil heeft z'n eigen afstand tot het centrum en zou dus overal hetzelfde moeten zijn – overal op dat schilletje dezelfde temperatuur, overal dezelfde dichtheid, alles hetzelfde. In werkelijkheid zal dat nooit zo zijn, maar omdat het onze berekeningen en stuk gemakkelijker maakt, nemen we gewoon aan dat het zo is. In plaats van een hele ster drie-dimensionaal uit te gaan rekenen, alsof het een bol is, kunnen we nu sterren één-dimensionaal doorrekenen: als we voor één punt op een schil weten bijvoorbeeld hoe heet het daar is, weten we dat voor alle punten, en hetzelfde geldt natuurlijk voor de dichtheid en alle andere dingen die we willen weten. Heel slim dus! Zo is een ster in onze computers niet meer een bol, maar een lijntje, dat loopt van het centrum van de ster naar de rand. Over dat lijntje verdelen we ongeveer 1000 punten, en voor ieder punt rekenen alles uit wat we willen weten (in onze code zijn dat ongeveer 70 verschillende dingen). Voor één bepaald moment weten we nu hoe de ster eruit ziet. Maar omdat sommige dingen in de ster veranderen, bijvoorbeeld omdat waterstof in helium wordt omgezet, moeten we, als we het hele leven van een ster willen begrijpen, keer op keer uitrekenen hoe dat de ster beïnvloed. Meestal beginnen we met een jonge ster, die net begonnen is met z'n leven, en rekenen we stapje voor stapje de hele evolutie van een ster door. Voor de meeste fases van het leven van een ster voldoet dit prima, en kunnen we in een paar minuten tot een paar uur (ook afhankelijk van de code) uitrekenen hoe zo'n ster evolueert. Maar sommige fases van het leven van een ster zijn erg moeilijk zo te simuleren, en het kost soms maanden voordat het programma er mee klaar is. Om toch iets te kunnen zeggen over zulke fases hebben we nóg een programma ontwikkeld dat het allemaal veel sneller kan, maar daar wordt het wel minder nauwkeurig van.

*Stap voor stap lopen we door het leven van een ster*

**SYNTHETISCHE STEREVOLUTIECODE** Een van die fases waarin het allemaal heel moeilijk gaat is de laatste fase van het leven van een AGB ster als hij bezig is met de pulsar in de heliumschil (zie hiervoor). Dat

is erg jammer, omdat juist dit de fase is waarin we erg geïnteresseerd zijn voor dit onderzoek. Gelukkig is er een oplossing, omdat heel veel eigenschappen van de ster gedurende deze fase maar heel langzaam veranderen, en je ze dus heel goed kunt benaderen met eenvoudige formules. Voor alle eigenschappen waarin we geïnteresseerd zijn hebben we zulke formules opgesteld, en die hebben we in een zogenaamde *synthetische code* aan elkaar geplakt, waardoor we in staat zijn om ook de evolutie van sterren in deze fase snel door te rekenen. In het onderzoek dat ik gedaan heb en dat in dit proefschrift staat beschreven, gebruik ik beide codes.

*Sterevo  
lucie met  
eenvoudige  
formules*

### 6.3.2 Resultaten

**HOOFDSTUK 2** In dit hoofdstuk doen we onderzoek naar Super-AGB sterren (sterren die tussen lichte en zware sterren invallen) in het huidige heelal (grofweg laten sterrenkundigen hieronder alle sterren vallen die dezelfde hoeveelheid metalen als de zon ook hebben, 2%). Met onze grote sterevo-luciecode kijken we hoe ze evolueren, welke dingen daar invloed op hebben en wat voor gevolgen dat heeft. Als we niet meer verder kunnen, gebruiken we de synthetische code om ook het laatste stuk van het leven van deze sterren te kunnen beschrijven. We vinden, dat sterren die tussen de 9 en 9.25 keer zo zwaar zijn als de zon, eerst een fase kennen die karakteristiek is voor AGB sterren, maar dat ze aan het einde daarvan toch exploderen als een supernova. Dit zou ongeveer 4% van alle supernova explosies moeten zijn. Als we alle onzekerheden meenemen zou dit maximaal 20% kunnen worden.

**HOOFDSTUK 3** In dit hoofdstuk richten we ons op Super-AGB sterren die een lagere metalliciteit hebben, en dus ouder zijn. We vinden dat als we naar oudere sterren kijken, er veel meer kans is dat een ster in het tussengebied tussen zware en lichte sterren zit. Voor sterren die tien keer minder metalen dan de zon bezitten, is het percentage “bijzondere” supernova’s al opgelopen tot zo’n 15%, voor 100 keer minder metalen tot 25% en voor 1000 keer minder metalen tot 35% van alle supernova’s. De reden voor deze oplopende percentages is dat de zuurstof-neon kern van deze sterren ongehinderd door kan groeien tot de kritische massa en de ster dus kan exploderen, omdat de mantel van de ster steeds langzamer wordt weggeblazen voor lagere metalliciteiten. We vinden dat er zelfs kans is op hele excentrieke supernova’s, waarvan het bestaan al lang vermoed is, maar die nog nooit zijn aangetoond. Deze supernova’s bestaan uit koolstofkernen die zwaar genoeg zijn om te exploderen, iets wat heel moeilijk realiseerbaar is, omdat de kern de kritische massa heeft bereikt, de kans al heel groot is dat de volledige mantel is verdwenen. Dit levert allerlei interessante voorspellingen op of we deze en eerder genoemde supernova’s ook kunnen waarnemen,

en hoe ze er dan uit zouden kunnen zien. Daarom vergelijken we onze bevindingen met een aantal onopgeloste waarnemingen, maar helaas kunnen we hier geen ondubbelzinnige conclusies uit trekken. Ook de vragen die er nog zijn over de chemische evolutie van het heelal, en dan vooral over de rol die supernova's van Super-AGB sterren hierin mogelijk zouden kunnen spelen, kunnen (nog) niet echt worden opgelost.

**HOOFDSTUK 4** In dit hoofdstuk bouwen we voort op de resultaten van hoofdstuk 2 en kijken we welke invloed Super-AGB sterren gedurende hun leven hebben op de chemische samenstelling van het huidige heelal. We komen tot de conclusie dat lichte sterren en zware sterren veel meer invloed hebben op de chemische samenstelling van het heelal, en dat de invloed van de sterren die er tussenin zitten, onze Super-AGB sterren, verwaarloosbaar is.

**HOOFDSTUK 5** In dit hoofdstuk, dat ook gebaseerd is op een gedeelte van de resultaten uit hoofdstuk 2, kijken we wat het verschil is tussen sterren die alleen zijn en sterren die samen een paar vormen, de zogenaamde dubbelsterren. We doen dit, omdat we hiermee een verklaring hopen te geven voor de twee groepen neutronensterren die we waarnemen; neutronensterren met die een lage snelheid hebben ( $\sim 50$  km/s) en neutronensterren die een hoge snelheid hebben ( $\sim 100 - 200$  km/s). We proberen aan te tonen dat neutronensterren met zowel een lage als een hoge snelheid hun oorsprong hebben in dubbelstersystemen, maar dat neutronensterren met een lage massa waarschijnlijk ontstaan zijn uit een supernova explosie die vergelijkbaar is met de explosie van een "alleenstaande" Super-AGB ster, en dat neutronensterren met een hoge snelheid ontstaan zijn zwaardere sterren.

## BIBLIOGRAPHY

---

- Aldering, G., Antilogus, P., Bailey, S., et al. 2006, astro-ph/0606499 (Cited on page 70.)
- Alexander, D. R. & Ferguson, J. W. 1994, *ApJ*, 437, 879 (Cited on page 76.)
- Allen, D. M. & Barbuy, B. 2006, *A&A*, 454, 895 (Cited on page 69.)
- Arzoumanian, Z., Chernoff, D. F., & Cordes, J. M. 2002, *ApJ*, 568, 289 (Cited on pages 68 and 100.)
- Barbuy, B., Spite, M., Spite, F., et al. 2005, *A&A*, 429, 1031 (Cited on page 6.)
- Baron, E., Cooperstein, J., & Kahana, S. 1987, *ApJ*, 320, 300 (Cited on page 41.)
- Becker, S. A. 1981, *ApJS*, 45, 475 (Cited on page 50.)
- Beers, T. C. & Christlieb, N. 2005, *ARA&A*, 43, 531 (Cited on pages 6 and 69.)
- Belczynski, K., Kalogera, V., & Bulik, T. 2002, *ApJ*, 572, 407 (Cited on page 81.)
- Bethe, H. A. & Wilson, J. R. 1985, *ApJ*, 295, 14 (Cited on page 41.)
- Bildsten, L., Chakrabarty, D., Chiu, J., et al. 1997, *ApJS*, 113, 367 (Cited on page 113.)
- Blöcker, T. 1995, *A&A*, 297, 727 (Cited on pages 14, 30, 46, 54, and 76.)
- Blöcker, T. & Schönberner, D. 1991, *A&A*, 244, L43 (Cited on page 81.)
- Bono, G., Caputo, F., Cassisi, S., et al. 2000, *ApJ*, 543, 955 (Cited on pages 45 and 50.)
- Boothroyd, A. I., Sackmann, I.-J., & Wasserburg, G. J. 1995, *ApJ*, 442, L21 (Cited on page 74.)
- Bowen, G. H. 1988, *ApJ*, 329, 299 (Cited on page 30.)
- Bowen, G. H. & Willson, L. A. 1991, *ApJ*, 375, L53 (Cited on pages 56, 61, and 66.)
- Brandt, N. & Podsiadlowski, P. 1995, *MNRAS*, 274, 461 (Cited on page 100.)
- Brown, G. E., Heger, A., Langer, N., et al. 2001, *New Astronomy*, 6, 457 (Cited on pages 101, 104, and 106.)
- Brown, G. E., Lee, C.-H., & Bethe, H. A. 1999, *New Astronomy*, 4, 313 (Cited on page 101.)
- Burgay, M., D'Amico, N., Possenti, A., et al. 2003, *Nature*, 426, 531 (Cited on page 114.)
- Burrows, A. & Lattimer, J. M. 1985, *ApJ*, 299, L19 (Cited on page 41.)
- Busso, M., Gallino, R., & Wasserburg, G. J. 1999, *ARA&A*, 37, 239 (Cited

- on page 20.)
- Carretta, E., Bragaglia, A., Gratton, R. G., et al. 2006, *A&A*, 450, 523 (Cited on page 95.)
- Cassisi, S. & Castellani, V. 1993, *ApJS*, 88, 509 (Cited on pages 50 and 53.)
- Castellani, V., Chieffi, A., & Straniero, O. 1990, *ApJS*, 74, 463 (Cited on page 50.)
- Chieffi, A., Domínguez, I., Limongi, M., & Straniero, O. 2001, *ApJ*, 554, 1159 (Cited on page 23.)
- Chieffi, A. & Limongi, M. 2004, *ApJ*, 608, 405 (Cited on page 81.)
- Chugai, N. N., Chevalier, R. A., & Lundqvist, P. 2004, *MNRAS*, 355, 627 (Cited on page 70.)
- Chugai, N. N. & Utrobin, V. P. 2000, *A&A*, 354, 557 (Cited on page 34.)
- Chugai, N. N. & Yungelson, L. R. 2004, *Astronomy Letters*, 30, 65 (Cited on page 70.)
- Clayton, D. D. 1983, *Principles of stellar evolution and nucleosynthesis* (Chicago: University of Chicago Press, 1983) (Cited on page 1.)
- Cordes, J. M. & Chernoff, D. F. 1998, *ApJ*, 505, 315 (Cited on page 100.)
- Deng, J., Kawabata, K. S., Ohya, Y., et al. 2004, *ApJ*, 605, L37 (Cited on page 70.)
- Denissenkov, P. A. & Tout, C. A. 2003, *MNRAS*, 340, 722 (Cited on page 14.)
- Doherty, C. L. & Lattanzio, J. C. 2006, *Memorie della Societa Astronomica Italiana*, 77, 828 (Cited on pages 22, 41, 56, 75, 79, 80, and 87.)
- Drukier, G. A. 1996, *MNRAS*, 280, 498 (Cited on page 100.)
- El Eid, M. F. & Langer, N. 1986, *A&A*, 167, 274 (Cited on page 76.)
- Eldridge, J. J. & Tout, C. A. 2004a, *MNRAS*, 348, 201 (Cited on page 62.)
- Eldridge, J. J. & Tout, C. A. 2004b, *Memorie della Societa Astronomica Italiana*, 75, 694 (Cited on pages 18, 62, and 74.)
- Eldridge, J. J. & Tout, C. A. 2004c, *MNRAS*, 353, 87 (Cited on pages 13, 44, 45, 71, 104, 108, and 113.)
- Falk, S. W. & Arnett, W. D. 1977, *ApJS*, 33, 515 (Cited on page 33.)
- Freytag, B., Ludwig, H.-G., & Steffen, M. 1996, *A&A*, 313, 497 (Cited on page 14.)
- Frost, C. A., Cannon, R. C., Lattanzio, J. C., Wood, P. R., & Forestini, M. 1998, *A&A*, 332, L17 (Cited on pages 7 and 12.)
- Fryer, C. L. 1999, *ApJ*, 522, 413 (Cited on page 106.)
- Fryer, C. L. 2004, *Stellar Collapse* (Stellar Collapse. Edited by Chris L. Fryer, Los Alamos National Laboratory, Los Alamos, NM, U.S.A. and University of Arizona, Tucson, AZ, U.S.A. Astrophysics and Space Science Library, Volume 302 Kluwer Academic Publishers, Dordrecht) (Cited on page 106.)

- Fryer, C. L., Heger, A., Langer, N., & Wellstein, S. 2002, *ApJ*, 578, 335 (Cited on page 106.)
- Fryer, C. L. & Kalogera, V. 2001, *ApJ*, 554, 548 (Cited on page 106.)
- Fryer, C. L. & Warren, M. S. 2002, *ApJ*, 574, L65 (Cited on pages 106 and 107.)
- Fryer, C. L. & Warren, M. S. 2004, *ApJ*, 601, 391 (Cited on pages 106 and 107.)
- García-Berro, E. & Iben, I. 1994, *ApJ*, 434, 306 (Cited on page 74.)
- García-Berro, E., Ritossa, C., & Iben, I. J. 1997, *ApJ*, 485, 765 (Cited on pages 7, 12, 13, 15, 18, 44, 74, and 104.)
- Gil-Pons, P., Suda, T., Fujimoto, M. Y., & García-Berro, E. 2005, *A&A*, 433, 1037 (Cited on page 45.)
- Girardi, L., Bressan, A., Bertelli, G., & Chiosi, C. . 2000, *A&AS*, 141, 371 (Cited on pages 15, 45, 50, and 74.)
- Goriely, S. & Siess, L. 2004, *A&A*, 421, L25 (Cited on page 96.)
- Grevesse, N. 1991, in *IAU Symp. 145: Evolution of Stars: the Photospheric Abundance Connection*, 63 (Cited on page 76.)
- Gutiérrez, J., Canal, R., & García-Berro, E. 2005, *A&A*, 435, 231 (Cited on pages 12, 59, 81, and 96.)
- Gutierrez, J., Garcia-Berro, E., Iben, I. J., et al. 1996, *ApJ*, 459, 701 (Cited on page 59.)
- Habets, G. M. H. J. 1986, *A&A*, 167, 61 (Cited on page 104.)
- Habing, H. J. 1996, *A&A Rev.*, 7, 97 (Cited on pages 12 and 54.)
- Hamuy, M., Phillips, M. M., Suntzeff, N. B., et al. 2003, *Nature*, 424, 651 (Cited on page 70.)
- Han, Z. 1998, *MNRAS*, 296, 1019 (Cited on page 114.)
- Han, Z., Podsiadlowski, P., & Eggleton, P. P. 1994, *MNRAS*, 270, 121 (Cited on page 108.)
- Hansen, B. M. S. & Phinney, E. S. 1997, *MNRAS*, 291, 569 (Cited on page 100.)
- Hartman, J. W. 1997, *A&A*, 322, 127 (Cited on page 101.)
- Hashimoto, M., Iwamoto, K., & Nomoto, K. 1993, *ApJ*, 414, L105 (Cited on pages 7, 12, and 44.)
- Heger, A. & Langer, N. 2000, *ApJ*, 544, 1016 (Cited on pages 15 and 20.)
- Heger, A., Langer, N., & Woosley, S. E. 2000, *ApJ*, 528, 368 (Cited on pages 14, 15, 19, 46, and 75.)
- Heger, A. & Woosley, S. E. 2003, in *AIP Conf. Proc. 662: Gamma-Ray Burst and Afterglow Astronomy 2001: A Workshop Celebrating the First Year of the HETE Mission*, 214–216 (Cited on page 102.)
- Heger, A., Woosley, S. E., Langer, N., & Spruit, H. C. 2004, in *IAU Symposium*, 591 (Cited on page 102.)
- Heger, A., Woosley, S. E., Rauscher, T., Hoffman, R. D., & Boyes, M. M.

- 2002, *New Astronomy Review*, 46, 463 (Cited on page 106.)
- Hendry, M. A., Smartt, S. J., Crockett, R. M., et al. 2006, *MNRAS*, 369, 1303 (Cited on page 34.)
- Herwig, F. 2000, *A&A*, 360, 952 (Cited on pages 14, 46, and 76.)
- Herwig, F. 2004a, *ApJ*, 605, 425 (Cited on pages 15, 23, 41, 45, 56, 75, and 76.)
- Herwig, F. 2004b, *ApJS*, 155, 651 (Cited on pages 15, 45, and 56.)
- Herwig, F. 2005, *ARA&A*, 43, 435 (Cited on pages 4, 12, and 20.)
- Herwig, F. & Austin, S. M. 2004, *ApJ Lett.*, 613, L73 (Cited on page 15.)
- Herwig, F., Blöcker, T., Schönberner, D., & El Eid, M. 1997, *A&A*, 324, L81 (Cited on pages 14, 46, and 76.)
- Herwig, F., Langer, N., & Lugaro, M. 2003, in *IAU Symposium*, 99 (Cited on page 15.)
- Hill, V., Barbuy, B., Spite, M., et al. 2000, *A&A*, 353, 557 (Cited on page 6.)
- Hillebrandt, W., Wolff, R. G., & Nomoto, K. 1984, *A&A*, 133, 175 (Cited on pages 41, 59, and 107.)
- Hurley, J. R., Pols, O. R., & Tout, C. A. 2000, *MNRAS*, 315, 543 (Cited on page 28.)
- Hurley, J. R., Tout, C. A., & Pols, O. R. 2002, *MNRAS*, 329, 897 (Cited on page 76.)
- Iben, I. 1974, *ARA&A*, 12, 215 (Cited on pages 103 and 107.)
- Iben, I. & Renzini, A. 1983, *ARA&A*, 21, 271 (Cited on pages 4, 6, 12, 20, 57, 58, 70, and 74.)
- Iben, I. J., Ritossa, C., & Garcia-Berro, E. 1997, *ApJ*, 489, 772 (Cited on pages 7, 12, 13, 15, 18, 44, 74, and 104.)
- Iglesias, C. A. & Rogers, F. J. 1996, *ApJ*, 464, 943 (Cited on pages 14, 46, and 76.)
- Iliadis, C., D'Auria, J. M., Starrfield, S., Thompson, W. J., & Wiescher, M. 2001, *ApJS*, 134, 151 (Cited on page 95.)
- Ishimaru, Y., Wanajo, S., Aoki, W., & Ryan, S. G. 2004, *ApJ*, 600, L47 (Cited on page 69.)
- Israelian, G., Rebolo, R., Basri, G., Casares, J., & Martín, E. L. 1999, *Nature*, 401, 142 (Cited on page 114.)
- Ivanova, N. & Podsiadlowski, P. 2003, in *From Twilight to Highlight: The Physics of Supernovae*, ed. W. Hillebrandt & B. Leibundgut, 19 (Cited on page 102.)
- Izzard, R., Lugaro, M., Iliadis, C., & Karakas, A. 2006a, astro-ph/0607536 (Cited on page 80.)
- Izzard, R. G. 2004, *Memorie della Societa Astronomica Italiana*, 75, 754 (Cited on page 96.)
- Izzard, R. G., Dray, L. M., Karakas, A. I., Lugaro, M., & Tout, C. A. 2006b, *A&A*, 460, 565 (Cited on pages 8 and 75.)



- Izzard, R. G., Tout, C. A., Karakas, A. I., & Pols, O. R. 2004, *MNRAS*, 350, 407 (Cited on pages 25, 26, 46, and 75.)
- Janka, H.-T., Buras, R., Kifonidis, K., Plewa, T., & Rampp, M. 2003, in *From Twilight to Highlight: The Physics of Supernovae*, ed. W. Hillebrandt & B. Leibundgut, 39 (Cited on page 106.)
- Johnston, S., Manchester, R. N., Lyne, A. G., et al. 1992, *ApJ*, 387, L37 (Cited on page 113.)
- Jonsell, K., Barklem, P. S., Gustafsson, B., et al. 2006, *A&A*, 451, 651 (Cited on pages 6 and 69.)
- Joss, P. C. & Becker, J. A. 2003, in *From Twilight to Highlight: The Physics of Supernovae*, ed. W. Hillebrandt & B. Leibundgut, 104 (Cited on page 102.)
- Karakas, A. I., Lattanzio, J. C., & Pols, O. R. 2002, *Publications of the Astronomical Society of Australia*, 19, 515 (Cited on pages 8, 25, 28, 29, 40, 48, 56, 59, 61, and 76.)
- Kaspi, V. M., Bailes, M., Manchester, R. N., Stappers, B. W., & Bell, J. F. 1996, *Nature*, 381, 584 (Cited on page 113.)
- Kaspi, V. M., Johnston, S., Bell, J. F., et al. 1994, *ApJ*, 423, L43 (Cited on page 113.)
- Katz, J. I. 1975, *Nature*, 253, 698 (Cited on page 101.)
- Katz, J. I. 1983, *A&A*, 128, L1+ (Cited on page 101.)
- Kippenhahn, R. & Weigert, A. 1967, *Zeitschrift fur Astrophysik*, 65, 251 (Cited on page 102.)
- Kitaura, F. S., Janka, H.-T., & Hillebrandt, W. 2006, *A&A*, 450, 345 (Cited on pages 34, 41, 59, 69, and 96.)
- Kroupa, P., Tout, C., & Gilmore, G. 1993, *MNRAS*, 262, 545 (Cited on page 93.)
- Kuranov, A. G. & Postnov, K. A. 2006, *Astronomy Letters*, 32, 393 (Cited on page 69.)
- Langer, N. 1991, *A&A*, 252, 669 (Cited on page 76.)
- Langer, N. 1998, *A&A*, 329, 551 (Cited on pages 14, 46, and 76.)
- Langer, N., Fricke, K. J., & Sugimoto, D. 1983, *A&A*, 126, 207 (Cited on pages 14 and 76.)
- Langer, N., Heger, A., Wellstein, S., & Herwig, F. 1999, *A&A*, 346, L37 (Cited on page 15.)
- Langer, N., Kiriakidis, M., El Eid, M. F., Fricke, K. J., & Weiss, A. 1988, *A&A*, 192, 177 (Cited on page 75.)
- Langer, N. & Norman, C. A. 2006, *ApJ*, 638, L63 (Cited on page 68.)
- Langer, N., Wellstein, S., & Petrovic, J. 2003, in *IAU Symposium*, 275 (Cited on page 102.)
- Langer, N., Yoon, S.-C., Petrovic, J., & Heger, A. 2004, in *IAU Symposium*, ed. A. Maeder & P. Eenens, 535 (Cited on page 102.)
- Lauterborn, D. 1970, *A&A*, 7, 150 (Cited on page 102.)

- Livio, M. & Riess, A. G. 2003, *ApJ*, 594, L93 (Cited on page 70.)
- Lyne, A. G., Burgay, M., Kramer, M., et al. 2004, *Science*, 303, 1153 (Cited on page 114.)
- Lyne, A. G. & Lorimer, D. R. 1994, *Nature*, 369, 127 (Cited on page 100.)
- Marietta, E., Burrows, A., & Fryxell, B. 2000, *ApJS*, 128, 615 (Cited on page 69.)
- Marigo, P., Bressan, A., & Chiosi, C. 1996, *A&A*, 313, 545 (Cited on page 14.)
- Maund, J. R. & Smartt, S. J. 2005, *MNRAS*, 360, 288 (Cited on page 34.)
- Mayle, R. & Wilson, J. R. 1988, *ApJ*, 334, 909 (Cited on page 41.)
- Miyaji, S. & Nomoto, K. 1987, *ApJ*, 318, 307 (Cited on pages 7, 12, 44, and 59.)
- Miyaji, S., Nomoto, K., Yokoi, K., & Sugimoto, D. 1980a, *PASJ*, 32, 303 (Cited on pages 7, 12, 44, and 59.)
- Miyaji, S., Sugimoto, D., Nomoto, K., & Yokoi, K. 1980b, in *International Cosmic Ray Conference*, 13–16 (Cited on page 59.)
- Nelemans, G., Yungelson, L. R., Portegies Zwart, S. F., & Verbunt, F. 2001, *A&A*, 365, 491 (Cited on page 114.)
- Nomoto, K. 1981, in *IAU Symp. 93: Fundamental Problems in the Theory of Stellar Evolution*, 295–314 (Cited on pages 24 and 59.)
- Nomoto, K. 1982, in *NATO ASIC Proc. 90: Supernovae: A Survey of Current Research*, 205–213 (Cited on page 59.)
- Nomoto, K. 1983, in *IAU Symp. 101: Supernova Remnants and their X-ray Emission*, 139–143 (Cited on pages 58 and 59.)
- Nomoto, K. 1984a, *ApJ*, 277, 791 (Cited on pages 12, 13, 41, 44, 59, and 104.)
- Nomoto, K. 1984b, in *ASSL Vol. 109: Stellar Nucleosynthesis*, 239 (Cited on page 59.)
- Nomoto, K. 1985, in *The Crab Nebula and Related Supernova Remnants*, 97–113 (Cited on page 59.)
- Nomoto, K. 1987a, *ApJ*, 322, 206 (Cited on pages 7, 12, 13, 41, 44, 59, 74, 81, and 104.)
- Nomoto, K. 1987b, in *IAU Symp. 125: The Origin and Evolution of Neutron Stars*, 281 (Cited on pages 44 and 114.)
- Nomoto, K. & Iben, I. 1985, *ApJ*, 297, 531 (Cited on page 114.)
- Nomoto, K. & Kondo, Y. 1991, *ApJ*, 367, L19 (Cited on page 114.)
- Nomoto, K., Miyaji, S., Sugimoto, D., & Yokoi, K. 1979, *BAAS*, 11, 725 (Cited on page 59.)
- Paczynski, B. 1976, in *IAU Symp. 73: Structure and Evolution of Close Binary Systems*, ed. P. Eggleton, S. Mitton, & J. Whelan, 75 (Cited on page 102.)
- Pannekoek, A. 1951, *De groei van ons wereldbeeld: een geschiedenis van de sterrenkunde* (Amsterdam, Nederland : Wereld-Bibliotheek,

- 1951.) (Cited on pages 1 and 2.)
- Pastorello, A., Turatto, M., Benetti, S., et al. 2002, *MNRAS*, 333, 27 (Cited on page 34.)
- Pfahl, E., Rappaport, S., & Podsiadlowski, P. 2002a, *ApJ*, 573, 283 (Cited on pages 69, 100, 109, and 113.)
- Pfahl, E., Rappaport, S., & Podsiadlowski, P. 2002b, *ApJ*, 571, L37 (Cited on page 109.)
- Pfahl, E., Rappaport, S., & Podsiadlowski, P. 2003, *ApJ*, 597, 1036 (Cited on page 109.)
- Pfahl, E., Rappaport, S., Podsiadlowski, P., & Spruit, H. 2002c, *ApJ*, 574, 364 (Cited on pages 100, 101, 102, and 109.)
- Podsiadlowski, P., Joss, P. C., & Hsu, J. J. L. 1992, *ApJ*, 391, 246 (Cited on page 102.)
- Podsiadlowski, P., Langer, N., Poelarends, A. J. T., et al. 2004, *ApJ*, 612, 1044 (Cited on pages 34, 68, and 69.)
- Podsiadlowski, P., Nomoto, K., Maeda, K., et al. 2002, *ApJ*, 567, 491 (Cited on page 114.)
- Podsiadlowski, P., Rappaport, S., & Han, Z. 2003, *MNRAS*, 341, 385 (Cited on page 108.)
- Poelarends, A. J. T., Herwig, F., Langer, N., & Heger, A. 2007, submitted to *ApJ* (Cited on pages 43, 44, 45, 75, 76, 79, 103, 105, 108, and 113.)
- Poelarends, A. J. T., Izzard, R. G., Herwig, F., Langer, N., & Heger, A. 2006, *Memorie della Societa Astronomica Italiana*, 77, 846 (Cited on page 56.)
- Pols, O. R. & Dewi, J. D. M. 2002, *Publications of the Astronomical Society of Australia*, 19, 233 (Cited on page 103.)
- Pols, O. R., Tout, C. A., Schroder, K.-P., Eggleton, P. P., & Manners, J. 1997, *MNRAS*, 289, 869 (Cited on page 108.)
- Pooley, D., Lewin, W. H. G., Anderson, S. F., et al. 2003, *ApJ*, 591, L131 (Cited on page 69.)
- Price, N. M. & Podsiadlowski, P. 1993, in *Bulletin of the American Astronomical Society*, 1439 (Cited on page 114.)
- Reimers, D. 1975, *Memoires of the Societe Royale des Sciences de Liege*, 8, 369 (Cited on pages 29 and 81.)
- Ritossa, C., Garcia-Berro, E., & Iben, I. J. 1996, *ApJ*, 460, 489 (Cited on pages 7, 12, 13, 15, 18, 20, 22, 41, 44, 46, 59, 74, 75, 87, and 104.)
- Ritossa, C., Garcia-Berro, E., & Iben, I. J. 1999, *ApJ*, 515, 381 (Cited on pages 7, 12, 13, 15, 18, 20, 44, 74, 79, and 108.)
- Romano, D., Chiappini, C., Matteucci, F., & Tosi, M. 2005, *A&A*, 430, 491 (Cited on page 95.)
- Schaller, G., Schaerer, D., Meynet, G., & Maeder, A. 1992, *A&AS*, 96, 269 (Cited on page 49.)
- Scheck, L., Plewa, T., Janka, H.-T., Kifonidis, K. ., & Müller, E. 2004,

- Physical Review Letters, 92, 011103 (Cited on page 107.)
- Schröder, K.-P. & Cuntz, M. 2005, ApJ, 630, L73 (Cited on page 29.)
- Schroder, K.-P., Pols, O. R., & Eggleton, P. P. 1997, MNRAS, 285, 696 (Cited on page 108.)
- Seeger, P. A., Fowler, W. A., & Clayton, D. D. 1965, ApJS, 11, 121 (Cited on page 5.)
- Siess, L. 2006, A&A, 448, 717 (Cited on pages 12, 13, 15, 18, 41, 44, 56, 59, 74, and 79.)
- Siess, L., Goriely, S., & Langer, N. 2004, A&A, 415, 1089 (Cited on pages 15 and 22.)
- Siess, L. & Pumo, M. L. 2006, Memorie della Societa Astronomica Italiana, 77, 822 (Cited on pages 22, 41, 44, 45, 50, 53, 75, and 87.)
- Smartt, S. J., Gilmore, G. F., Tout, C. A., & Hodgkin, S. T. 2002, ApJ, 565, 1089 (Cited on page 114.)
- Sollerman, J., Kozma, C., & Lundqvist, P. 2001, A&A, 366, 197 (Cited on page 34.)
- Spruit, H. C. & Phinney, E. S. 1998, Nature, 393, 139 (Cited on page 102.)
- Stairs, I. H., Manchester, R. N., Lyne, A. G., et al. 2001, MNRAS, 325, 979 (Cited on page 113.)
- Sugimoto, D. & Nomoto, K. 1980, Space Science Reviews, 25, 155 (Cited on page 24.)
- Sumiyoshi, K., Terasawa, M., Mathews, G. J., et al. 2001, ApJ, 562, 880 (Cited on pages 41, 106, and 107.)
- Tornambe, A. & Chieffi, A. 1986, MNRAS, 220, 529 (Cited on page 50.)
- Tsujimoto, T. & Shigezama, T. 2006, ApJ, 638, L109 (Cited on page 70.)
- van Loon, J. T. 2005, astro-ph/0512326 (Cited on page 56.)
- van Loon, J. T., Cioni, M.-R. L., Zijlstra, A. A., & Loup, C. 2005, A&A, 438, 273 (Cited on pages 8, 29, 48, 55, 57, 81, 82, 84, and 86.)
- Vassiliadis, E. & Wood, P. R. 1993, ApJ, 413, 641 (Cited on pages 30, 48, 54, 56, 57, and 81.)
- Ventura, P., Castellani, M., & Straka, C. W. 2005, A&A, 440, 623 (Cited on page 13.)
- Ventura, P. & D'Antona, F. 2005, ApJ, 635, L149 (Cited on pages 74 and 95.)
- Vink, J. S. & de Koter, A. 2005, A&A, 442, 587 (Cited on page 67.)
- Wagenhuber, J. & Groenewegen, M. A. T. 1998, A&A, 340, 183 (Cited on page 28.)
- Wanajo, S. 2005, in Origin of Matter and Evolution of Galaxies, 279 (Cited on page 59.)
- Wanajo, S., Nomoto, K., Iwamoto, N., Ishimaru, Y., & Beers, T. C. 2006, ApJ, 636, 842 (Cited on pages 6 and 69.)
- Wanajo, S., Tamamura, M., Itoh, N., et al. 2003, ApJ, 593, 968 (Cited on

- pages 12, 41, 59, 69, 96, 104, and 114.)
- Weaver, T. A., Zimmerman, G. B., & Woosley, S. E. 1978, *ApJ*, 225, 1021 (Cited on pages 3, 14, and 46.)
- Wellstein, S. & Langer, N. 1999, *A&A*, 350, 148 (Cited on page 103.)
- Wellstein, S., Langer, N., & Braun, H. 2001, *A&A*, 369, 939 (Cited on pages 103, 105, and 108.)
- Wheeler, J. C., Cowan, J. J., & Hillebrandt, W. 1998, *ApJ*, 493, L101 (Cited on pages 12 and 41.)
- Woosley, S. E., Heger, A., & Weaver, T. A. 2002, *Reviews of Modern Physics*, 74, 1015 (Cited on pages 3 and 15.)
- Woosley, S. E., Langer, N., & Weaver, T. A. 1995, *ApJ*, 448, 315 (Cited on page 103.)
- Woosley, S. E. & Weaver, T. A. 1995, *ApJS*, 101, 181 (Cited on pages 54 and 105.)
- Yoon, S.-C. & Langer, N. 2005, *A&A*, 443, 643 (Cited on page 67.)
- Yoon, S.-C., Langer, N., & Norman, C. 2007, *A&A* in press, astro-ph/0606637 (Cited on pages 67 and 68.)
- Yoon, S.-C., Langer, N., & van der Sluys, M. 2004, *A&A*, 425, 207 (Cited on pages 12 and 44.)
- Young, P. A., Meakin, C., Arnett, D., & Fryer, C. L. 2005, *ApJ Lett.*, 629, L101 (Cited on page 14.)
- Young, T. R. 2004, *ApJ*, 617, 1233 (Cited on page 33.)
- Zijlstra, A. 2006, astro-ph/0605097 (Cited on pages 56 and 66.)
- Zijlstra, A. A. 2004, *MNRAS*, 348, L23 (Cited on pages 6, 56, 57, 61, 66, and 70.)



*The search for understanding,  
which is so natural to a scientist,  
is, in the end, the search for God.*

— John Polkinhorne, physicist & theologian

*The Word became flesh and lived among us... full of grace and truth.*

— John 1:14

## ACKNOWLEDGMENTS / DANKWOORD

---

At the end of this thesis I would like to thank a couple of people. Norbert, over the last five and a half years you have had the difficult task to supervise and advise me. Times of excitement and rapid scientific developments were alternated by times of almost no progress. Thank you, for your confidence in what I was doing, even if it was different from what you had in mind.

Many thanks to Alexander Heger for inviting me to Los Alamos, one of the most remarkable physics laboratories of the world, and giving me the opportunity to look and work beyond the boundaries of science in Utrecht and the Netherlands, in a way that had much more impact than a short visit or conference. Thanks also to Falk Herwig, whose ambition stirred up my research a lot, and thanks also for the many helpful discussions, both about science and life.

Een hartelijk “bedankt” ook voor alle (oud)collega’s op het instituut. Ik denk met veel plezier terug aan de borrels en etentjes, maar ook aan de dagelijkse lunches, de zeiltochten en alle andere dingen die we samen gedaan hebben. A special word of thanks to Sung-Chul Yoon for assistance with the stellar evolution code, to Ed, Marion and Sake for practical assistance, to Alfred and Cees for L<sup>A</sup>T<sub>E</sub>X and IDL help, to Onno for many helpful discussions about almost everything, to Rob for doing together the nucleosynthesis paper, and to the rest of the stellar evolution group for nice – but sometimes long – groupmeetings. In het bijzonder ook de studenten met wie ik heb samengewerkt, Rob, Maarten, Frank, Hesdy en Marcel.

Cees (en Gemma natuurlijk ook), bedankt voor de vriendschap van de afgelopen jaren. We zijn meer dan collega’s geworden, en dat heeft een hoop bij gedragen aan het plezier waarmee ik naar m’n werk ging.

Iets verder terug in de tijd staan de docenten van het *Greijdanus College* in Zwolle. Bert, Jan Jaap, Hans en Ieke, ieder op jullie eigen manier hebben jullie bijgedragen aan de persoon die ik nu ben. Bedankt voor manier waarop jullie me enthousiast hebben gemaakt voor de wetenschap, bedankt ook voor het vertrouwen dat jullie me de afgelopen jaren hebben gegeven in de steeds weer terugkerende uitnodiging om een bijdrage te geven aan de ANW-dagen. Het waren niet alleen waardevolle dagen voor de leerlingen, maar het heeft ook mij gedwongen om steeds opnieuw na te denken over de relatie tussen wetenschap en geloof. De ontwikkeling die ik daarin heb doorgemaakt hebben jullie zelf kunnen zien.

Gerrit Glas, you encouraged me to pursue a scientific career and showed from your own life how to face the questions you can encounter as a Christian in science. I have learned a lot from your wisdom, broad knowledge and view on reality and will always remember your advice to be a Christian in science "with open eyes."

As a lot of people will know, the time that I spend in Los Alamos during Summer and Fall of 2004 has made a huge impact on my life. Mainly responsible for that, were the people from Bryce Avenue Presbyterian Church in White Rock whose love I will always remember, especially of my fellow brothers and sisters from the Sunday Evening Home Fellowship in Los Alamos: David & Chris, David & Amy, John & Catherine, Kendall & Kris, Craig & Shirley, Jim, Gregg, Kurt Andrew & Natashja, Bob & Anne, Doug, thank you very much! Also thanks to pastor Henry and his wife Cindy Fernandez. We'll meet again!

Ook in Utrecht (en daarbuiten) heb ik gelukkig veel vrienden. Omdat ik niet het gevaar wil lopen in een lange opsomming iemand te vergeten, begin ik gewoon niet aan die opsomming. Als je dit leest, weet dan dat ik je betrokkenheid bij mijn leven en werk – op wat voor manier dan ook – erg waardeer en blij ben je tot mijn vriendenkring te kunnen rekenen. Bedankt!

Christiaan, Eline & Peter en Arieke & Maurijn, hoewel jullie waarschijnlijk weinig snappen van waar ik nu die vier jaar mee bezig ben geweest, zijn jullie wel belangrijk geweest, omdat ik thuis echt thuis kon zijn en het altijd goed en gezellig is.

Papa en mama, in de moeilijkste jaren van jullie leven, hebben jullie de kracht gekregen om ons op te voeden en ons liefde te geven. Nu ik zelf de leeftijd begin te naderen waarop jullie stil werden gezet, begin ik een klein beetje te beseffen welke impact jullie ziekten gehad moeten hebben. Ik wordt dan stil, leg de hand op mijn mond, en ben jullie diep dankbaar voor jullie liefde in al die jaren, tot op de dag van vandaag.



The years that I worked on this thesis were in more than one way exceptional. The changes in my personal life were without doubt more radical than what I scientifically achieved. But as I learned more and more about this fascinating universe, the more I became overwhelmed by a sense of wonder. This world is not a world of chaos and random chance, but of order and meaning and beauty. The world we study as scientists, is only a small fraction of the reality we live in, a reality that is only worth living in because of love — Love that no scientist can ever unravel, love that's transcendent and ultimately heavenly: full of grace and truth. Therefore, the only thing I can say at the end of this thesis, are the words that I've learned from the English theologian N.T. Wright, and that have sunk deep into my heart: *This is my Father's world.*



## CURRICULUM VITAE

---

Ik ben geboren op 31 augustus 1979 te Zwolle en opgegroeid in de kleine hanzestad Hasselt. Mijn eerste onderwijs kreeg ik op de gereformeerde basisschool *Op de Hoeksteen* te Hasselt en voortgezet onderwijs volgde ik op de Gereformeerde Scholengemeenschap *Greijdanus College* te Zwolle, waar ik in 1997 mijn VWO diploma behaalde.

In september 1997 begon ik met een studie Technische Natuurkunde aan de *Universiteit Twente*, waarvan ik in augustus 1998 een propaedeutisch diploma in ontvangst mocht nemen. Ondertussen was ik ook begonnen met het volgen van vakken aan de *Universiteit Utrecht*, en in september 1998 ben ik volledig overgestapt naar de opleiding Natuur- en Sterrenkunde. Onder begeleiding van prof. dr. N. Langer begon ik in september 2001 met een afstudeeronderzoek naar hoofdreekssterren in een dubbelster met een zwart gat als begeleider, wat resulteerde in een scriptie waarin ik een nieuwe methode beschrijf om de massa van de hoofdreeksster, en daarmee ook van het begeleidende zwarte gat, te bepalen. Op 28 oktober 2002 behaalde ik het doctoraal diploma Natuur- en Sterrenkunde (met een specialisatie in de theoretische sterrenkunde).

Op 1 januari 2003 ben ik opnieuw onder begeleiding van prof. dr. N. Langer begonnen als assistent in opleiding in het Sterrenkundig Instituut Utrecht. Dit boekwerkje is het verslag van afgelopen vier jaar. Tijdens mijn promotieonderzoek heb ik deelgenomen aan conferenties in Brussel, Vancouver, Santa Fe, Leiden en Granada. Daarnaast heb ik drie maanden doorgebracht op *Los Alamos National Laboratory* in Los Alamos, NM, USA, waar ik samenwerkte met dr. A. Heger en dr. F. Herwig.